

AD-757 871

A SIMPLIFIED APPROACH TO THE ANALYSIS OF
TURBULENT BONDARY LAYERS IN TWO AND
THREE DIMENSIONS

F. M. White, et al

Rhode Island University

Prepared for:

Air Force Flight Dynamics Laboratory

November 1972

DISTRIBUTED BY:

NTIS

National Technical Information Service
U. S. DEPARTMENT OF COMMERCE
5285 Port Royal Road, Springfield Va. 22151

AD 757871

**A SIMPLIFIED APPROACH TO THE
ANALYSIS OF TURBULENT BOUNDARY
LAYERS IN TWO AND THREE DIMENSIONS**

*F. M. WHITE
R. C. LESSMANN
G. H. CHRISTOPH*

*DEPARTMENT OF MECHANICAL ENGINEERING
AND APPLIED MECHANICS
UNIVERSITY OF RHODE ISLAND
KINGSTON, RHODE ISLAND*

TECHNICAL REPORT AFFDL-T^o-136

NOVEMBER 1972

Approved for
Distribution by
NATIONAL TECHNICAL
INFORMATION SERVICE
Department of Commerce
Springfield, VA 22151

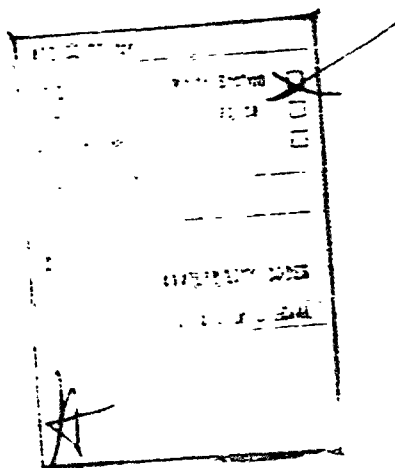
DD
FORM 1
MAR 28 1973
RECEIVED
E

Approved for public release; distribution unlimited.

**AIR FORCE FLIGHT DYNAMICS LABORATORY
AIR FORCE SYSTEMS COMMAND
WRIGHT-PATTERSON AIR FORCE BASE, OHIO 45433**

NOTICE

When Government drawings, specifications, or other data are used for any purpose other than in connection with a definitely related Government procurement operation, the United States Government thereby incurs no responsibility nor any obligation whatsoever; and the fact that the government may have formulated, furnished, or in any way supplied the said drawings, specifications, or other data, is not to be regarded by implication or otherwise as in any manner licensing the holder or any other person or corporation, or conveying any rights or permission to manufacture, use, or sell any patented invention that may in any way be related thereto.



Copies of this report should not be returned unless return is required by security considerations, contractual obligations, or notice on a specific document.

UNCLASSIFIED

Security Classification

DOCUMENT CONTROL DATA - R&D		
<i>(Security classification of title, body of abstract and indexing annotation must be entered when the overall report is classified)</i>		
1. ORIGINATING ACTIVITY (Corporate author) Division of Engineering Research & Development University of Rhode Island Kingston, Rhode Island 02881		2a. REPORT SECURITY CLASSIFICATION Unclassified
		2b. GROUP N/A
3. REPORT TITLE A SIMPLIFIED APPROACH TO THE ANALYSIS OF TURBULENT BOUNDARY LAYERS IN TWO AND THREE DIMENSIONS		
4. DESCRIPTIVE NOTES (Type of report and inclusive dates) Final Report - June 1971 through July 1972		
5. AUTHOR(S) (Last name, first name, initial) White, F.M. Lessmann, R.C. Christoph, G.H.		
6. REPORT DATE November 1972	7a. TOTAL NO. OF PAGES 228/41	7b. NO. OF REFS 71
8a. CONTRACT OR GRANT NO. F33615-71-C-1585	9a. ORIGINATOR'S REPORT NUMBER(S)	
b. PROJECT NO. 1426		
c. Task No. 04	9b. OTHER REPORT NO(S) (Any other numbers that may be assigned this report) AFFDL-TR-72-136	
d. Work Unit 17		
10. AVAILABILITY/LIMITATION NOTICES Approved for public release, distribution unlimited.		
11. SUPPLEMENTARY NOTES	12. SPONSORING MILITARY ACTIVITY Department of the Air Force AF Flight Dynamics Laboratory (AFSC) Wright-Patterson AFB, Ohio 45433	
13. ABSTRACT This report deals with a new method of calculation of coupled skin friction and heat transfer in two-dimensional turbulent boundary layers and also with the calculation of axisymmetric and three-dimensional turbulent skin friction. It is based upon an integral approach which assumes analytic law-of-the-wall velocity and temperature profiles through the boundary layer. In the two-dimensional and axisymmetric cases, this results in ordinary differential equations which have the skin friction and/or wall heat transfer as the only dependent variables. No shape factors or integral thicknesses appear in this theory. Flow separation is predicted by the explicit criterion $C_f = 0$. The three-dimensional boundary layer analysis results in two coupled partial differential equations for 1) the freestream component of skin friction; and 2) the tangent of the angle between the total surface shear stress and the freestream direction. The new theory is compared to several important experimental studies and the general agreement is excellent. Also, even at its most complicated, the present theory is considerably simpler than other currently available calculation schemes. This is particularly true of the three-dimensional analysis.		

DD FORM 1473
1 JAN 64

I-a

UNCLASSIFIED

Security Classification

14 KEY WORDS	LINK A		LINK B		LINK C	
	ROLE	WT	ROLE	WT	ROLE	WT
Aerodynamic drag Aerodynamic heating Boundary Layer flow Compressible flow Law of the wall Skin friction Supersonic flow Turbulent boundary layer Three-dimensional boundary layer						

INSTRUCTIONS

1. **ORIGINATING ACTIVITY:** Enter the name and address of the contractor, subcontractor, grantee, Department of Defense activity or other organization (corporate author) involving the report.
- 2a. **REPORT SECURITY CLASSIFICATION:** Enter the overall security classification of the report. Indicate whether "Restricted Data" is included. Marking is to be in accordance with appropriate security regulations.
- 2b. **GROUP:** Automatic downgrading is specified in DoD Directive 5200.10 and Armed Forces Industrial Manual. Enter the group number. Also, when applicable, show that optional markings have been used for Group 3 and Group 4 as authorized.
3. **REPORT TITLE:** Enter the complete report title in all capital letters. Titles in all cases should be unclassified. If a meaningful title cannot be selected without classification, show title classification in all capitals in parentheses immediately following the title.
4. **DESCRIPTIVE NOTES:** If appropriate, enter the type of report, e.g., interim, progress, summary, annual, or final. Give the inclusive dates when a specific reporting period is covered.
5. **AUTHOR(S):** Enter the name(s) of author(s) as shown on the report. Enter last name, first name, middle initial. If military, show rank and branch of service. The name of the principal author is an absolute minimum requirement.
6. **REPORT DATE:** Enter the date of the report as day, month, year, or month, year. If more than one date appears on the report, use date of publication.
- 7a. **TOTAL NUMBER OF PAGES:** The total page count should follow annual pagination procedures, i.e., enter the number of pages containing information.
- 7b. **NUMBER OF REFERENCES:** Enter the total number of references cited in the report.
- 8a. **CONTRACT OR GRANT NUMBER:** If appropriate, enter the applicable number of the contract or grant under which the report was written.
- 8b, 8c, & 8d. **PROJECT NUMBER:** Enter the appropriate military department identification, such as project number, subproject number, system number, task number, etc.
- 9a. **ORIGINATOR'S REPORT NUMBER(S):** Enter the official report number by which the document will be identified and controlled by the originating activity. This number must be unique to this report.
- 9b. **OTHER REPORT NUMBER(S):** If the report has been assigned any other report numbers (either by the originator or by the sponsor), also enter this number(s).
10. **AVAILABILITY/LIMITATION NOTICES:** Enter any limitations on further dissemination of the report, other than those

imposed by security classification, using standard statements such as:

- (1) "Qualified requesters may obtain copies of this report from DDC."
- (2) "Foreign announcement and dissemination of this report by DDC is not authorized."
- (3) "U. S. Government agencies may obtain copies of this report directly from DDC. Other qualified DDC users shall request through _____."
- (4) "U. S. military agencies may obtain copies of this report directly from DDC. Other qualified users shall request through _____."
- (5) "All distribution of this report is controlled. Qualified DDC users shall request through _____."

If the report has been furnished to the Office of Technical Services, Department of Commerce, for sale to the public, indicate this fact and enter the price, if known.

11. **SUPPLEMENTARY NOTES:** Use for additional explanatory notes.
12. **SPONSORING/MONITORING AGENCY NAME(S) AND ADDRESS(ES):** Enter the name of the departmental project office or laboratory sponsoring (paying for) the research and development. Include address.
13. **ABSTRACT:** Enter an abstract giving a brief and factual summary of the document indicative of the report, even though it may also appear elsewhere in the body of the technical report. If additional space is required, a continuation sheet shall be attached.

It is highly desirable that the abstract of classified reports be unclassified. Each paragraph of the abstract shall end with an indication of the military security classification of the information in the paragraph. (TS) (S) (C) (U)

There is no limitation on the length of the abstract. However, the suggested length is from 150 to 225 words.
14. **KEY WORDS:** Key words are technically meaningful terms or short phrases that characterize a report and may be used as index entries for cataloging the report. Key words must be selected so that no security classification is required. Identifiers, such as equipment model designation, trade name, military project code name, geographic location, may be used as key words but will be followed by an indication of technical context. The assignment of links, roles, and weights is optional.

Th

FOREWORD

This final technical report was prepared by F.M. White, R.C. Lessmann, and G.H. Christoph of the Department of Mechanical Engineering and Applied Mechanics of the University of Rhode Island under Contract F33615-71-C-1585, "Analysis of the Turbulent Boundary Layer in Axisymmetric and Three-Dimensional Flows."

The contract was initiated under Project No. 1426, "Experimental Simulation of Flight Mechanics," Task No. 142604, "Theory of Dynamic Simulation of Flight Environment." The work was administered by the Air Force Flight Dynamics Laboratory, Wright-Patterson Air Force Base, Ohio, Dr. James T. Van Kuren (PX), Project Engineer.

The work was accomplished during the period 1 June 1971 through 30 June 1972.

The report was submitted by the authors in July 1972.

A supplement containing an outline of the theoretical method for engineering use is available under the title "Rapid Engineering Calculation of Two-Dimensional Turbulent Skin Friction."

This technical report has been reviewed and is approved.



PHILIP P. ANTONATOS
Chief, Flight Mechanics Division
Air Force Flight Dynamics
Laboratory

TABLE OF CONTENTS

<u>Chapter</u>		<u>page</u>
	INTRODUCTION	1
1	HEAT TRANSFER ANALYSIS	4
	1.1 Introduction	4
	1.2 Development of the New Method	4
	1.3 Comparison with Heat Transfer Experiments	21
	1.3.1 Flat Plate Data	21
	1.3.2 Data of Moretti & Kays	24
	1.4 Conclusion	30
2	AXISYMMETRIC COMPRESSIBLE FLOW	32
	2.1 Introduction	32
	2.2 The Axisymmetric Law-of-the-Wall	33
	2.3 Derivation of the Basic Differential Equation	38
	2.4 Comparison with Experiment	45
	2.4.1 Compressible Flow along a Slender Cylinder	47
	2.4.2 Supersonic Attached Flow Past a Cone	53
	2.4.3 Supersonic Flow with Pressure Gradient	59
	2.5 Summary	62
3	THE PREDICTION OF THREE-DIMENSIONAL SKIN FRICTION	63
	3.1 Introduction	63
	3.2 Specification of Velocity Correlations	69
	3.3 The Method of Solution	75

Preceding page blank

TABLE OF CONTENTS (Continued)

<u>Chapter</u>		<u>Page</u>
3	3.4 Comparison with Experiment	80
	3.4.1 The Rotating Disc Problem	80
	3.4.2 Johnston's Swept, Forward-Facing Step	92
	3.4.3 Data of Francis and Pierce	97
	3.4.4 Data of Klinksiek and Pierce	104
	3.5 Summary	107
Appendix A	INTEGRAL COEFFICIENTS	109
	REFERENCES	118

LIST OF ILLUSTRATIONS

<u>Figure</u>		<u>Page</u>
1.1	Illustration of the Effect of Various Parameters on the Velocity Law-of-the-Wall for Compressible Turbulent Flow	11
1.2	Illustration of the Effect of Various Parameters on the Temperature Law-of-the-Wall for Compressible Turbulent Flow	12
1.3	Comparison of the Present Near-Wall Theory with the Actual Law-of-the-Wake	20
1.4	Comparison of Theory with Zero Pressure Gradient Data of Moretti and Kays (1965)	26
1.5	Comparison of Theory with Mild Favorable Pressure Gradient Data of Moretti and Kays (1965)	27
1.6	Comparison of Theory with Severe Favorable Pressure Gradient Data of Moretti and Kays (1965)	28
1.7	Comparison of Theory with Adverse Pressure Gradient Data of Moretti and Kays (1965)	29
2.1	Definition Sketch Illustrating Coordinates for Axisymmetric Boundary Layer Flow	34
2.2	Some Examples of the Axisymmetric Law-of-the-Wall, Computed From Equations (2-10) and (2-12)	39
2.3	The Compressibility and Wall Temperature Parameter A, from Equation (2-32)	46
2.4	Skin Friction on an Adiabatic Cylinder at a Freestream Mach Number of 5 for Various Values of $R_a = U r_o / \nu_e$, Computed from Eqn. (2-34).	50
2.5	Skin Friction Determination for Supersonic Flow along a Slender Cylinder by a Modified Axisymmetric Clauser-Plot, Eqn. (2-40)	52

LIST OF ILLUSTRATIONS (Continued)

<u>Figure</u>		<u>Page</u>
2.6	Illustration of the Turbulent Cone Rule	56
2.7	Comparison of Theory and Experiment for Supersonic Flow past a Body of Revolution, After Allen (1970)	61
3.1	Three-Dimensional Boundary Layer Coordinate System with Skewing in One Direction Only	65
3.2	Three-Dimensional Boundary Layer with Bilateral Skewing	68
3.3	Sketch of the Triangular Hodograph Approximation, after Johnston (1957)	73
3.4	Verification of the Streamwise Law-of-the-Wall for Turbulent Flow on a Rotating Disc	83
3.5	Verification of Mager's Hodograph for Rotating Disc Flow	84
3.6	Comparison of Theory and Experiment for Streamwise Skin Friction on a Rotating Disc	87
3.7	Comparison of Theory and Experiment for the Wall Streamline Tangent on a Rotating Disc	88
3.8	Comparison of Rotating Disc Crossflow Velocity Profiles with the Hodograph of Von Karman (1946)	91
3.9	Comparison of Present Theory for Three Pressure Distribution Assumptions with the Streamwise Skin Friction Data of Johnston (1970) for Flow near a 45° Swept Step	95
3.10	Comparison of Present Theory for Three Pressure Distribution Assumptions with the Wall Streamline Tangent Data of Johnston (1970) for Flow Near a Swept Step	95

LIST OF ILLUSTRATIONS (Continued)

<u>Figure</u>		<u>Page</u>
3.11	Comparison of Present Theory With the Curved Duct Experiment of Francis and Pierce (1967), Series 5	99
3.12	Comparison of Theory With Wall Streamline Tangent Data of Francis and Pierce (1967), Series 5	100
3.13	Comparison of Present Theory With Experimental Skin Friction as Estimated in a Curved Duct by Francis and Pierce (1967), Series 2	101
3.14	Comparison of Theory With Wall Streamline Tangent Data of Francis and Pierce (1967), Series 2	102
3.15	Comparison of Present Theory With Estimated Skin Friction in the Curved Duct Experiment of Klinksiek and Pierce (1970)	105
3.16	Comparison of Present Theory With Wall Streamline Tangent Data of Klinksiek and Pierce (1971)	106

LIST OF TABLES

<u>Table</u>		<u>Page</u>
1-1	Comparison of Six Theories with Flat Plate Friction Data	23
2-1	Comparison of Theory with the Data of Richmond (1957) for Supersonic Flow Along a Slender Cylinder at $M_e = 5.8$	58

LIST OF SYMBOLS

English

A	van Driest factor defined by Eqn. (2-32)
A_i	Integral coefficients defined by Eqns. (2-26,27,28)
c_D	Drag coefficient
c_f	Local skin friction coefficient, $c_f = 2\tau_w/\rho_e U_e^2$
c_h	Local Stanton number, $c_h = q_w/\rho_e c_p U_e (T_{aw} - T_w)$
c_p	Specific heat at constant pressure
C_p	Pressure coefficient
D_i	Integral coefficients defined by Eqns. (3-53) to (3-58)
F_c, F_{Rx}	Transformation functions defined by Eqn. (1-38)
G_i	Integral coefficients defined by Eqns. (3-38,39)
h_o	Stagnation enthalpy, $h_o = h + u^2/2$
h_{1s}	Direction along an external streamline
h_{2n}	Direction normal to an external streamline
H_i	Integral coefficients defined by Eqns. (1-29,30)
k	Specific heat ratio, $k = c_p/c_v$
k_w	Fluid thermal conductivity at the wall
L	Reference length
M	Mach number
P	Pressure
P_T	Turbulent Prandtl number, ≈ 0.9
q	Heat flux
r_o	Body radius
r_o^+	Dimensionless body radius, $r_o^+ = r_o u^*/\nu_w$

LIST OF SYMBOLS (Continued)

r	Defined in Figure 2.1
\hat{r}	Recovery factor, $\hat{r} \doteq 0.89$
R	Perfect gas constant
R_a	Radius Reynolds number, $R_a = U_e r_o / \nu_e$
R_x	Local Reynolds number, $R_x = U_e x / \nu_e$
R_L	Effective Reynolds number defined by Eqn. (1-31)
t	Dimensionless wall temperature, $t = T_w / T_{w0}$
T	Absolute temperature
T_{w0}	Reference wall temperature
T^+	Temperature ratio, $T^+ = T / T_w$
u, v, w	Velocities in the x, y, z directions respectively
u^*	Friction velocity, $u^* = (\tau_{ws} / \rho_w)^{1/2}$
u^+	Dimensionless velocity, $u^+ = u / u^*$
U_e	Freestream velocity
U_o	Reference velocity
v^*	Friction velocity, $v^* = (\tau_{wn} / \rho_w)^{1/2}$
V	Dimensionless freestream velocity, $V = U_e / U_o$
w^+	Dimensionless velocity, $w^+ = w / u^*$
x, y	Coordinates parallel and normal to the wall
x^*	Dimensionless coordinate, $x^* = x / L$
y^+	Dimensionless coordinate, $y^+ = y u^* / \nu_w$
Y	Coordinate, $Y = r_o \ln(r / r_o)$
Y^+	Dimensionless coordinate, $Y^+ = Y u^* / \nu_w$

LIST OF SYMBOLS (Continued)

Greek

α	Dimensionless pressure gradient parameter, Eqn. (1-12)
β	Dimensionless heat transfer parameter, Eqn. (1-16)
γ	Dimensionless compressibility parameter, Eqn. (1-16)
δ	Boundary layer thickness
δ^+	Dimensionless boundary layer thickness, $\delta^+ = \delta u^* / \nu_w$
ϵ	Eddy viscosity
θ	Tangent of the angle between the total surface shear stress vector and the freestream direction
κ	von Karman's constant, $\kappa \doteq 0.4$
λ_1	Dimensionless skin friction variables, $\lambda_1 = (\epsilon / c_f)^{1/2}$
λ_2	Dimensionless heat transfer variable, $\lambda_2 = \frac{q_w}{\rho_w U_e^3} \left(\frac{T_e}{T_w} \right)$
μ	Absolute viscosity
ν	Kinematic viscosity
ρ	Density
τ	Shear stress
ψ	Stream function
ω	Viscosity power-law exponent, $\omega \doteq 0.67$
Ω	Angular velocity of rotating disc

Subscripts

aw	Adiabatic wall
e	Freestream
n	Normal
o	Initial value
s	Streamwise
w	Wall

earlier report, White and Christoph (1970), which considered skin friction only and eliminated the temperature through a Crocco approximation. The new theory results in two first-order coupled differential equations for skin friction coefficient and Stanton number. The theory is compared with variable wall temperature and pressure gradient experiments, and an approximate correlation is found which relates the Reynolds analogy factor (c_h/c_f) to the local pressure gradient.

The second chapter develops an analysis for compressible axisymmetric flow with pressure gradients. The boundary layer is assumed to be thick, so that transverse curvature is important, and temperature is eliminated through the Crocco approximation. The result is a single first-order differential equation for the skin friction coefficient. Comparison is made with experiments for supersonic flow along thin cylinders and bodies of revolution. The transverse curvature effect can be quite large, causing skin friction increases of 100% or more in both subsonic and supersonic flows. Some earlier work on this type of analysis was given in a paper by White (1972).

The third and final chapter is concerned with three-dimensional incompressible turbulent skin friction. The distinguishing characteristic of a three-dimensional boundary layer is a crossflow normal to the freestream direction, resulting in a vector wall shear stress which has both streamwise and crossflow components. Since both shear

components vary with both surface coordinates, partial differential equations are inevitable. The present analysis uses both a streamwise and a crossflow law-of-the-wall to derive two first order coupled partial differential equations for the two surface shear components. As with previous work, there are no shape factors or integral thickness present. Also, the partial differential equations are of such simple form that they lend easily to a very simple finite difference technique. The equations are applied to several experimental flows, and the agreement is very promising, particularly considering the relative inaccuracy of present three-dimensional flow measurements.

Heat Transfer Analysis

1.1 Introduction

The purpose of this chapter is to develop a method for calculating heat transfer coefficients for arbitrarily high Mach numbers, variable wall temperatures, and variable streamwise pressure gradients. The present analysis is restricted to steady, two-dimensional flow of a perfect gas in a compressible turbulent boundary layer. The lateral pressure gradient will be neglected since, although the lateral gradient strongly influences the momentum thickness in high Mach number flows, it appears to have negligible effect on the approach proposed here. Two coupled, first order, ordinary differential equations are derived which have for dependent variables only the skin friction coefficient and the Stanton number. Stanton numbers are calculated and compared to the data of Moretti and Kays (1965). A relationship among skin friction, heat transfer, and pressure gradient is presented.

1.2 Development of the New Method

The equations governing compressible, two-dimensional turbulent boundary layer mean flow analyses were apparently first given by Young (1953) in the following form:

a) The continuity equation:

$$\frac{\partial}{\partial x}(\rho u) + \frac{\partial}{\partial y}(\rho v) = 0 \quad (1-1)$$

b) The momentum equation:

$$\rho u \frac{\partial u}{\partial x} + \rho v \frac{\partial u}{\partial y} = - \frac{dp}{dx} + \frac{\partial \tau}{\partial y} \quad (1-2)$$

c) The energy equation:

$$\rho u \frac{\partial h_o}{\partial x} + \rho v \frac{\partial h_o}{\partial y} = \frac{\partial}{\partial y}(q + u\tau) \quad (1-3)$$

d) The perfect gas law:

$$p = \rho RT, \text{ or: } T/T_w = \rho_w/\rho \quad (1-4)$$

Here $h_o = c_p T + u^2/2$ is the stagnation enthalpy, and the symbols q and τ represent the heat flux and shear stress, respectively. That is,

$$q = k \frac{\partial T}{\partial y} - \rho \overline{h'v'}; \quad \tau = \mu \frac{\partial u}{\partial y} - \rho \overline{u'v'} \quad (1-5)$$

There are six unknowns (ρ, u, v, h_o, q, τ) and only four equations, so that further relations are needed. The finite difference methods model the eddy viscosity and eddy conductivity, thus correlating the variables q and τ with

local conditions, and then attack the complete governing equations. The so-called von Kármán integral methods eliminate ρv from equations (1-2) and (1-3) by equation (1-1) and then integrate with respect to y across the entire boundary layer, thus obtaining the von Kármán integral relations. Additional relations for these integral methods are then brought in as correlations between integral parameters.

The compressible flow analysis of White and Christoph (1970, 1972) was based on Crocco's approximation for the energy equation - cf. Schlichting (1968):

$$\text{Prandtl number} = \text{unity}; \quad T = a + bu + cu^2, \quad (1-6)$$

where a, b, c are determined from boundary conditions.

Basically, the analysis of White and Christoph (1970, 1972) non-dimensionalizes the velocity u with respect to wall quantities and then integrates equations (1-1) and (1-2) with respect to the law-of-the-wall variable $y^+ = yu^*/\nu_w$, where $u^* = (\tau_w/\rho_w)^{1/2}$ is the friction velocity. With Crocco's approximation one can compute local heat transfer only through a Reynolds analogy. Crocco's approximation will not be made here. Instead, the energy equation, as given by equation (1-3), will be used. The velocity u and the temperature T are non-dimensionalized as follows:

$$u^+ = u(x,y)/u^*(x) \quad \text{and} \quad T^+ = T(x,y)/T_w(x) . \quad (1-7)$$

Quantitative expressions for u^+ and T^+ are needed. The simple incompressible formula

$$u^+ = 2.5 \ln(y^+) + 5.5 \quad (1-8)$$

and a similar expression for T^+ are not adequate, because we need to include compressibility, heat transfer, and pressure gradient effects in the velocity and temperature correlations. An analytical approach of finding expressions for u^+ and T^+ was desired, so that as little empiricism as possible would be introduced into the present method. The scheme adopted was based on the eddy viscosity approach of Deissler (1959), which assumed that the Prandtl mixing length approximation could be extended to the variable density case with no further changes. Let us first derive an expression for u^+ . The total shear stress is related to an eddy viscosity and mixing length as follows:

$$\tau = (\mu + \epsilon) \frac{\partial u}{\partial y} , \quad (1-9)$$

$$\text{where} \quad \epsilon = \rho \kappa^2 y^2 \left| \frac{\partial u}{\partial y} \right|$$

and $\kappa = 0.4$ is von Kármán's constant. Also, near the wall,

the boundary layer is approximately a Couette flow with negligible acceleration, so that equation (1-2) becomes

$$\tau \doteq \tau_w + \frac{dp}{dx} y \quad (1-10)$$

Non-dimensionalizing equations (1-9) and (1-10) with respect to wall variables, we neglect the laminar portion of the total shear in equation (1-9) (This step greatly simplifies the final form of u^+ but has a negligible effect on the numerical values of u^+). Equating equations (1-9) and (1-10) results in

$$\frac{\partial u^+}{\partial y^+} = \frac{(T^+(1 + \alpha y^+))^{1/2}}{\kappa y^+} \quad (1-11)$$

where

$$\alpha = \frac{v_w}{\tau_w u^*} \frac{dp}{dx} \quad (1-12)$$

This is the same parameter α , termed the "pressure gradient" parameter, which appeared in White's (1969) analysis, and which was suggested by the work of Mellor (1966). It is an ideal parameter for this method because it is directly related to the shear stress without any

integral thicknesses. We now need an expression for T^+ . Following the same approach, the total heat flux is related to an eddy conductivity as follows:

$$q = \frac{c_p}{Pr_T} (\mu + \epsilon) \frac{\partial T}{\partial y} \quad (1-13)$$

where Pr_T is the turbulent Prandtl number. Near the wall, one obtains from equation (1-3)

$$q_w = u\tau + q \quad (1-14)$$

Again, non-dimensionalizing equations (1-13) and (1-14), neglecting the laminar portion of the total heat flux in equation (1-13), and equating equations (1-13) and (1-14) results in

$$\frac{\partial T^+}{\partial y^+} = \frac{(\beta - 2\gamma u^+(1 + \alpha y^+))T^{+1/2}}{\kappa y^+ (1 + \alpha y^+)^{1/2}} \quad (1-15)$$

where

$$\beta = \frac{Pr_T q_w}{\rho_w u_w^* c_p T_w} \quad \text{and} \quad \gamma = \frac{Pr_T u_w^{*2}}{2c_p T_w} \quad (1-16)$$

The parameters β and γ will be referred to as the "heat

transfer" parameter and the "compressibility" parameter, respectively. The effects of the parameters α , β , and γ on u^+ are shown in Figure (1-1). Positive α (adverse pressure gradient) and positive β (cold wall heat transfer) raise u^+ above the incompressible logarithmic law, and negative α (favorable pressure gradient) and negative β (hot wall heat transfer) have the opposite effect. The parameter γ , which is always positive, lowers u^+ below the incompressible result. If more than one of these parameters are nonzero, the effect is roughly an additive one. Precisely these effects have been found experimentally, e.g., Kepler and O'Brien (1959), Lee et al (1969), and Brott et al (1969). The "heat transfer" and "compressibility" parameters have the same qualitative effect on T^+ as they do on u^+ . The "pressure gradient" parameter alone does not affect T^+ . However, a positive α combined with either a positive β or a negative β depresses the β effect on T^+ . A negative α has the opposite effect. The compressibility effect is increased with a positive α and decreased with a negative β . These results are shown in Figure (1-2).

Equations (1-11) and (1-15) give, for zero pressure gradient,

$$\frac{\partial T^+}{\partial u^+} = \frac{\partial T^+}{\partial y^+} \frac{\partial y^+}{\partial u^+} = \beta - 2 \gamma u^+ \quad (1-17)$$

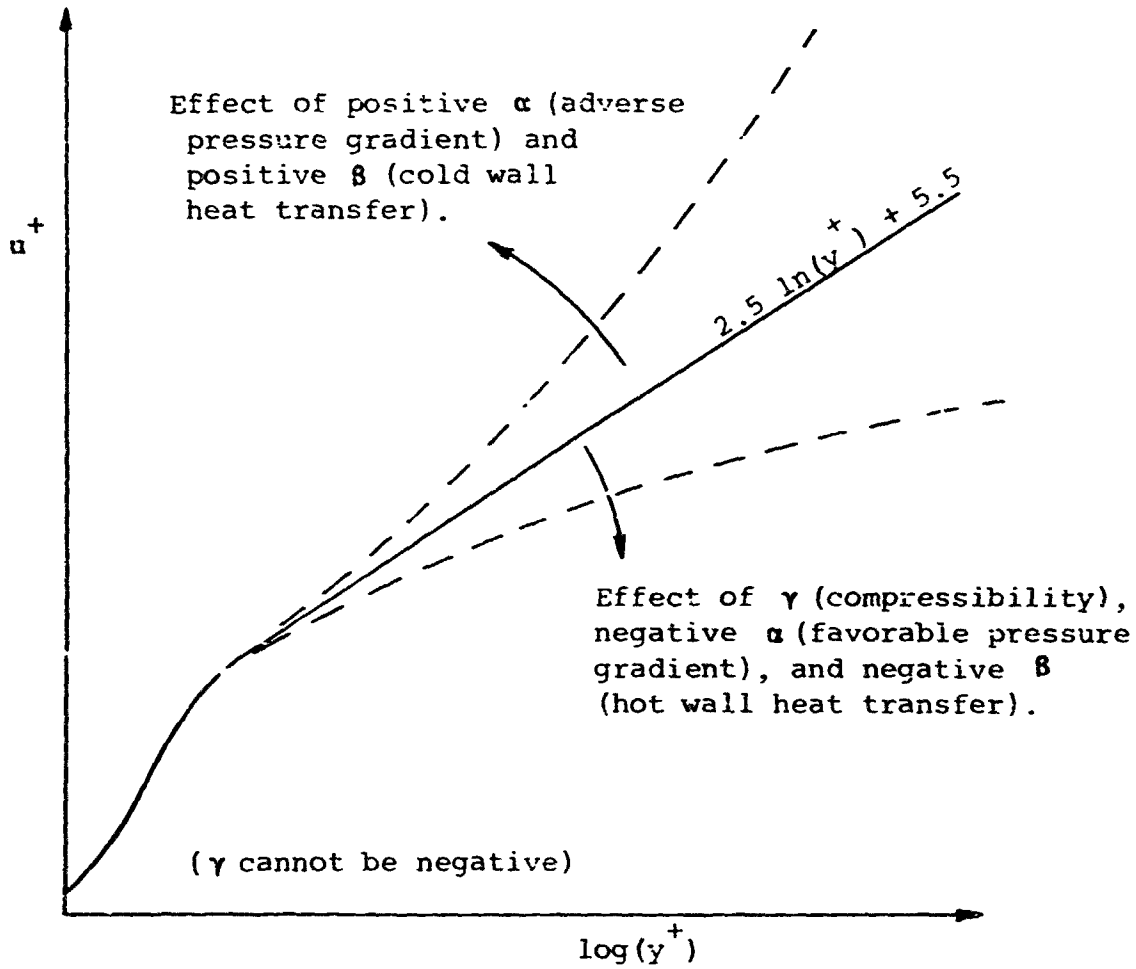


Figure 1.1. ILLUSTRATION OF THE EFFECT OF VARIOUS PARAMETERS ON THE VELOCITY LAW-OF-THE-WALL FOR COMPRESSIBLE TURBULENT FLOW.

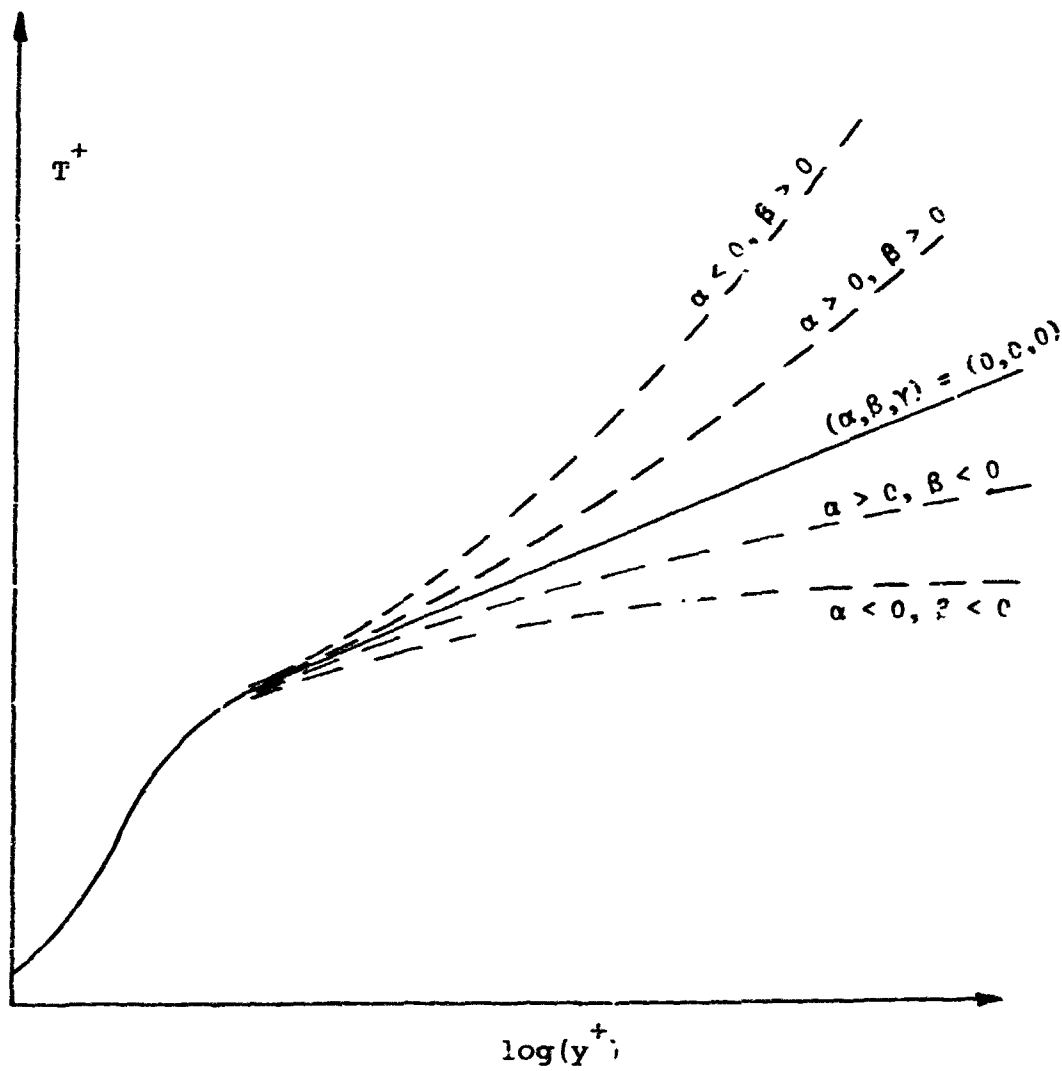


Figure 1.2. ILLUSTRATION OF THE EFFECT OF VARIOUS PARAMETERS ON THE TEMPERATURE LAW-OF-THE-WALL FOR COMPRESSIBLE TURBULENT FLOW.

Integrating equation (1-17) gives

$$T^+ = 1 + \beta u^+ - \gamma u^{+2}, \quad (1-18)$$

which is the form of Crocco's relation used by White and Christoph (1970, 1972). If α does not equal zero, one then obtains

$$\frac{\partial T^+}{\partial u^+} = \frac{\beta - 2\gamma u^+(1 + \alpha y^+)}{1 + \alpha y^+}, \quad (1-19)$$

which is not a Crocco relation.

Let us continue the method of solution, by first defining a compressible stream function ψ as follows

$$\frac{\partial \psi}{\partial y} = \rho u; \quad \frac{\partial \psi}{\partial x} = -\rho v \quad (1-20)$$

Eliminating ρv from equations (1-2) and (1-3) by equation (1-20), and non-dimensionalizing u and T as in equation (1-7) gives

$$\begin{aligned} \rho u^* u^+ \frac{\partial}{\partial x} (u^* u^+) - \frac{\partial \psi}{\partial x} \frac{u^*}{v_w} \frac{\partial}{\partial y^+} (u^* u^+) = \\ - \frac{dp}{dx} + \frac{u^*}{v_w} \frac{\partial \tau}{\partial y^+} \end{aligned} \quad (1-21)$$

and

$$\left(\rho u^{*+} \frac{\partial}{\partial x} - \frac{\partial \rho}{\partial x} \frac{u^*}{v_w} \frac{\partial}{\partial y^+} \right) \left(c_p T_w T^+ + \frac{u^{*2} u^{+2}}{2} \right) = \frac{u^*}{v_w} \frac{\partial}{\partial y^+} (u\tau + q) \quad (1-22)$$

The pressure gradient in equation (1-21) is related to the freestream conditions by the inviscid Bernoulli relation:

$$\frac{dp}{dx} = - \rho_e U_e \frac{dU_e}{dx} \quad (1-23)$$

The y^+ -derivatives in equations (1-21) and (1-22) are no problem because these equations are going to be integrated with respect to y^+ , but the x -derivatives must be calculated. The functional relationships of u^+ , T^+ , and μ_w (μ has dimensions of viscosity) are

$$u^+, T^+, \mu_w = \text{fcn}(y^+, \alpha, \beta, \gamma) \quad (1-24)$$

The x -derivatives are calculated by using the chain rule:

$$\frac{\partial}{\partial x} = \frac{\partial y^+}{\partial x} \frac{\partial}{\partial y^+} + \frac{\partial \alpha}{\partial x} \frac{\partial}{\partial \alpha} + \frac{\partial \beta}{\partial x} \frac{\partial}{\partial \beta} + \frac{\partial \gamma}{\partial x} \frac{\partial}{\partial \gamma} \quad (1-25)$$

For skin friction and heat transfer calculations, it is convenient to define further non-dimensionalizations:

$$x^* = x/L \quad ; \quad \bar{v} = U_e/U_0 \quad ; \quad \lambda_1 = (\epsilon/c_f)^{1/2} \quad (1-26)$$

$$t = T_w/T_{w0} \quad ; \quad \lambda_2 = q_w T_e / (\rho_w U_e^3 T_w) \quad ,$$

where L , U_0 , and T_{w0} are constant reference values. Now use equations (1-26) in the definitions for y^+ , α , β , and v and carry out the partial derivatives in equation (1-25). In so doing, derivatives of v_w , ρ_w , and T_e will arise. Eliminate such derivatives in favor of (dT_w/dx^*) and (dv/dx^*) through equation (1-4) and a viscosity power-law assumption $\mu \propto T^r$, where r is taken here as 0.67 for air. Also use the relation between velocity, pressure, and temperature in the freestream:

$$k M_e^2 \frac{dv}{v} = - \frac{dp}{p} = \frac{-k}{k-1} \frac{dT_e}{T_e} \quad , \quad (k = c_p/c_v) \quad (1-27)$$

The net result is that equation (1-25) can now be written as:

$$\begin{aligned} \frac{\partial}{\partial x^*} = & \frac{1}{\lambda_1} \frac{d\lambda_1}{dx^*} \left[-y^+ \frac{\partial}{\partial y^+} + 3\alpha \frac{\partial}{\partial \alpha} + \beta \frac{\partial}{\partial \beta} - 2v \frac{\partial}{\partial v} \right. \\ & + \frac{v^{\Gamma}}{v} y^+ \frac{\partial}{\partial y^+} + 2\beta \frac{\partial}{\partial \beta} + 2v \frac{\partial}{\partial v} \left. \right] \lambda_1^3 \left(\frac{1/V}{R_L} \right)^n \frac{\partial}{\partial \alpha} \\ & + \frac{t^{\Gamma}}{t} \left[-y^+ \left(n + 1/2 \right) \frac{\partial}{\partial y^+} + \alpha \left(n + 1/2 \right) \frac{\partial}{\partial \alpha} - \frac{\beta}{2} \frac{\partial}{\partial \beta} \right] \\ & + \frac{1}{\lambda_2} \frac{d\lambda_2}{dx^*} \left[\beta \frac{\partial}{\partial \beta} + \frac{(k+1)}{\epsilon} M_e^2 \frac{v^{\Gamma}}{v} \alpha \frac{\partial}{\partial \alpha} - y^+ \frac{\partial}{\partial y^+} - \beta \frac{\partial}{\partial \beta} - v \frac{\partial}{\partial v} \right] \end{aligned} \quad (1-28)$$

where the primes denote differentiation with respect to x^* .

Equation (1-28) is now substituted into equations (1-21)

and (1-22) and the resulting equations integrated from

$y^+ = 0$ ($\tau = -w$) to $y^+ = \delta^+$ ($\tau = 0$). The result is

$$\begin{aligned} \frac{d\lambda_1}{dx^*} (H_1 - 3\alpha H_2) - \frac{\lambda_1^4 (1/V)'' H_2}{R_L} - \frac{\lambda_1}{\lambda_2} \frac{d\lambda_2}{dx^*} H_3 \\ + \lambda_1 \frac{V'}{V} \lambda_1^2 \delta^+ - H_1 - 3H_3 - \frac{(k+1)}{2} M_e^2 (\alpha H_2 - H_1 - H_3) \\ - \lambda_1 \frac{t'}{t} [\alpha(\tau+1) H_2 + H_4] = R_L V \end{aligned} \quad (1-29)$$

and

$$\begin{aligned} \frac{d\lambda_1}{dx^*} (H_5 - 3\alpha H_6) - \frac{\lambda_1^4 (1/V)'' H_6}{R_L} - \frac{\lambda_1}{\lambda_2} \frac{d\lambda_2}{dx^*} H_7 \\ - \lambda_1 \frac{V'}{V} H_5 + 3H_7 + \frac{(k+1)}{2} M_e^2 (\alpha H_6 - H_5 - H_7) \\ - \lambda_1 \frac{t'}{t} [\alpha(\tau+1/2) H_6 + H_8] = R_L (T_e/T_w)^{\tau+1} \lambda_2 \lambda_1^3 v \end{aligned} \quad (1-20)$$

where R_L is an effective Reynolds number defined as:

$$R_L = \frac{U_o L}{\nu_e} \left(\frac{\mu_e}{\mu_w} \right) \left(\frac{T_e}{T_w} \right)^{1/2} \quad (1-31)$$

The H_i coefficients are integrals involving u^+ , T^+ and the law-of-the-wall parameters; they are listed in Appendix A.

It is possible to numerically evaluate these H_i 's once expressions for the derivatives $\frac{\partial u^+}{\partial \alpha}$, $\frac{\partial u^+}{\partial \beta}$, $\frac{\partial u^+}{\partial \gamma}$, $\frac{\partial T^+}{\partial \alpha}$, $\frac{\partial T^+}{\partial \beta}$, $\frac{\partial T^+}{\partial \gamma}$,

$\frac{\partial \psi}{\partial \beta}$, and $\frac{\partial \psi}{\partial \gamma}$ are found. Expressions for these derivatives are obtained by differentiating, with respect to α , β , and γ , the previously derived integrals for u^+ , T^+ , and ψ , Eqns. (1-11, 15, 20) respectively, at a fixed y^+ . Integral expressions for these partial derivatives are given in Appendix A; the change of variables $du^+ = (\lambda u^+ / \lambda y^+) dy^+$ has been made. The coefficients H_i are then evaluated by integrating the relations in Appendix A from $u^+ = 0$ to $u^+ = u_e^+ = \lambda_1 (T_e / T_w)^{1/2}$ for various values of α , β , and γ . The turbulent Prandtl number P_T is taken as 0.9^* . The starting value of T^+ is 1.0, and the initial value of y^+ is taken to be $0.1108 = \exp(-5.5/2.5)$ to match with the incompressible logarithmic law (Eqn. 1-8) in the limit. Curve fit expressions for the coefficients H_i are also given in Appendix A.

The parameters α , β , and γ are related to the dependent variables λ_1 and λ_2 as follows:

$$\begin{aligned}
 \alpha &= \lambda_1^3 (1/V)' / R_L \\
 \gamma u_e^{+2} &= P_T \frac{(k-1)}{2} M_e^2 (T_e / T_w) \\
 \beta u_e^+ &= P_T \lambda_1^2 \lambda_2 M_e^2 (k-1) (T_e / T_w)
 \end{aligned}
 \tag{1-32}$$

^{*} $P_T \doteq 0.9$ was found experimentally by Simpson, Whitter and Moffat (1970). It is also the value assumed in most finite-difference calculations, e.g. Cebeci (1971).

Equations (1-29) and (1-30) are, then, two coupled, first order, nonlinear, ordinary differential equations in λ_1 and λ_2 only. The freestream Mach number and wall temperature distributions must be known, plus the values of λ_1 and λ_2 at some initial x^* . Unfortunately, δ^+ appears in equation (1-29) and must be calculated. However, δ^+ need not be known precisely for accurate calculations of λ_1 and λ_2 . An approximate way of calculating δ^+ , and the one recommended, is to first assume a Crocco law of the form in equation (1-18). With this expression for T^+ , equation (1-11) may be integrated analytically as

$$\sin^{-1} \left(\frac{2\gamma u^+ - \beta}{Q} \right) = \sin^{-1} \left(\frac{2\gamma u_0^+ - \beta}{Q} \right) + \frac{\sqrt{\gamma}}{\kappa} \left[2(P - P_0) + \ln \left(\frac{P-1}{P+1} \frac{P_0+1}{P_0-1} \right) \right], \quad (1-33)$$

where $Q = (\beta^2 + 4\gamma)^{1/2}$ and $P = (1 + \alpha y^+)^{1/2}$.

Equation (1-33) needs to be initialized. By plotting u^+ versus y^+ , as in Figure 1-1, it is seen that the curves for various values of α , β and γ converge at y^+ slightly less than ten. The initial conditions $u_0^+ = 0$ and $y_0^+ = 0.1108$ were taken. Unfortunately, y^+ is an implicit function of u^+ so that an iteration scheme must be used.

The dependent variable λ_2 is directly related to the Stanton number

$$c_h = \frac{\lambda_2 (k-1) M_e^2 (\bar{T}_e / \bar{T}_w)}{(\bar{T}_{aw} / \bar{T}_w - 1)} \quad (1-34)$$

where the Stanton number has been defined as

$$c_h = \frac{q_w}{\rho_e c_p U_e (T_{aw} - T_w)} \quad (1-35)$$

Since λ_1 is defined as $(2/c_f)^{1/2}$, equations (1-29) and (1-30) give c_f and c_h directly - no auxiliary information is needed about the behavior of integral thickness or shape factors. Another important and unique property of equations (1-29) and (1-30) is an explicit flow separation criterion. As separation is approached, $d\lambda_1/dx^*$ approaches infinity and hence c_f approaches zero - which is precisely the definition of two-dimensional separation. One need not worry about attempting to predict separation according to a particular value of the shape factor.

One basic assumption is made in the development of the present method; that is, that the velocity and the temperature profiles, correlated by inner variables only, are valid all the way to the edge of the boundary layer. This assumption leads to a slight miscalculation in δ^+ , as seen by Figure 1-3. The outer wake is not predicted accurately. But, as was pointed out earlier, it is not terribly important to know δ^+ precisely in order to obtain accurate skin friction and heat transfer coefficients. Also, in a supersonic turbulent boundary layer, the wake almost disappears. Of course, there will be some error in the momentum and the displacement thicknesses, if one wishes to calculate them. In passing, it should be noted that, from

1
2
3
4
5
6
7
8
9
10
11
12
13
14
15
16
17
18
19
20

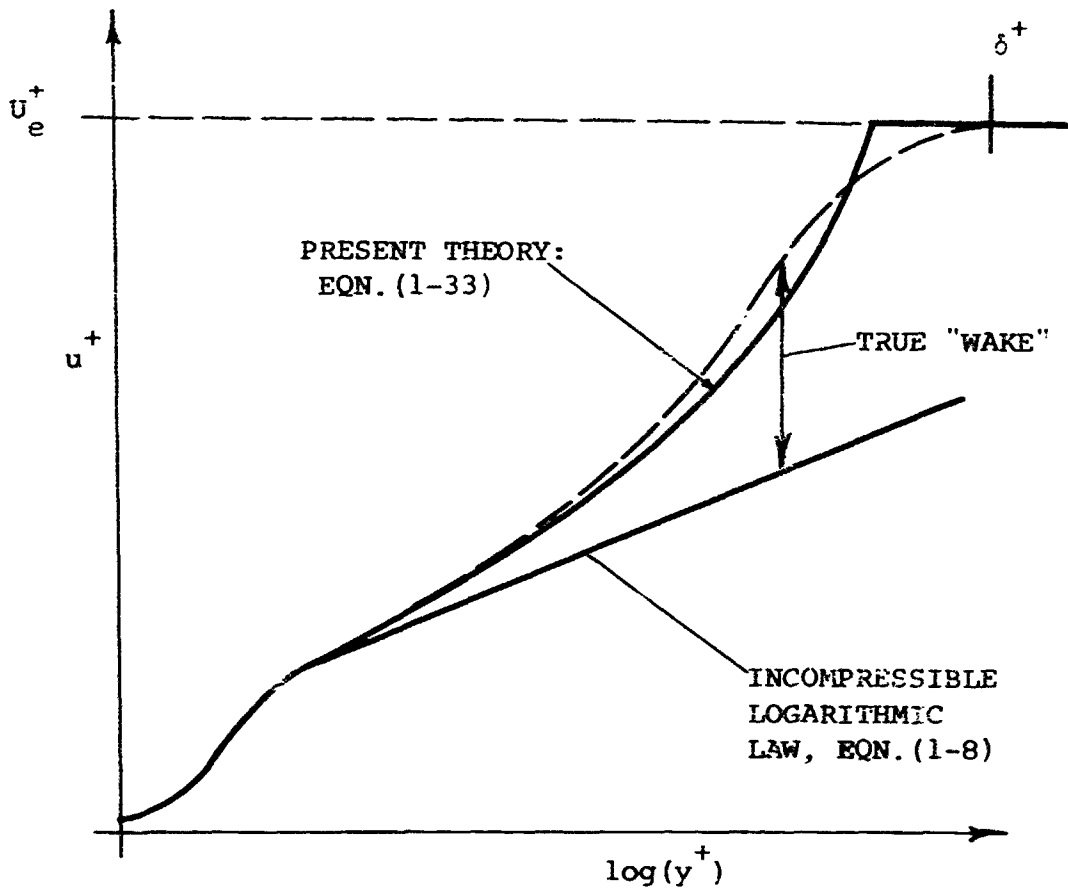


Figure 1-3. COMPARISON OF THE PRESENT NEAR-WALL THEORY WITH THE ACTUAL LAW-OF-THE-WAKE.

equation (1-11), if λy^+ is greater than minus one, then $\frac{\lambda u^+}{\lambda y^+} | \frac{\lambda u^+}{\lambda y^+} | < 0$. Thus the velocity gradient is negative, or the velocity inside the boundary layer has become greater than the freestream velocity. To avoid this difficulty, it is suggested that one take $\delta_{\max}^+ = -1/\alpha$ in the case of a favorable pressure gradient. This is not believed to handicap the present method.

1.3 Comparison With Heat Transfer Experiments

1.3.1 Flat Plate Data

First, it seems appropriate to consider a special case, namely when $\frac{dT_w}{dx} = \frac{dq_w}{dx} = \frac{dp}{dx} = 0$. For this case, the present analysis reduces to the analysis given by White and Christoph (1970, 1972). Equation (1-29) reduces to:

$$\bar{h}_1 \frac{d\lambda_1}{dx^*} = \frac{R_x}{2}, \quad (1-36)$$

which integrates to:

$$c_f = \frac{0.455}{A^2 \ln^2 \frac{R_x}{0.06 (T_e/T_w)^{1/4} R_x/A}} \quad (1-37)$$

where A is the van Driest flat plate parameter, given by equation (2-32) and plotted in Figure 2-3.

This result is expressed in terms of a flat plate compressibility transformation for skin friction as follows (in the notation of Spalding and Chi (1964)):

$$c_f = \frac{1}{F_c} c_{f_{inc.}} (R_x F_{Rx}) \text{ where } F_c = A^2 \quad (1-38)$$

$$\text{and } F_{Rx} = (\tau_e / \tau_w)^{1+n} / A$$

The present theory and five other theories, the five most popular and accurate known, were compared to 427 adiabatic and 230 cold wall heat transfer data points. The five other theories were cast in the same form as equation (1-38), but of course F_c and F_{Rx} were different for each theory. All theories were computed with the incompressible skin friction formula of Spalding and Chi (1964), which apparently gives the best agreement with incompressible friction data. Both the root mean square error and the mean absolute error were computed. The results are shown in Table 1-1. For adiabatic wall, the methods of Spalding and Chi (1964), van Driest (1956b) and the present theory are equally accurate. For cold wall heat transfer, the present theory has the lowest percent error, with Moore (1962) second. The present method is thus the most accurate flat plate theory available at the present time, with the added advantage that it can be extended to more general freestream and wall conditions (White and Christoph 1971).

TABLE 1-1

COMPARISON OF SIX THEORIES WITH FLAT PLATE FRICTION DATA

	ADIABATIC: 427 POINTS		COLD WALL: 230 POINTS	
AUTHOR	RMS % ERROR	ABS % ERROR	RMS % ERROR	ABS % ERROR
Eckert (1955)	12.44	9.06	29.45	25.56
Moore (1962)	8.87	6.54	17.69	13.08
Sommer and Short (1955)	9.40	7.77	23.55	20.14
Spalding & Chi (1964)	7.59	5.46	21.13	16.94
Van Eriest #2 (1956b)	7.55	5.45	17.49	13.81
Present Theory, Eqn. (1-37)	7.80	5.26	14.31	11.28

Note: RMS Error = $\left(\frac{1}{N} \sum e_i^2\right)^{1/2}$;

MEAN ABS Error = $\frac{1}{N} \sum |e_i|$

Data Source: White and Christoph (1970).

1.3.2 Data of Moretti and Kays

Next, the present method was compared to the data of Moretti and Kays (1965). Their data were taken in a rectangular duct which followed a system of rectangular nozzles. This test section was designed to provide various desired distributions of stream velocity and surface temperature. The velocities and heat transfer rates for these experiments were low, so the boundary layers were essentially constant property layers. However, the important effects of wall temperature variation and freestream velocity variation were present. In fact, predicting heat transfer under varying freestream conditions, especially accelerating flows, has become of practical concern in such problems as cooling of gas turbine blades and rocket nozzles.

Figure 1-4 shows the Stanton number as a function of position along the rectangular duct for a constant freestream velocity and for a sharp decrease in the wall temperature. No data was given by Moretti and Kays (1965) over the first one-third of the flow field. Since the Stanton number must be known at the starting point of integration of equations (1-29) and (1-30), and since it was desired to predict the effect of the wall temperature decrease which occurred in the first one-third of the flow field, equations (1-29) and (1-30) were integrated forward and backward from the first data point. Skin friction coefficients were not given by Moretti and Kays, so the starting value of λ_1 was

chosen such that $c_h = 0.5 c_f$. The curve-fit wall temperature distribution was chosen to be of the form

$$\frac{T_w}{T_\infty} = a + b \cos \left[\pi(x^* - x_1^*)/c \right] \quad (1-39)$$

where (a,b,c) were fitted constants and x_1^* was the x^* position where the wall temperature change started. The present theory and the digital computer finite difference method of Herring and Mellor (1968) are compared to the data in Figure 1-4. Agreement by both methods is excellent.

The second Stanton number distribution measured by Moretti and Kays consisted of a wall temperature change plus an accelerating freestream velocity. Again, the wall temperature distribution was fitted by equation (1-39), but the freestream velocity distribution was fitted by a polynomial. The present method and the method of Herring and Mellor are compared with the data in Figure 1-5. Once again both methods accurately predict the data. A more severe test of the present method, and of the method of Herring and Mellor, is the steep favorable pressure gradient as given by Moretti and Kays' data in Figure 1-6. If one believes in a constant Reynolds analogy factor, one would expect an increase in the Stanton number or at most a constant or slightly decreasing Stanton number. As seen in Figure 1-6, the Stanton number decreases considerably. Both the present theory and the method of Herring and Mellor

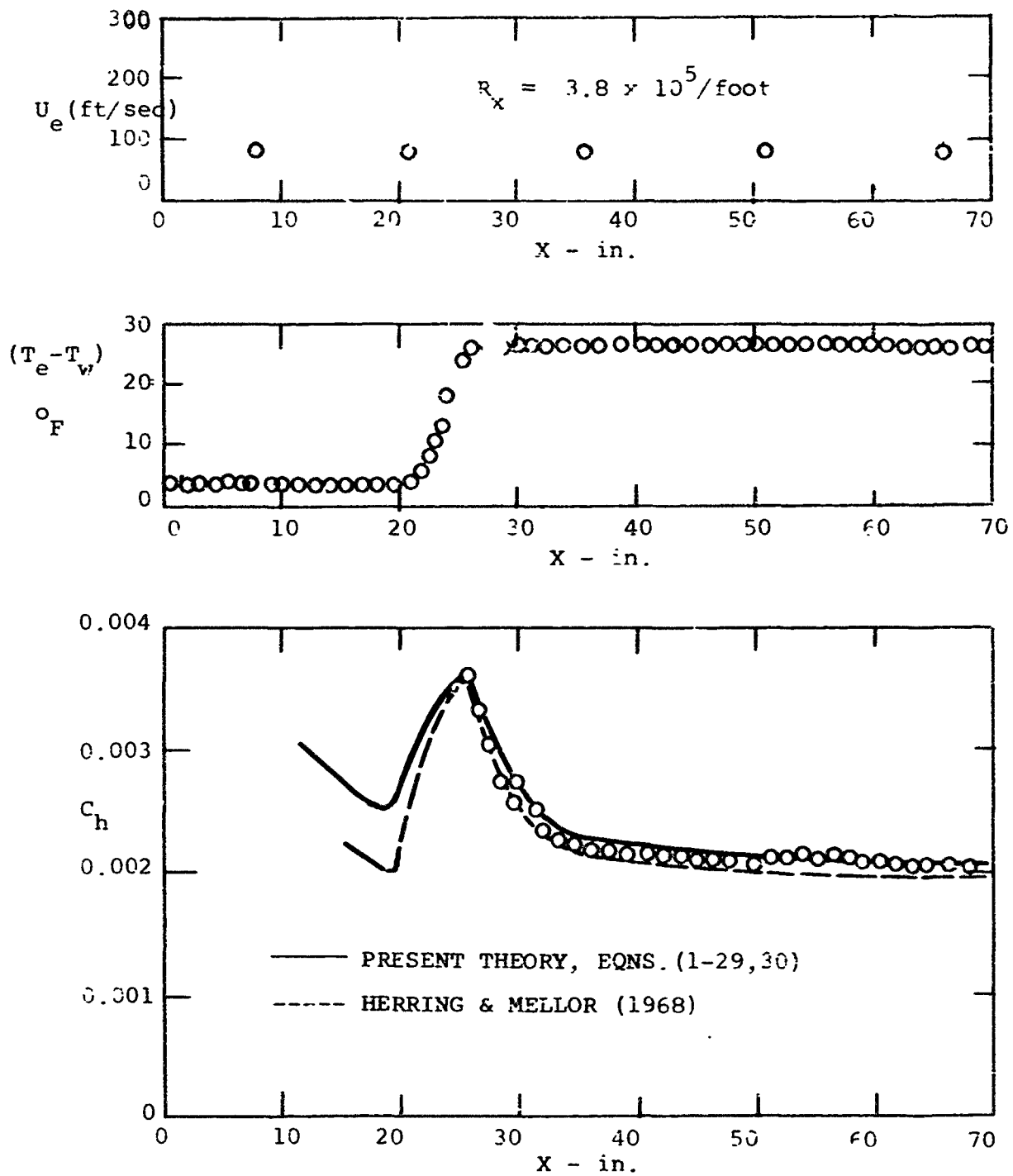


Figure 1.4. COMPARISON OF THEORY WITH ZERO PRESSURE GRADIENT DATA OF MORETTI AND KAYS (1965).

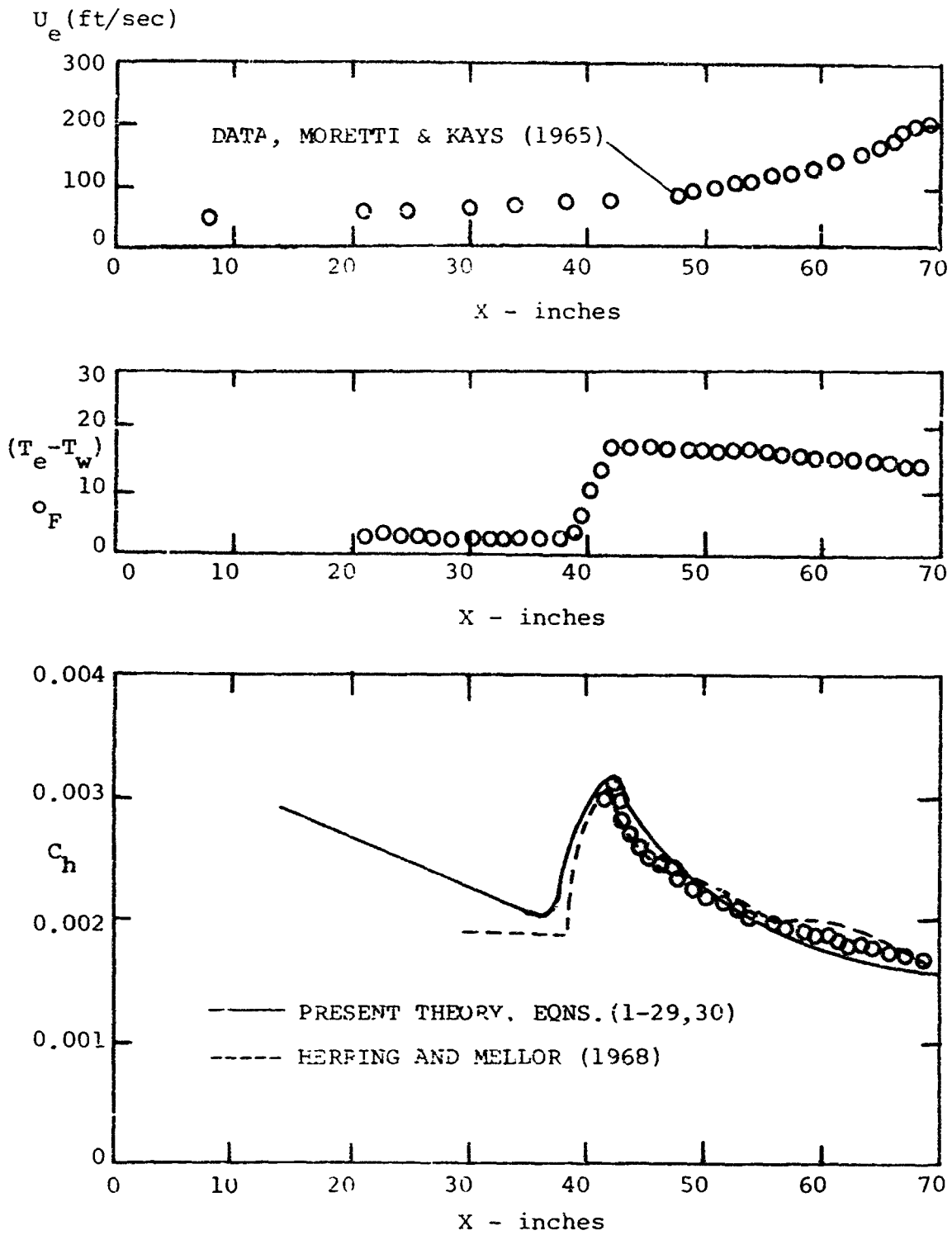


Figure 1.5. COMPARISON OF THEORY WITH MILD FAVORABLE PRESSURE GRADIENT DATA OF MORETTI & KAYS (1965).

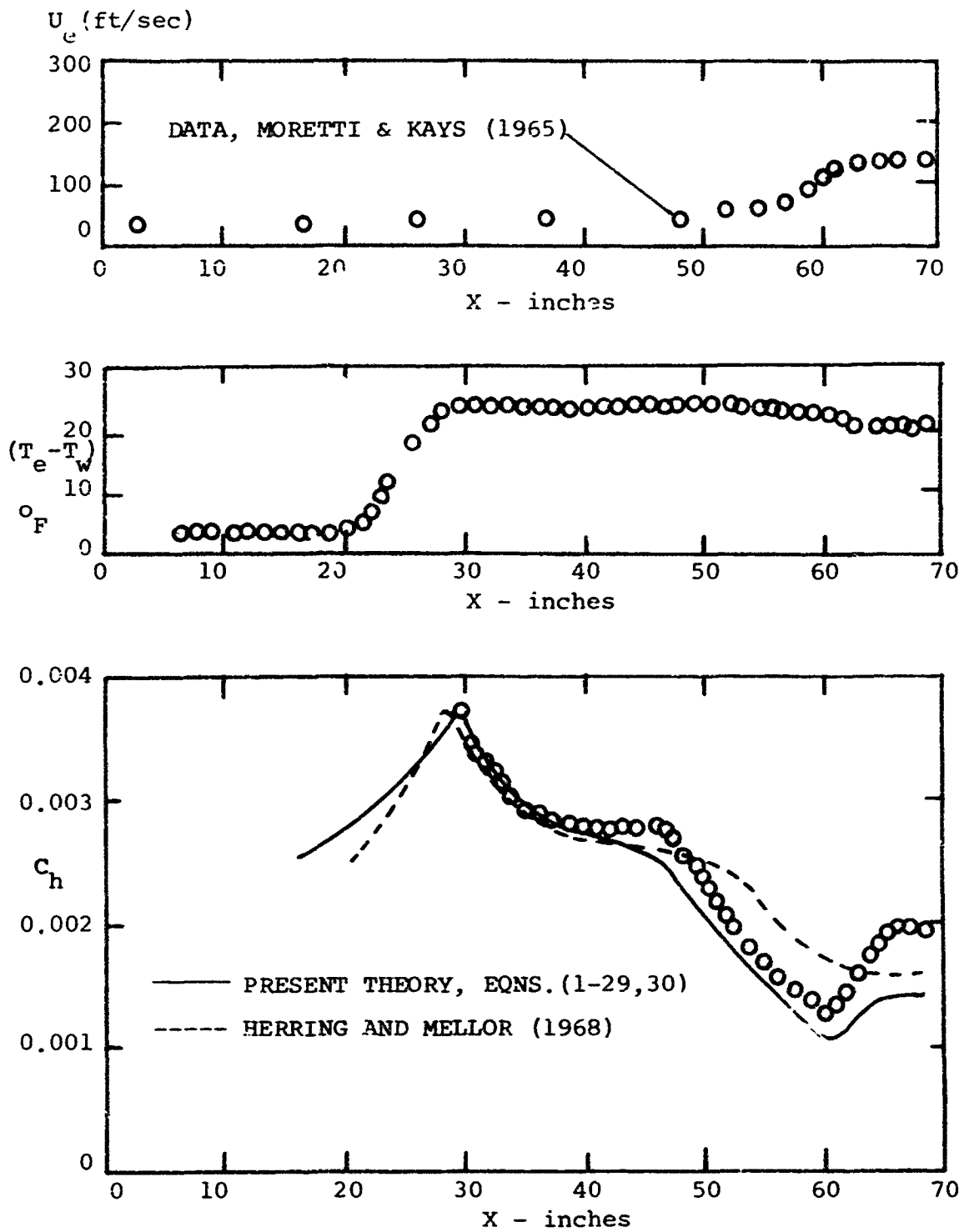


Figure 1.6. COMPARISON OF THEORY WITH SEVERE FAVORABLE PRESSURE GRADIENT DATA OF MORETTI & KAYS (1965).

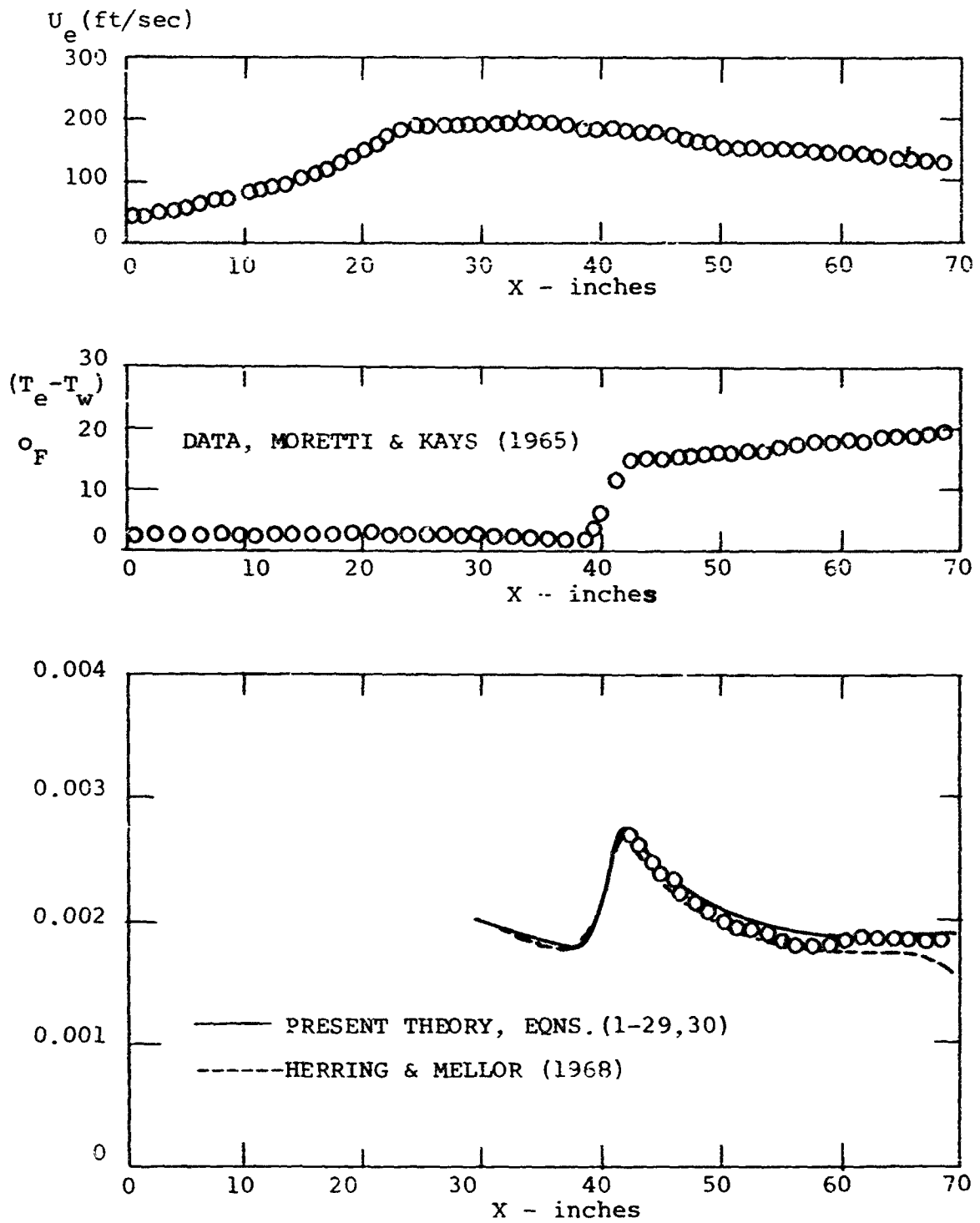


Figure 1.7. COMPARISON OF THEORY WITH ADVERSE PRESSURE GRADIENT DATA OF MORETTI & KAYS (1965).

qualitatively predict this decrease. However, neither the present method nor the method of Herring and Mellor are able to fully recover after the favorable pressure gradient has ended - the present method doing somewhat better than the method of Herring and Mellor.

The effect of an adverse pressure gradient on the Stanton number is shown in Figure 1-7. There is a noticeable difference between the present method and the method of Herring and Mellor toward the end of the flow region. The present method shows a slight increase in the Stanton number, whereas Herring and Mellor show a slight decrease. The data of Moretti and Kays remain approximately constant and are in reasonable agreement with either theory.

1.4 Conclusion

The purpose of this chapter was to develop a simple and accurate method for analyzing heat transfer and skin friction in two-dimensional, compressible turbulent boundary layers. This method uses law-of-the-wall velocity and temperature correlations which include pressure gradient, heat transfer, and compressibility effects. After integrating the continuity, momentum, and energy equations across the boundary layer, two coupled differential equations result which have as their dependent variables the skin friction coefficient and the Stanton number. Contrary to the von Karman technique, integral thicknesses and shape

factors are not used. The present heat transfer analysis, which is for arbitrary freestream velocity and wall temperature distributions, compares favorably with the data of Moretti and Kays (1965) and is as accurate as the sophisticated finite difference technique of Herring and Mellor (1968).

Chapter Two

Axisymmetric Compressible Flow

2.1 Introduction.

In this chapter, our basic approach is applied to derive a method for computing skin friction in a thick axisymmetric, compressible turbulent boundary layer. The analysis is restricted to steady flow and a perfect gas is assumed for convenience. The freestream Mach number and pressure gradient may be arbitrarily large and variable. Nonadiabatic wall temperature is allowable, but the variations should be "modest", that is, the streamwise derivative of wall temperature is neglected. The temperature is eliminated in favor of velocity through the Crocco approximation. It has already been shown that this simplification has little effect on the accuracy of skin friction computation (White and Christoph 1972).

The transverse curvature effect is introduced through a coordinate change suggested by Rao (1967). The resulting differential equation for skin friction (Eq. 2-25) is thus valid for arbitrarily large ratios of the boundary layer thickness to the body radius.

Rao's transformation was used by White (1972) to compute the skin friction in turbulent incompressible flow past a long cylinder of constant radius. The basic results of that paper can be summarized as two formulas for turbu-

lent incompressible skin friction on very long cylinders:

$$C_f \doteq 0.0015 + \left[0.20 + 0.016 \left(x/r_0 \right)^{0.4} \right] R_x^{-1/3}$$

$$C_D \doteq 0.0015 + \left[0.30 + 0.015 \left(L/r_0 \right)^{0.4} \right] R_L^{-1/3} \quad (2-1)$$

Here r_0 is the cylinder radius, x is the axial distance from the leading edge, and $R_x = U_0 x / \nu$ is the local Reynolds number for an assumed constant freestream velocity U_0 . The quantity C_D is the total friction drag coefficient on a cylinder of length L . Equations (2-1) are accurate to $\pm 5\%$ over the entire turbulent flow range ($10^6 < R_x < 10^9$) and for cylinder lengths up to $(L/r_0) = 10^6$. Similar results will be obtained here for compressible flow along a cylinder.

2.2 The Axisymmetric Law-of-the-Wall

In order to use the present method, it is necessary to have a realistic expression for the law-of-the-wall in a thick axisymmetric boundary layer. This law differs considerably from the two-dimensional law because of the effect of the radial variable in the momentum equation. With reference to Figure 2-1, let the body radius be $r_0(x)$. Within the sublayer, both the convective acceleration and the pressure gradient terms in the momentum equation are negligible. The equation reduces to:

$$\frac{\lambda}{\lambda r} (r\tau) \doteq 0 \quad ,$$

$$\text{or: } r\tau = r_0 \tau_w = \text{constant} \doteq r \mu_w \frac{\partial u}{\partial r} \quad (2-2)$$

With τ thus approximated by the viscous stress only, we may integrate Eqn. (2-2) to obtain an approximate velocity profile in the sublayer:

$$\mu_w u \doteq r_0 \tau_w \ln(r/r_0) \quad (2-3)$$

If we now define the shear velocity u^* such that $\tau_w = \rho_w u^{*2}$, Eqn. (2-3) may be rewritten in law-of-the-wall form:

$$u^+ = r_0^+ \ln(r/r_0) \quad , \quad (\text{SUBLAYER}) \quad (2-4)$$

where $u^+ = u/u^*$ and $r_0^+ = \rho_w u^* r_0 / \mu_w$. Equation (2-4) is in marked contrast to the two-dimensional sublayer, for which

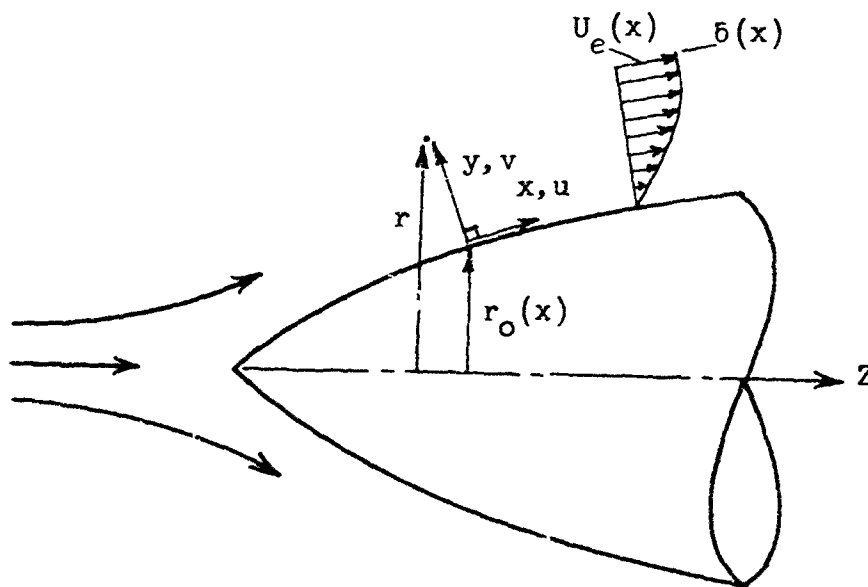


Figure 2.1. DEFINITION SKETCH ILLUSTRATING COORDINATES FOR AXISYMMETRIC BOUNDARY LAYER FLOW.

u^+ simply equals y^+ , as in Chapter 1. Since y^+ correlates the entire wall region in two-dimensional flow, it was suggested by Rao (1967) that the variable $r_0^+ \ln(r/r_0)$ in Eqn. (2-4) would similarly correlate an axisymmetric flow. Thus Rao's hypothesis for incompressible axisymmetric flow is that

$$u^+ = \text{fcn}(Y^+), \text{ where } Y = r_0 \ln(r/r_0) . \quad (2-5)$$

Equation (2-4) would hold in the sublayer, while the logarithmic overlap layer would be characterized by the relation

$$u^+ = \frac{1}{\kappa} \ln(Y^+) + B \quad (\kappa \doteq 0.40, B \doteq 5.5) \quad (2-6)$$

Rao (1967) and later White (1972) showed that Eqn. (2-6) is an excellent approximation for a wide variety of thick axisymmetric boundary layers. As the boundary layer becomes thicker, this axisymmetric wall law becomes valid across the entire boundary layer, that is, the outer or "wake" layer becomes vanishingly small.

Note that Eqn. (2-6) is consistent with a turbulent eddy viscosity ϵ and mixing length l given by

$$\epsilon = \rho \kappa^2 Y^2 (r/r_0) \frac{\partial u}{\partial y} \cos(\alpha) , \quad (2-7)$$

$$\text{or } l = \kappa Y (r/r_0)^{1/2} ,$$

where $\alpha = \tan^{-1}(dr_0/dx)$. For this report, we shall take

$\alpha \approx 0^\circ$, that is, we neglect the slope of the body and take, approximately, $r = r_0 + y$. The error is negligible except near the stagnation point, which does not concern us. Since Y as defined by Eqn. (2-5) is smaller than y , l as defined by Eqn. (2-7) is smaller than its two-dimensional equivalent $l = \kappa y$, the physical explanation being that a cylinder has less ability to create turbulent shear than a plane surface.

Equation (2-7) may be used to derive a law-of-the-wall for compressible flow with pressure gradient. As in the two-dimensional case (White and Christoph 1971), we neglect the convective acceleration, and the axisymmetric streamwise momentum equation becomes

$$\frac{\lambda}{2r} (r \tau) - r \frac{dp_e}{dx} = 0 \quad (2-8)$$

Integrating from the wall ($r=r_0$) outward, we have:

$$r \tau = r_0 \tau_w + \frac{1}{2} \frac{dp_e}{dx} (r^2 - r_0^2) \quad (2-9)$$

This may be integrated again by assuming that viscous shear is negligible and that $\tau = \epsilon (\lambda u / \lambda y)$, where ϵ is given by Eqn. (2-7). Substituting for τ and rearranging in terms of law-of-the-wall variables, we obtain:

$$\frac{du^+}{dY^+} = \frac{1}{\kappa Y^+} (\rho_w / \rho)^{1/2} \left[1 + \frac{\alpha}{2} r_0^+ (e^{2Y^+ / r_0^+} - 1) \right]^{-1/2}, \quad (2-10)$$

$$\text{where } \alpha = \frac{v_w}{\tau_w} \frac{dp_e}{dx}.$$

The pressure gradient parameter α is the same quantity which appeared in previous analyses for two-dimensional flow (Chapter 1 and White 1969).

Equation (2-10) can be integrated for the velocity profile $u^+(Y^+)$ if we make an assumption about the density variation. Since we are concerned only with predicting skin friction, we assume a perfect gas,

$$p = \rho R T, \text{ or: } \rho_w/\rho \doteq T_w/T \quad (2-11)$$

plus a Crocco approximation, $T \doteq a + b u + c u^2$, which may be rewritten in terms of wall variables as follows:

$$T/T_w = 1 + \beta u^+ - \gamma u^{+2} \doteq \rho_w/\rho \quad (2-12)$$

where β and γ are the same parameters used in previous work (White and Christoph 1970, 1972):

$$\begin{aligned} \beta &= q_{w,v_w}/(T_w k_w u^*) = \text{heat transfer parameter;} \\ \gamma &= \hat{r} u^{*2}/(2c_p T_w) = \text{compressibility parameter.} \end{aligned} \quad (2-13)$$

Equations (2-10) and (2-12) may now be combined and integrated to obtain the desired law-of-the-wall $u^+(Y^+, \alpha, \beta, \gamma)$. Of particular interest is a closed form which can be obtained for the special case ($\alpha=0, \beta=0$):

$$u^+(Y^+, 0, 0, \gamma) = \frac{1}{\sqrt{\gamma}} \sin^{\sqrt{\gamma}} \frac{1}{\kappa} \ln(Y^+/Y_0^+) \quad (2-14)$$

where we take $Y_0^+ = 0.1108$ so that the formula reduces in the limit of large radius to the two-dimensional law-of-the-wall.

Equation (2-14) corresponds to supersonic adiabatic flow along a cylinder, for which experimental thick boundary layer data is available (Richmond 1957).

Some velocity profiles obtained from integrating Eqn. (2-10) are shown in Figure 2-2. The effect is generally the same as in the two-dimensional flow study (White and Christoph 1970), with positive α (adverse pressure gradient) raising the curves above the incompressible log law and γ (the compressibility effect) tending to lower the curves. Note that the parameter r_0^+ has no effect on the curves unless α is finite.

2.3 Derivation of the Basic Differential Equation

We now assume that the compressible law-of-the-wall for a thick axisymmetric turbulent boundary layer is known as the integrated combination of Equations (2-10) and (2-12):

$$u^+(Y^+, \alpha, \beta, \gamma, r_0^+) = \int_0^{Y^+} \frac{1}{\kappa Y^+} (1 + \beta u^+ - \gamma u^{+2})^{\frac{1}{2}} \left[1 - \frac{\alpha r_0^+}{2} (1 - e^{2Y^+/r_0^+}) \right]^{\frac{1}{2}} dY^+ \quad (2-15)$$

This relation, if accepted as a reasonable approximation across the entire boundary layer, provides closure to the problem of computing the wall shear stress on a body of revolution. That is, we can now derive a single differential equation for $C_f(x)$ under arbitrary flow conditions.

The boundary layer equations for compressible, axisymmetric, turbulent boundary layer flow are given by, for

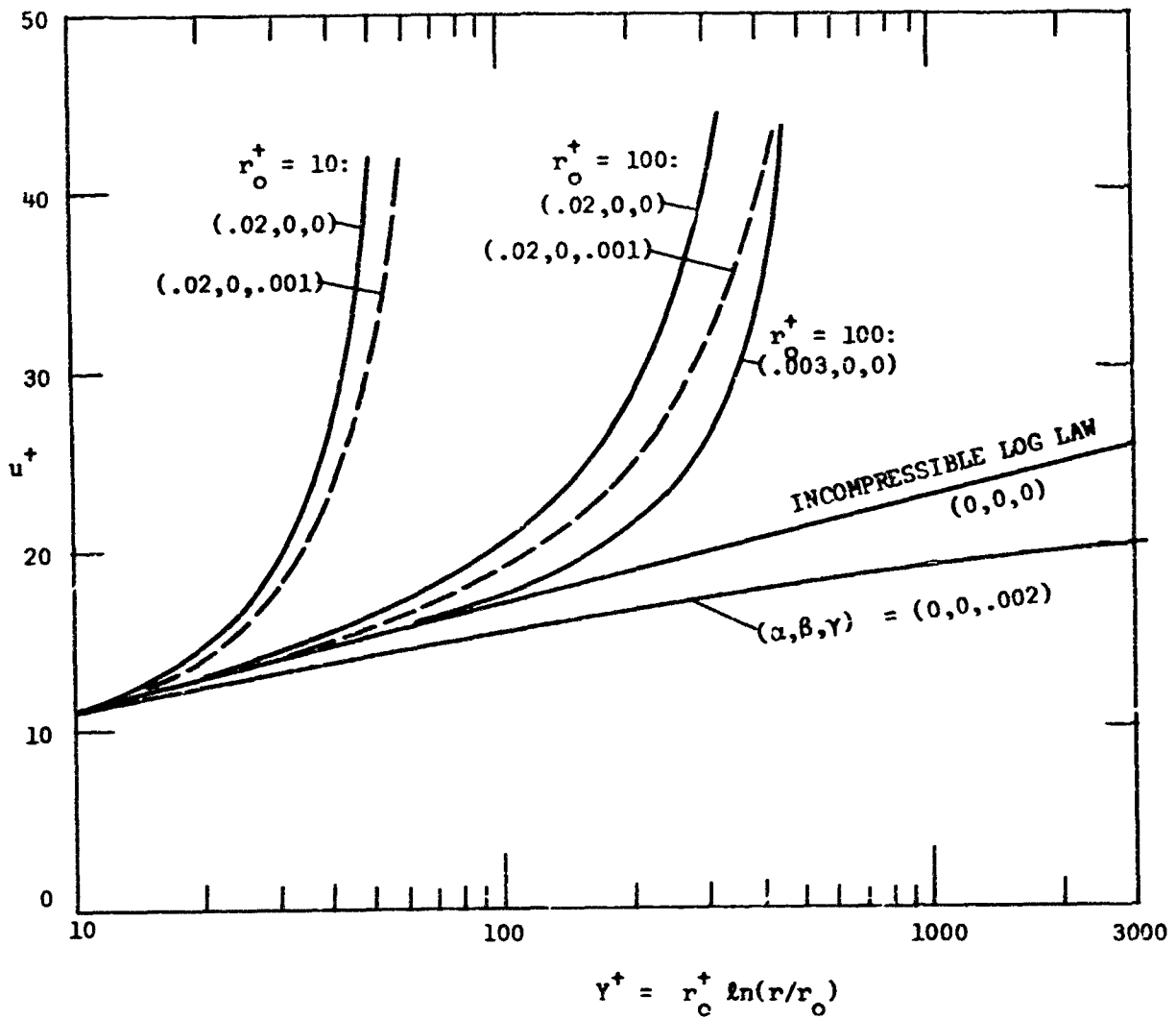


Figure 2-2. SOME EXAMPLES OF THE AXISYMMETRIC LAW-OF-THE-WALL, COMPUTED FROM EQUATIONS (2-10) and (2-12).

Reproduction of this figure is authorized by the U.S. Government.

example, Herring and Mellor (1968):

a) Continuity:

$$\frac{\partial}{\partial x}(\rho u r) + \frac{\partial}{\partial y}(\rho v r) = 0 \quad (2-16)$$

b) Momentum:

$$\rho u r \frac{\partial u}{\partial x} + \rho v r \frac{\partial u}{\partial y} = - r \frac{dp_e}{dx} + \frac{\partial}{\partial y}(r\tau) \quad (2-17)$$

c) Energy:

$$\rho u r \frac{\partial h_o}{\partial x} + \rho v r \frac{\partial h_o}{\partial y} = \frac{\partial}{\partial y} [r(q + \tau)] \quad (2-18)$$

where the notation is the same as in Figure 2-1. As in Chapter 1, the quantity $h_o = h + u^2/2$ is the stagnation enthalpy. Now in fact Eqn. (2-16), although included for completeness, is not needed here, since the temperature relates directly to velocity through the Crocco approximation, Eqn. (2-12). As mentioned, the effect of this simplification upon skin friction is slight, but knowledge of the Stanton number distribution is lost. If desired, one could extend the temperature wall law technique of Chapter 1 to this axisymmetric case for computing wall heat transfer.

The continuity relation (2-16) is satisfied identically by defining an axisymmetric stream function ψ such that:

$$\frac{\partial \psi}{\partial y} = \rho u r ; \quad \frac{\partial \psi}{\partial x} = - \rho v r \quad (2-19)$$

Since ρ , u , r , and y are each related to wall variables, it follows from the first of Eqns. (2-19) that y^+ itself is a law-of-the-wall variable:

$$y^+/\mu_w r_0 = \int_0^{y^+} \frac{\rho}{\rho_w} \left(\frac{r}{r_0}\right)^2 u^+ dy^+ = \text{fcn}[Y^+, \alpha, \beta, \gamma, r_0^+] \quad (2-20)$$

This fact is important in computing the velocity v from the second of Eqns. (2-19). Utilizing wall law variables wherever possible, the momentum relation, Eqn. (2-17), now becomes:

$$\begin{aligned} \rho r u^* u^+ \frac{\partial}{\partial x}(v^* u^+) - \frac{\partial \tau}{\partial x} \frac{u^*}{v_w} \frac{\partial}{\partial y^+}(u^* u^+) = - r \frac{dp_e}{dx} \\ + \frac{u^*}{v_w} \frac{\partial}{\partial y^+}(r \tau) \end{aligned} \quad (2-21)$$

where $u^* = (\tau_w/\rho_w)^{1/2}$ is the wall friction velocity. The y^+ derivatives are related to Rao's variable Y^+ through the relation

$$\frac{\partial}{\partial y^+} = \frac{r}{r_0} \frac{\partial}{\partial Y^+}, \quad (2-22)$$

which follows from Eqn. (2-5). The x derivatives must be handled by the chain rule, since each of the parameters $(\alpha, \beta, \gamma, r_0^+)$ in the law-of-the-wall is a function of x .

Thus we substitute

$$\begin{aligned} \frac{\partial}{\partial x} = \frac{\partial Y^+}{\partial x} \frac{\partial}{\partial Y^+} + \frac{\partial \alpha}{\partial x} \frac{\partial}{\partial \alpha} + \frac{\partial \beta}{\partial x} \frac{\partial}{\partial \beta} + \frac{\partial \gamma}{\partial x} \frac{\partial}{\partial \gamma} \\ + \frac{\partial r_0^+}{\partial x} \frac{\partial}{\partial r_0^+} \end{aligned} \quad (2-23)$$

In carrying out the partial derivatives in Eqn. (2-23), we retain our previous approximation (White and Christoph 1970, 1972) of neglecting the derivatives with respect to x of ρ_w , T_w , μ_w , and q_w wherever they appear in α, β, γ , etc. It is felt that these terms have only a small effect on wall skin friction.

It remains only to carry out our basic integral procedure, namely, combining Eqns. (2-21, 22, 23) and integrating the entire equation with respect to Y^+ across the boundary layer from ($Y^+ = 0, \tau = \tau_w$) to ($Y^+ = Y_e^+, \tau = 0$). The result is a single first order differential equation for the wall friction velocity $u^*(x)$. It is convenient to define dimensionless variables as in Chapter 1:

$$\lambda = \sqrt{2/C_f} ; \quad x^* = x/L ; \quad V = U_e(x)/U_0 , \quad (2-24)$$

where $C_f = 2\tau_w/(\rho_e U_e^2)$, and L and U_0 are suitable reference values. In terms of these variables, the final integral momentum equation becomes

$$\frac{d\lambda}{dx^*} (A_1 - 3\alpha A_2) + \frac{V}{\lambda} (F - A_1) - \frac{\lambda^4}{R_L} A_2 (1/V)'' = R_L V - A_3 \frac{1}{r_0} \frac{dr_0}{dx^*} , \quad (2-25)$$

where $R_L = (U_0 L / \nu_e) (\mu_e / \mu_w) (T_e / T_w)^{\frac{1}{2}}$ and $F = \frac{1}{2} \lambda^2 r_0^2 (e^{2Y_e^+ / r_0^+} - 1)$.

Equation (2-25) is the central result of this chapter - a first order ordinary differential equation for $\lambda(x^*)$, subject only to some assumed initial condition $\lambda(x^*_0)$ and known flow conditions $U_e(x)$, $T_e(x)$, $T_w(x)$, $r_0(x)$, and $M_e(x)$.

The functions (A_1 , A_2 , A_3) arise from the integration across the boundary layer and are defined as follows:

$$A_1 = \int_0^{Y_e^+} \left\{ (T_e/T_w) \exp(2Y^+/r_0^+) \left[u^{+2} - \beta u^+ \frac{\partial u^+}{\partial \beta} + 2\gamma u^+ \frac{\partial u^+}{\partial \gamma} \right] + \frac{\beta}{\mu_w r_0} \frac{\partial \psi}{\partial \beta} \frac{\partial u^+}{\partial Y^+} - \frac{2\gamma}{\mu_w r_0} \frac{\partial \psi}{\partial \gamma} \frac{\partial u^+}{\partial Y^+} \right\} dY^+ \quad (2-26)$$

$$A_2 = \int_0^{Y_e^+} \left\{ \frac{T_e}{T_w} \exp(2Y^+/r_0^+) u^+ \frac{\partial u^+}{\partial \alpha} - \frac{1}{\mu_w r_0} \frac{\partial \psi}{\partial \alpha} \frac{\partial u^+}{\partial Y^+} \right\} dY^+ \quad (2-27)$$

$$A_3 = \int_0^{Y_e^+} \left\{ (u^+/T^+) \exp(2Y^+/r_0^+) \Gamma(u^+) - \frac{r_0^+}{\mu_w r_0} \Gamma(\psi) \right\} dY^+ \quad (2-28)$$

$$\text{where } \Gamma(\) = (Y^+ - r_0^+) \frac{\partial}{\partial Y^+} + r_0^+ \frac{\partial}{\partial r_0^+} .$$

In order for Eqn. (2-25) to be viable, it is necessary to have analytic approximations for these coefficient functions. After extensive numerical computation of Eqns. (2-26, 27, 28), using Eqn. (2-15) for the wall law, we offer the following curve-fit approximations:

$$A_1 \doteq \frac{1}{2} A_3 \doteq 8.0 \exp\left\{ \frac{0.48 \lambda + 0.2 S + 0.0018 S^2}{A (1 + 0.2 Q)} \right\}, \quad (2-29)$$

$$\text{where } S = \exp(0.4 \lambda / A) / r_o^+,$$

$$r_o^+ = R_L r_o / (\lambda L),$$

$$Q = \frac{1}{2} \alpha r_o^+ \{ \exp(2 Y_e^+ / r_o^+) - 1 \}.$$

$$A_2 \doteq 0.066 \exp\left\{ \frac{0.84 \lambda + 0.2 S + 0.0018 S^2}{A (1 + 0.2 Q)} \right\} \quad (2-30)$$

and where

$$Y_e^+ \doteq 0.1108 \exp(0.4 \xi - 2.2 Q^{2/3}), \quad (2-31)$$

$$\text{where } \xi = \frac{1}{\sqrt{\gamma}} \sin^{-1} \left\{ (2\gamma u^+ - \beta) / (\beta^2 + 4\gamma)^{1/2} \right\}.$$

Equation (2-31) is a curve-fit to the law-of-the-wall itself, Eqn. (2-15), and Y_e^+ is needed to evaluate the pressure gradient parameter Q above. Note that, in the limit of very large r_o^+ , Q approaches $(\alpha \delta^+)$, which is the incompressible two-dimensional parameter originally used by White (1969).

The parameter "A" in these formulas accounts for the combined effect of wall temperature and Mach number, as was done in White and Christoph (1972). It is the same parameter defined in a flat plate analysis by van Driest (1956):

$$A = (T_{aw}/T_e - 1)^{1/2} / [\sin^{-1}(a/c) + \sin^{-1}(b/c)] \quad (2-32)$$

$$\text{where } a = (T_{aw} + T_w)/T_e - 2 \quad ; \quad b = (T_{aw} - T_w)/T_e \quad ;$$

$$c^2 = [(T_{aw} + T_w)/T_e]^2 - 4T_w/T_e \quad .$$

Values of A for various Mach numbers and wall temperature ratios are shown in Figure 2-3. Note that the incompressible adiabatic limit is $A = 1$.

2.4 Comparison with Experiment

Equation (2-25) may be used to compute the turbulent skin friction distribution $C_f(x) = 2/\lambda^2(x)$ along a body of revolution in arbitrary subsonic or supersonic flow, providing only that variations in wall temperature are not too great. A starting value $\lambda_0(x=x_0)$ is needed; if the computation is started at the transition point, the value $\lambda_0 = 20$ is recommended. The solution of (2-25) may be continued downstream until the separation point (if any) is predicted to occur when the coefficient $(A_1 - 3\alpha A_2)$ vanishes.

We now consider three applications: a) flow along a slender cylinder; b) supersonic attached flow past a cone;

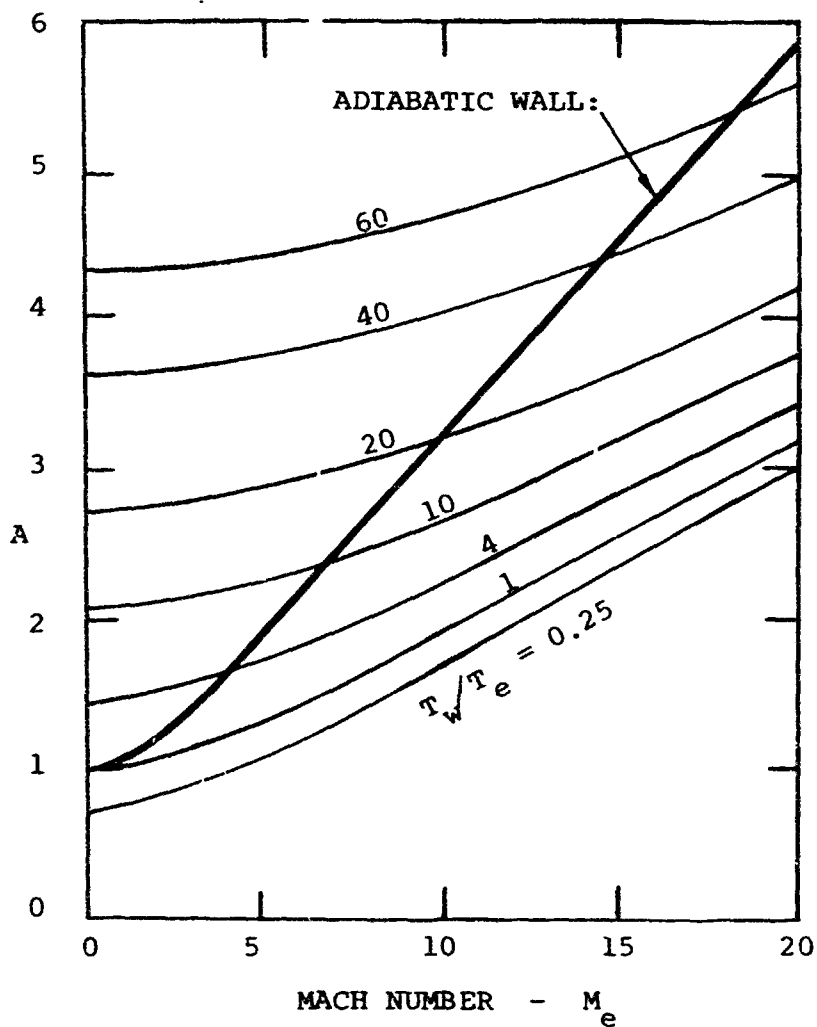


Figure 2.3. THE COMPRESSIBILITY AND WALL TEMPERATURE PARAMETER A, FROM EQN. (2-32).

and c) supersonic flow past a slender body of revolution.

2.4.1 Compressible Flow Along a Slender Cylinder

The application of the present theory is to consider the effect of compressibility and transverse curvature with no pressure gradient. A cylinder has $r_0 = \text{constant}$ and, to excellent approximation, $U_e = U_0 = \text{constant}$. Equation (2-25) reduces to:

$$A_1 \frac{d\lambda}{dx^*} = R_L, \quad (2-33)$$

which may be separated and integrated for a direct relation between skin friction and local Reynolds number:

$$R_x = (\mu_w/\mu_e)(T_w/T_e)^{1/2} \int_0^\lambda A_1(\lambda, 0, \beta, \nu, r_0^+) d\lambda \quad (2-34)$$

With zero pressure gradient, the curve-fit approximation to A_1 is:

$$A_1 \doteq 8.0 \exp\left[\frac{1}{A} (0.48 \lambda + 0.20 Z + 0.0018 Z^2)\right], \quad (2-35)$$

$$\text{where } Z = \exp(0.4 \lambda / A) / r_0^+.$$

Further, r_0^+ is directly related to λ and the radius Reynolds number $R_a = U_e r_0 / \nu_e$, as follows:

$$r_0^+ = R_a / \left[\lambda (\mu_w/\mu_e)(T_w/T_e)^{1/2} \right] \quad (2-36)$$

Since R_a is constant for the cylinder, Eqs. (2-35, 36) may be substituted into Eqn. (2-34) and the integration carried

out for the desired relation $R_x(\lambda)$, or better, its inverse $C_f = C_f(R_x, R_a)$. As an example, the computed skin friction on an adiabatic cylinder at a Mach number $M_e = 5$ is shown in Figure 2-4. It is seen that there are substantial transverse curvature effects which raise the skin friction over its flat plate value. As R_a becomes very large, which is equivalent to the cylinder being very short, the flat plate skin friction is approached from above.

Since the integral in Eqn. (2-34) cannot be found in closed form, it is appropriate to find a curve-fit formula for the results, in the spirit of the correlations (2-1) proposed for incompressible flow. It was found that the flat plate formula of White and Christoph (1972) could be generalized to include the effect of $x/r_o = R_x/R_a$ as follows:

$$C_f \doteq 0.455 / \left[A^2 \ln^2 \left(b R_x \left(\rho_e / \mu_w \right) \left(T_e / T_w \right)^{\frac{1}{2}} / A \right) \right] \quad (2-37)$$

$$\text{where } b \cong 0.06 / \left[1 + 0.025 (x/r_o)^{6/7} \right].$$

This formula is valid with accuracy to $\pm 10\%$ over the entire turbulent Reynolds number range (10^5 - 10^9) and for Mach numbers from zero to ten. The slenderness ratio (x/r_o) may be as high as 10^6 ; note that the formula predicts a roughly 5% increase in skin friction for (x/r_o) as low as ten. For very small (x/r_o), the formula reduces to the compressible flat plate formula, Equation (24) of White and Christoph (1972).

Equations (2-34) or (2-37) may be compared with experimental data of Richmond (1957) for supersonic turbulent flow past long cylinders. Richmond generated a supersonic flow at $M_e \doteq 5.8$ past three cylinders: $r_0 = 0.012$, 0.032 , and 0.125 inches, respectively. For the largest cylinder ($0.125''$), skin friction was measured with a floating element balance for one condition ($R_a = 20,400$) and was estimated from the velocity profiles for the other two cylinders. The authors attempted an alternate skin friction determination, using a sort of axisymmetric "Clauser-plot" which may be inferred from our postulated law-of-the-wall, Eqn. (2-15). Since the cylinders are assumed adiabatic and the pressure gradient is zero ($\alpha=\beta=0$), Eqn. (2-15) may be integrated in closed form to give the following expression:

$$u^+(Y^+, 0, 0, \nu, r_0^+) = \frac{1}{\sqrt{Y}} \sin^{-1} \frac{\sqrt{Y}}{\kappa} \ln(Y^+/Y_0^+) \quad , \quad (2-38)$$

where $Y_0^+ = 0.1108$ - to match with the incompressible log law in the limit. By introducing the definition of v from Eqn. (2-13) and rearranging, we obtain an equivalent logarithmic law:

$$\hat{u}/u^* = \frac{1}{\kappa} \ln(Y^+/0.1108) \quad , \quad \text{where } \hat{u} = U_r \sin^{-1}(u/U_r) \quad (2-39)$$

$$\text{and where } U_r = (2c_{pT_w}/\hat{r})^{1/2} .$$

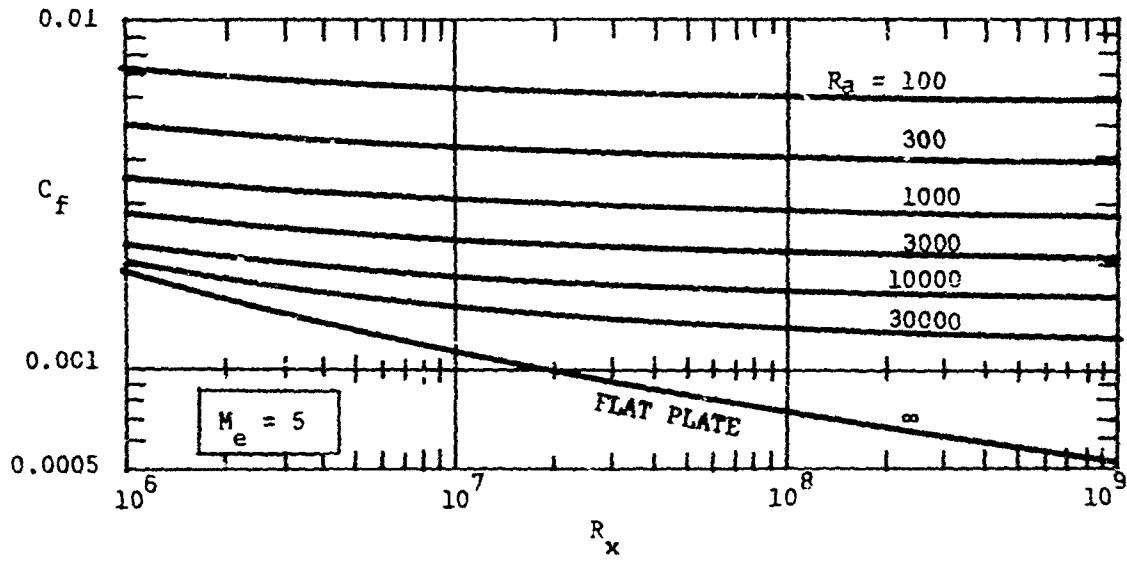


Figure 2-4. SKIN FRICTION ON AN ADIABATIC CYLINDER AT
 A FREESTREAM MACH NUMBER OF 5 FOR VARIOUS VALUES
 OF $R_a = U_e r / \nu_e$, COMPUTED FROM EQUATION (2-34).

This relation shows that a plot of the "reduced" velocity \hat{u} versus Rao's variable Y^+ should be semi-logarithmic and follow the incompressible law. Further, if the velocity profile $u(y)$ is known, one may use Eqn. (2-39) to infer the friction velocity u^* and hence C_f itself. That is, if we eliminate u^* in favor of C_f , Eqn. (2-39) may be rewritten as follows:

$$\zeta = \sqrt{C_f/2} \left[\frac{1}{\kappa} \ln(\tau \sqrt{C_f/2}) + 5.5 \right], \quad (2-40)$$

where $\tau = (\hat{u}/U_e)(T_e/T_w)^{1/2}$ and $\tau = R_a \ln(r/r_0)$

$$(\mu_e/\mu_w)(T_e/T_w)^{1/2}.$$

Equation (2-40) may be plotted with C_f as a parameter, as shown in Figure 2-5. When data for ζ versus τ is placed on this chart, it should possess a logarithmic overlap layer from which one can infer C_f by interpolating between the plotted parametric lines. This has been done in Figure 2-5 for four supersonic cylindrical profiles given by Richmond (1957). Note that all profiles demonstrate the proper slope and behavior and thus substantiate the present law-of-the-wall approach. In all four cases, the inferred C_f is lower than that reported by Richmond (1957). Table 2.1 summarizes the skin friction data and compares with two theories: the more "exact" integral computation of Eqn. (2-34) and the curve-fit formula of Eqn. (2-37). Also included for comparison is a flat plate computation for R_x in the same

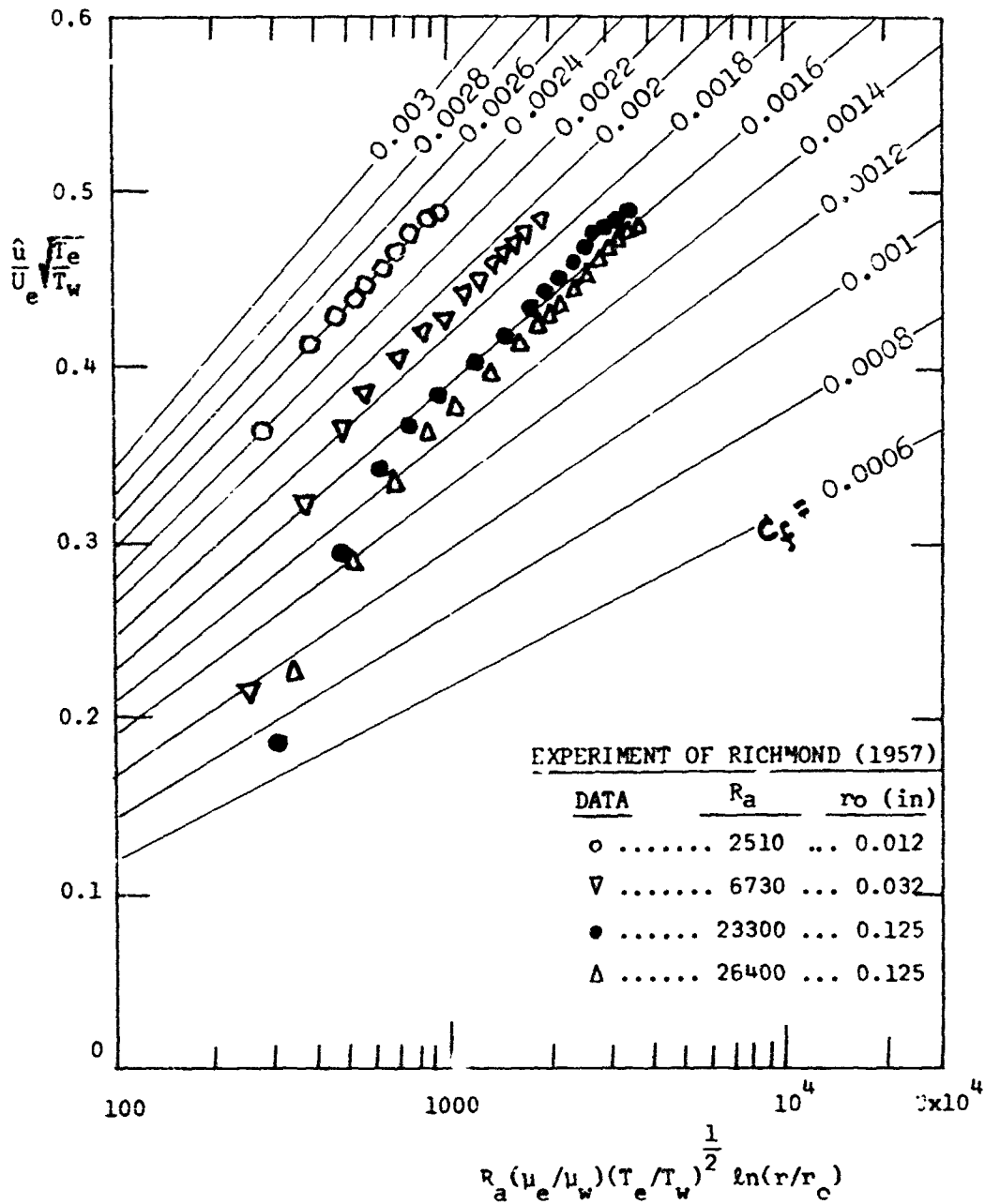


Figure 2.5. SKIN FRICTION DETERMINATION FOR SUPERSONIC FLOW ALONG A SLENDER CYLINDER BY A MODIFIED AXISYMMETRIC CLAUSER-PLOT (EQ. 2-40).

range. Note that transverse curvature has increased C_f by at least 40% to as much as 100%. The present theory seems in good agreement, falling between the two skin friction estimates (Richmond and the "Clauser-plot"). To the author's knowledge, no other theory, whether integral or finite difference in nature, has been applied to these important thick axisymmetric supersonic boundary layer experiments. Richmond (1957) also reported low speed friction and velocity profile measurements along slender cylinders; these were analyzed in the incompressible theory of White (1972).

2.4.2 Supersonic Attached Flow Past a Cone

A classic problem in the literature is that of supersonic flow past a cone at zero incidence. If the resulting shock wave is attached to the cone vertex, the freestream flow along the cone surface is approximately constant velocity ($\alpha = 0$). This is somewhat analogous to the cylinder case of the previous example, except that here the surface radius r_0 varies. If x is along the cone generators, we have

$$r_0 = x \sin \omega \quad , \quad (2-41)$$

where ω is the cone half-angle. It is of interest to try and relate the cone skin friction to an equivalent flat plate or cylinder at the same Reynolds number R_x . According

to the classic turbulent analysis by van Driest (1952), C_f at position R_x on the cone is equal to C_f on a flat plate at position $(R_x/2)$. Thus, for equal R_x , the cone skin friction is 10-15% higher than the plate C_f . This analysis of course does not account for boundary layer thickness effects, which the present theory includes as the (r_0^+) effect on the law-of-the-wall. With $U_e = \text{constant}$, Eqn. (2-25) reduces for cone flow to:

$$A_1 \frac{d\lambda}{dx^*} + A_3 \frac{1}{r_0} \frac{dr_0}{dx^*} = R_L \quad , \quad (2-42)$$

and, since ϕ is constant, $(1/r_0)(dr_0/dx^*) = 1/x^*$ from Eqn. (2-41). If transverse curvature is important, i.e. if the boundary layer is thick compared to the cone radius, then A_1 and A_3 depend upon $r_0^+(\lambda, x^*)$ and the variables are not separable in Eqn. (2-42). However, if we assume a thin boundary layer (large r_0^+), then our curve-fit approximations give:

$$A_1 \doteq \frac{1}{2} A_3 \doteq a e^{b\lambda} \quad (a \doteq 0.0, \quad b \doteq 0.48/A) \quad (2-43)$$

For this case, Eqn. (2-42) has a closed form solution:

$$\lambda = \frac{1}{b} \ln \frac{-b R_L x^*}{a(1 + 2b)} \quad , \quad (2-44)$$

which may be compared to the analogous solution for flat plate flow, Eqn. (2-37) or (1-36):

$$\lambda = \frac{1}{b} \ln \left[b R_L x^*/a \right] \quad (2-46)$$

By comparing (2-44) and (2-45), one may deduce a first-order turbulent "cone rule":

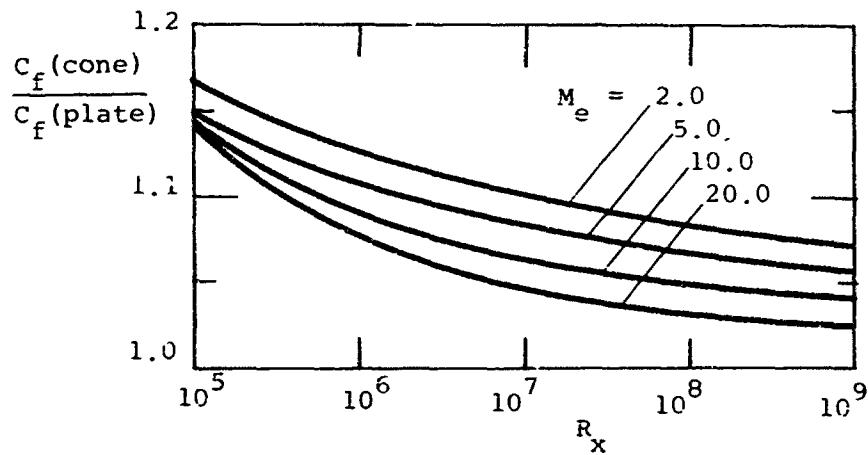
$$C_{f_{\text{cone}}} (at R_x) = C_{f_{\text{plate}}} (at R_x / [1 + 0.96/A]) \quad (2-46)$$

This may be compared with the classic cone rule developed by van Driest (1952):

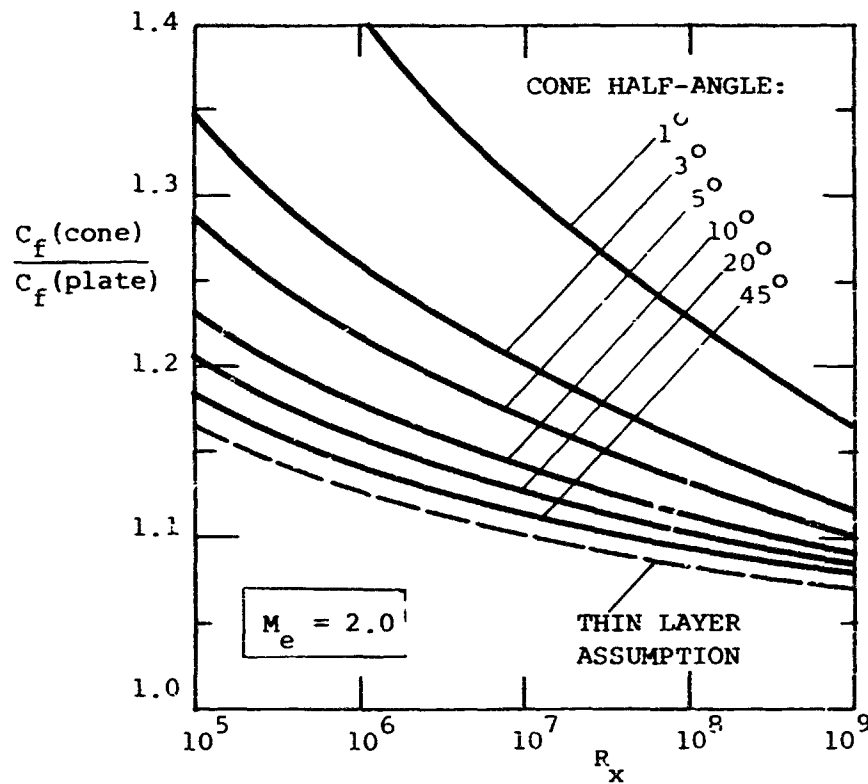
$$C_{f_{\text{cone}}} (R_x) = C_{f_{\text{plate}}} (R_x/2) \quad (2-47)$$

From Figure 2-3, $A \doteq 1.0$ at low Mach numbers, so that the correction factor for Reynolds number equals 1.96 approximately, or very close to van Driest's factor of 2.0. A later analysis by Tetervin (1969) gives a factor of $(2.0 + 1/N)$, where N is the exponent in an assumed $(1/N^{\text{th}})$ power-law relation between C_f and momentum thickness Reynolds number. Since N is of the order of 5 to 9, increasing with Reynolds number and Mach number, Tetervin's factor is also about two. Figure 2-6.a shows values of the ratio of cone to plate friction coefficient as calculated from Eqn. (2-46). The predicted increase in cone friction is of the order of 5 to 15%, being higher at low Reynolds numbers.

In fact, however, neither Eqn. (2-46) nor the van Driest or Tetervin analysis is accurate for small cone



a) THIN BOUNDARY LAYER ASSUMPTION: EQN. (2-46).



b) EXACT CALCULATIONS FOR $M_e = 2.0$, EQN. (2-42).

Figure 2.6. ILLUSTRATION OF THE TURBULENT CONE RULE.

angles, because of the transverse curvature effect (large δ/r_0). That is, a numerical or graphical solution of Eqn.(2-42), using the actual formulas for A_1 and A_3 from Eqns.(2-29,31), shows a further increase in cone skin friction at the smaller cone angles. These numerical solutions are illustrated in Figure 2.6.b for a freestream Mach number of 2.0 along the cone surface. Thus transverse curvature adds an additional 10 to 30% to the skin friction, and only the thicker cones (20° to 45° half angle) approximate the first order cone rule above (2-46,47). By analogy with the cylinder analysis (Eqn.2-37), the relevant transverse curvature parameter is $(x/r_0) = \csc(\varphi)$ for a cone. Hence the numerical solutions in Figure 2.6.b may be correlated into the following formula for constant pressure (attached) flow along a cone:

$$C_f(\text{cone}) = \frac{0.455}{A^2 \ln^2 \left\{ b R_x (T_e/T_w)^{1/2} (\mu_e/\mu_w)/A \right\}}, \quad (2-48)$$

$$\text{where } b = 0.06(1 + 0.96/A)^{-1}(1 + 0.03 \csc \varphi)^{-1}.$$

This formula is accurate to about $\pm 3\%$ over the complete supersonic turbulent cone flow range, including constant nonadiabatic wall temperature, which is accounted for by the van Driest parameter A in the formula (Eqn.2-32).

TABLE 2-1
 COMPARISON OF THEORY WITH THE DATA OF RICHMOND (1957)
 FOR SUPERSONIC FLOW ALONG A SLENDER CYLINDER AT $M_e = 5.8$

r_0 (in.)	R_R	R_x ($\times 10^{-6}$)	C_f (exp)	C_f (Figure 2-5)	C_f (Eqn. 2-34)	C_f (Eqn. 2-37)
0.125	26400.	2.17	0.00185	0.00155	0.00162	0.00164
0.125	23300.	1.88	0.00194	0.0016	0.00168	0.00170
0.125	20400.	1.70	0.00203*	0.0017	0.00172	0.00174
0.032	6730.	4.20	0.00213	0.0019	0.00188	0.00191
0.012	2510.	4.18	0.00234	0.0024	0.00231	0.00236
----	∞	4.0	-----	-----	0.00121	0.00121

*Skin friction balance - other values estimated.

2.4.3 Supersonic Flow with Pressure Gradient:

For flow past a general body of revolution, the complete differential equation for skin friction, Eqn.(2-25), should be used, since $\alpha \neq 0$ and $r_0 = r_0(x)$. In one sense, these effects are mutually exclusive, because if pressure gradients are important, transverse curvature is probably not important, and vice versa. That is, only a slender body can have large (δ/r_0) , but a slender body cannot have large pressure gradients. However, the shape effect term $(A_3/r_0)(dr_0/dx^*)$ is nearly always important.

We give here a typical solution of the general theory by comparing Eqn.(2-25) with the skin friction measurements of Allen (1970) for supersonic flow past a so-called Haack-Adams body of revolution, shown to scale in Figure 2.7. The shape of the body is given by the following formula:

$$r_0/r_{\max} = 0.707(1-t^2)^{1.5} + 0.16934 \cos^{-1} t + t(1-t^2)^{1/2} \quad (2-49)$$

$$\text{where } t = (1 - 2Z/L).$$

Note that Z is the axial, not the surface, coordinate (see Figure 2.1). Allen (1970) tested a wind tunnel model with $L = 36$ inches and $r_{\max} = 1.8$ inches. Skin friction at seven stations was measured with a Preston tube and also estimated by 1) the Baronti-Libby law; and 2) the Fenter-Stalmach law. The upstream Mach number was varied from 2.5 to 4.5, and

the example shown ($M_\infty = 2.96$) is typical of both the data and the theory. With $L = 36$ inches, the Reynolds number R_L in Eqn.(2-25) was equal to 3.0×10^6 . The freestream Mach number distribution $M_e(x)$ is shown, and the velocity distribution is of a similar shape and was curve-fit by the expression

$$V(x^*) \doteq 1 + 0.156(t - t^2), \quad t = x^* - 0.139. \quad (2-50)$$

Figure 2.7 shows three different analytical estimates: 1) the exact theory, Eqn.(2-25); 2) a flat plate theory based on local R_x , Eqn.(1-36); and 3) a long cylinder theory, Eqn.(2-37), based on local R_x and $r_o(x)$. It is seen that the cylinder and flat plate formulas give an estimate of the average skin friction on the body. The difference between these two is about 5%, which represents the transverse curvature effect. The exact theory is in excellent agreement with the data over the entire body. The higher values of C_f (compared to a flat plate) at the front of the body are due to roughly equal contributions from 1) the term $(A_3/r_o)(dr_o/dx^*)$; and 2) the favorable pressure gradient. Similarly, the lower values at the rear are due to 1) a change in sign of (dr_o/dx^*) ; and 2) the adverse pressure gradient. The same excellent agreement with experiment was found for the other three conditions ($M_\infty = 2.5, 3.95, 4.5$) investigated by Allen (1970).

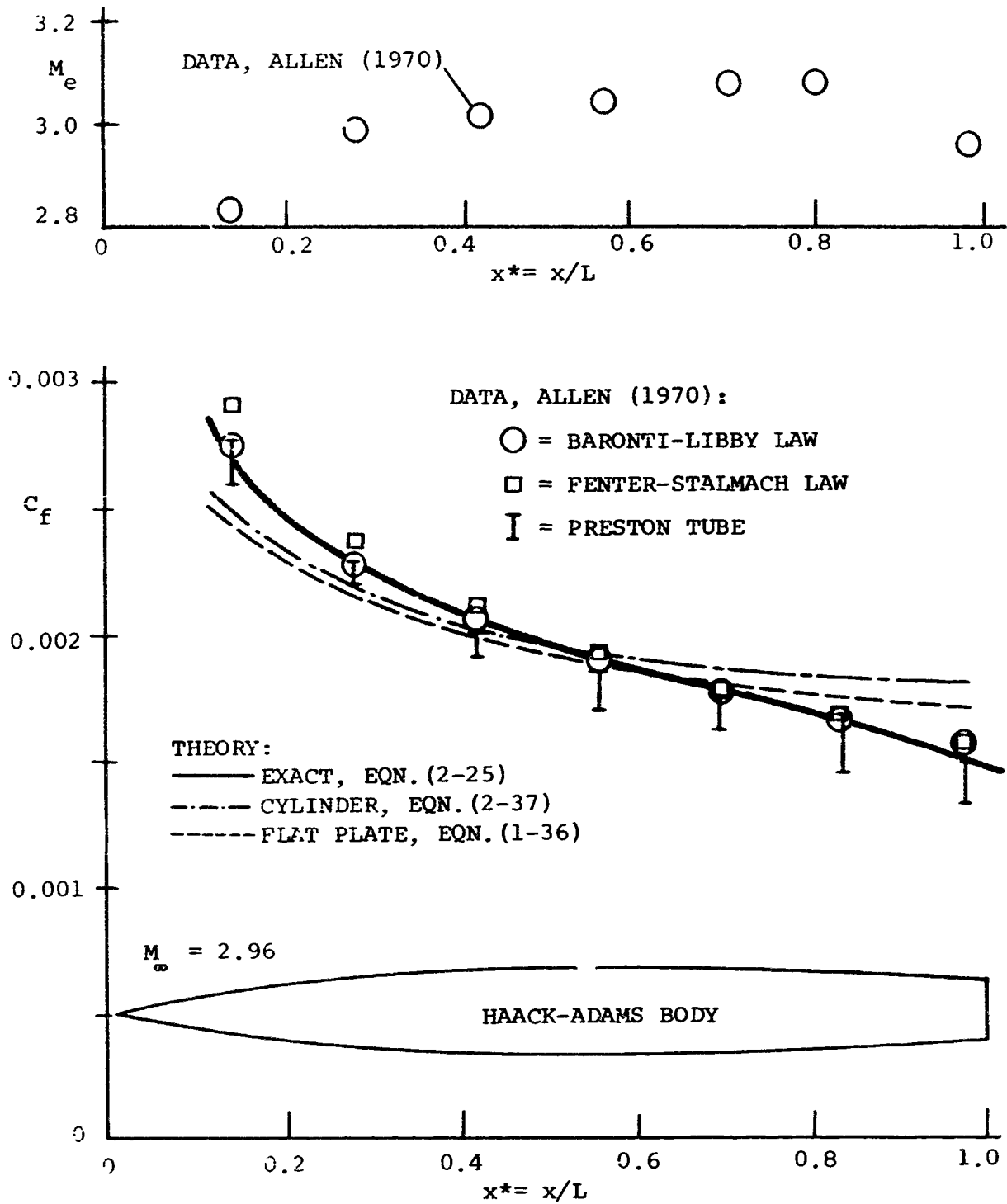


Figure 2.7. COMPARISON OF THEORY AND EXPERIMENT FOR SUPERSONIC FLOW PAST A BODY OF REVOLUTION AFTER ALLEN (1970).

2.5 Summary

This chapter has presented a complete theory for the computation of turbulent skin friction in compressible axisymmetric flow past arbitrary bodies of revolution. The approach leads to a single first order ordinary differential equation, Eqn.(2-25), for $C_f(x)$ and accounts for supersonic flow, nonadiabatic wall temperature, and extremely thick boundary layers, where a transverse curvature correction is necessary. Applications to cylinder flow, cone flow, and flow past a pointed body of revolution all show good agreement with experiment. It is therefore thought that the present theory has no significant deficiencies. Since this theory is also apparently the simplest comparable analysis to be found in the literature, we therefore recommend it to engineers for general usage.

The Prediction of Three Dimensional Skin Friction

3.1 Introduction

The most common type of boundary layer encountered in practice, and the most intractable from the standpoint of analysis, is the three-dimensional turbulent boundary layer. Reviews of the state of the art with respect to this important class of flows have been given by Cocke and Hall (1962), Joubert, Perry and Brown (1967) and more recently by Nash and Patel (1972). Existing theories are few and seem unduly complicated while available experimental data are usually unreliable. Historically, two approaches have been used to analyze three dimensional turbulent boundary layers; the integral approach and the differential approach.

Typical of the integral approach is the work of Smith (1966), and Cumpsty and Head (1967). These authors used two momentum integral equations plus an auxiliary equation to account for variations in the streamwise shape factor. They extended Head's (1958) two-dimensional entrainment relation to three dimensions but retained his two-dimensional empirical functions.

Differential methods have been given by Bradshaw (1971) and Nash (1969); both are extensions of the two-dimensional method of Bradshaw et al (1967) which utilizes the turbulent energy equation. The major difficulty with differential

methods is in the specification of boundary conditions. For a given domain, boundary conditions must be specified along all surfaces where fluid is entering from the outside.

In this chapter a new integral method is developed which greatly reduces the computational difficulties inherent in the calculation of three dimensional skin friction. The analysis results in two coupled, non linear partial differential equations with the skin friction coefficient and the tangent of the angle between the total surface shear stress vector and the shear stress vector in the freestream direction as the only unknowns. This is accomplished by assuming suitable "law-of-the-wall" velocity correlations for both the freestream and cross flow directions and then integrating the governing equations with respect to the law-of-the-wall coordinate y^+ . The resulting partial differential equations may be easily solved by finite difference techniques since they require initial data along only a single curve.

Thus the new method is a compromise between the "classical" integral and differential techniques. It is much more straight-forward and contains considerably less empirical content than the former, and is computationally much simpler than the latter.

At the present time this method is limited to incompressible flows; however, extending it to account for compressibility, heat transfer, and variable fluid properties should be possible in view of chapter 1 of this report and the past

efforts of White and Christoph (1970).

In order to discuss three-dimensional boundary layer flows it is most appropriate to work in a curvilinear coordinate system composed, in part, of the projection of the free streamlines onto the boundary surface. The coordinate along these free streamline curves is designated as s , while the coordinate along the orthogonal trajectories of the free streamlines, in the surface, is designated as n , and the coordinate normal to the surface is designated as y . Corresponding to these three coordinate directions are the metric coefficients h_1 , h_2 , and h_3 , and the mean velocity components u , w , and v respectively. For simplicity, it shall be assumed that the curvature of the bounding surface does not change abruptly and that the boundary layer thickness is small compared with the principal radii of curvature of the bounding surface, so that h_3 may be taken equal to unity and y becomes a simple distance normal to the surface. As a consequence, h_1 and h_2 are known functions of s and n provided that the inviscid flow over the surface is known. This coordinate system is shown in Figure 3.1.

$$\frac{1}{h_1 h_2} \frac{\partial}{\partial s} (h_2 u) + \frac{1}{h_1 h_2} \frac{\partial}{\partial n} (h_1 w) + \frac{\partial v}{\partial y} = 0 \quad , \quad (3-1)$$

the s component of the momentum equation

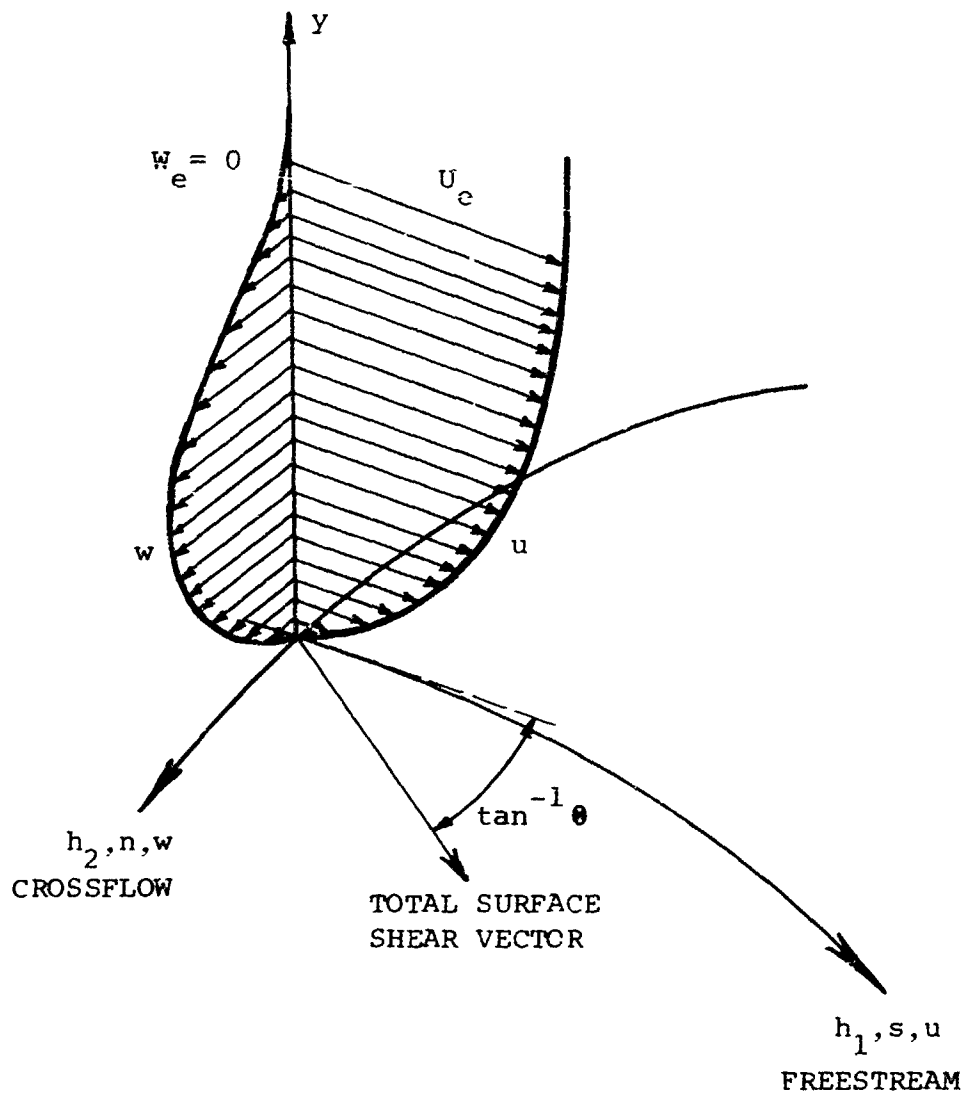


Figure 3.1. THREE-DIMENSIONAL BOUNDARY LAYER
 COORDINATE SYSTEM WITH SKEWING
 IN ONE DIRECTION ONLY.

$$\begin{aligned} \frac{u}{h_1} \frac{\partial u}{\partial s} + \frac{w}{h_2} \frac{\partial u}{\partial n} + v \frac{\partial u}{\partial y} + \frac{uw}{h_1 h_2} \frac{\partial h_1}{\partial n} - \frac{w^2}{h_1 h_2} \frac{\partial h_2}{\partial s} \\ = - \frac{1}{\rho h_1} \frac{\partial p}{\partial s} + \frac{1}{\rho} \frac{\partial \tau_s}{\partial y} \end{aligned} \quad (3-2)$$

and the n component of the momentum equation

$$\begin{aligned} \frac{u}{h_1} \frac{\partial w}{\partial s} + \frac{w}{h_2} \frac{\partial w}{\partial n} + v \frac{\partial w}{\partial y} + \frac{uw}{h_1 h_2} \frac{\partial h_2}{\partial s} - \frac{u^2}{h_1 h_2} \frac{\partial h_1}{\partial n} \\ = - \frac{1}{\rho h_2} \frac{\partial p}{\partial n} + \frac{1}{\rho} \frac{\partial \tau_n}{\partial y} \end{aligned} \quad (3-3)$$

In these equations τ_s and τ_n represent total shearing stresses and include the effects of viscosity and Reynolds stress. Since only incompressible flow is to be considered, the energy equation is not needed.

The distinguishing feature of a three dimensional boundary layer is crossflow (the w component of velocity) and the resulting vector character of the surface shear stress. Crossflow occurs when the freestream streamlines are curved, which gives rise to an unbalanced centrifugal pressure gradient in the boundary layer. Such crossflow imposes a shear stress on the surface, normal to the freestream direction (τ_n), which skews the total surface stress vector. If the direction of curvature of the freestream streamline is reversed, skewing in two lateral directions can occur in a single velocity profile. Typical velocity profiles showing skewing in one and two directions are shown

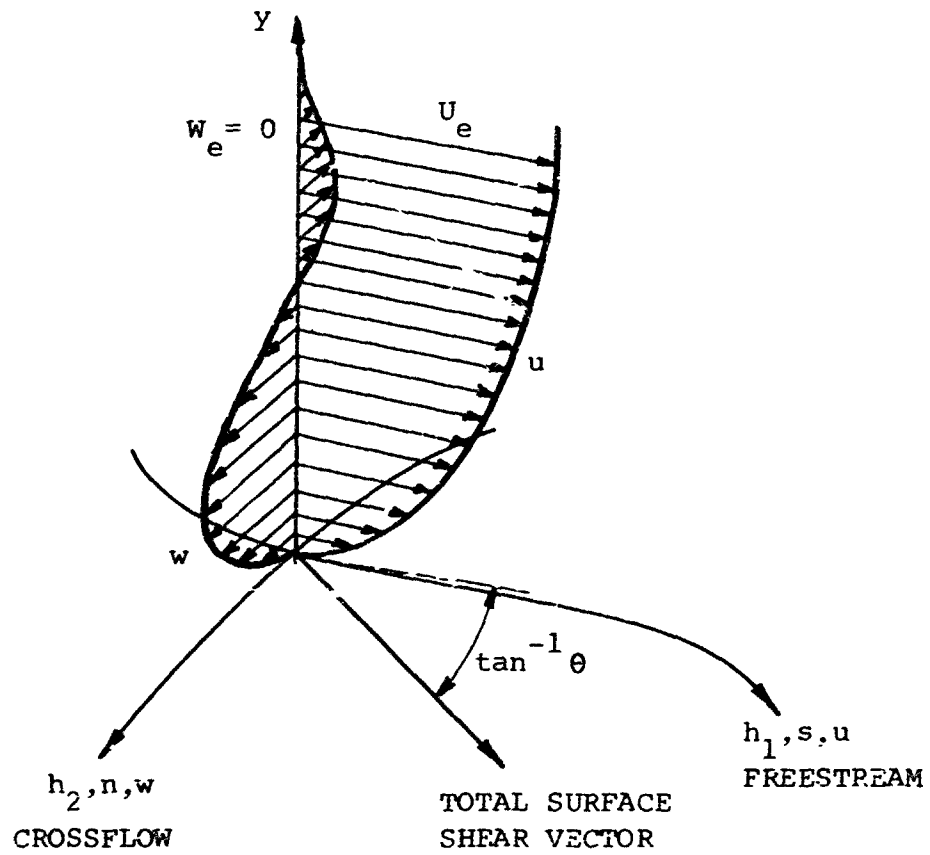


Figure 3.2. THREE-DIMENSIONAL BOUNDARY LAYER
WITH BILATERAL SKEWING.

in Figures 3.1 and 3.2.

Since the present method depends upon an a priori specification of velocity correlations in both the free-stream direction and the crossflow direction it would seem appropriate to discuss these in some detail.

3.2 Specification of Velocity Correlations

In general, integral techniques are insensitive to details of the assumed velocity correlations. However, this does not mean that one can be completely cavalier in their specification. In order to insure that the chosen correlations incorporate the correct physical parameters, consider that near the wall the force balances given by equations (3-2) and (3-3) reduce to

$$\tau_s \doteq \tau_{sw} + \frac{1}{h_1} \frac{\partial p}{\partial s} y \quad (3-4)$$

and

$$\tau_n \doteq \tau_{nw} + \frac{1}{h_2} \frac{\partial p}{\partial n} y \quad (3-5)$$

Assuming that the shear stress in the freestream direction in a three-dimensional boundary layer may be represented by the same eddy viscosity relation as for a two dimensional boundary layer gives

$$\tau_s = \rho \kappa^2 y^2 \left| \frac{\partial u}{\partial y} \right| \frac{\partial u}{\partial y} \quad (3-6)$$

with von Kármán's constant κ equal to 0.4. Nondimensional-

izing equations (3-4) and (3-6) with respect to wall quantities and solving for the velocity gradient gives

$$\frac{\partial u^+}{\partial y^+} = \frac{(1 + \alpha_s y^+)^{1/2}}{\tau_{sw}^+} \quad (3-7)$$

The pressure gradient parameter α_s is defined by

$$\alpha_s = \frac{v}{\tau_{sw} u^*} \frac{1}{h_1} \frac{\partial p}{\partial s} \quad (3-8)$$

where $u^* = (\tau_{sw}/\rho)^{1/2}$ is the shear velocity in the free-stream direction. Equations (3-7) and (3-8) are exactly the same results as have been previously obtained by White and Christoph (1972) for the two-dimensional case; except that here α_s includes the curvilinear scale factor h_1 .

Therefore, it will be assumed that the law-of-the-wall correlation for the streamwise velocity component, in a three-dimensional boundary layer (Eqn. 3-7) does not differ from the two-dimensional correlation. This is a reasonable assumption as has been pointed out by Lesch (1969) and others.

It would be extremely attractive to carry through similar arguments for the crossflow correlation. However, this immediately leads to excessive complication. The reason is that the simple eddy viscosity approximation of equation (3-6) does not appear adequate to describe the crossflow profile. Instead one must invoke a coupled eddy viscosity expression such as suggested by Cousteix, Quemard and Michel (1971):

$$\tau_n = \rho F^2 l^2 \left| \frac{\partial u}{\partial y} \right| \frac{\partial w}{\partial y} \quad (3-9)$$

where F is a sublayer damping factor suggested by van Driest (1956)

$$F = 1 - \exp \left[-\frac{1}{26\kappa\mu} (\tau\rho)^{1/2} \right] \quad (3-10)$$

and

$$l = 0.085 \delta \tanh \left(\frac{\kappa}{0.085} \frac{y}{\delta} \right) \quad (3-11)$$

Nondimensionalizing and combining (3-5) and (3-9)

leads to

$$\frac{\partial w^+}{\partial y^+} = \frac{(\alpha + \alpha_n y^+)}{\left| \frac{\partial u^+}{\partial y^+} \right| l^2 F^2} \quad (3-12)$$

with

$$\alpha_n = \frac{v}{\tau_{nw}} \frac{1}{u^+} \frac{\partial p}{\partial n} \quad (3-13)$$

The symbol α stands for the tangent of the angle between the total surface shear vector and the shear stress vector in the freestream direction.

Expression (3-12) is obviously much too complicated to be tractable as a crossflow velocity correlation. Fortunately an alternative exists in the simple hodograph models, which often give a better representation of the crossflow velocity profile than does (3-12).

The earliest hodograph model was proposed by Prandtl

(1946) who speculated that

$$w = ueg\left(\frac{y}{\delta}\right) \quad (3-14)$$

where g was a function such that $g(0) = 1$ and $g(1) = 0$. He took g to be

$$g\left(\frac{y}{\delta}\right) = 1 - \frac{y}{\delta} \quad (3-15)$$

Mager (1951) suggested a more accurate form in which

$$g\left(\frac{y}{\delta}\right) = \left(1 - \frac{y}{\delta}\right)^2 \quad (3-16)$$

Recently, several more sophisticated hodograph models have been proposed. Johnston (1957) represented the crossflow velocity by a triangular hodograph such that

$$\frac{w}{U_e} = \rho \frac{u}{U_e} \quad ; \quad \frac{u}{U_e} < \left(\frac{u}{U_e}\right)_p \quad (3-17)$$

$$\frac{w}{U_e} = \rho \left(1 - \frac{u}{U_e}\right) \quad ; \quad \frac{u}{U_e} > \left(\frac{u}{U_e}\right)_p \quad (3-$$

where $(u/U_e)_p$ corresponds to the apex of the triangle and is given by

$$\left(\frac{u}{U_e}\right)_p = \left(1 + \frac{\rho}{\tan \beta}\right)^{-1} \quad (3-18)$$

and U_e is the freestream velocity. Johnston's model is sketched in Figure 3-3. This model has several shortcomings. There are situations in which the outer region is not adequately represented by a straight line and there are situations in which the apex of the triangle is not well

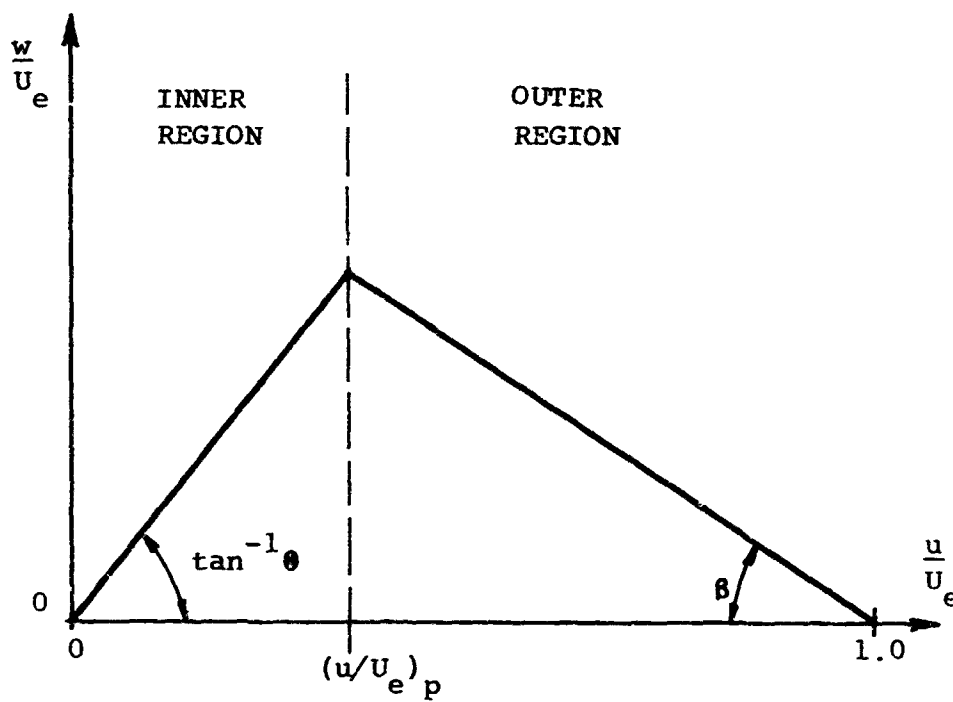


Figure 3.3. SKETCH OF THE TRIANGULAR HODOGRAPH APPROXIMATION, AFTER JOHNSTON (1957).

defined. Also, the experimental determination of β is very difficult due to the fact that the inner region of the model actually corresponds to the viscous sub layer. Eichelbrenner and Peube (1966) modeled the crossflow velocity by a polynomial of the form

$$\frac{w}{U_e} = \frac{u}{U_e} \rho \left[1 + a\left(\frac{u}{U_e}\right) + b\left(\frac{u}{U_e}\right)^2 + c\left(\frac{u}{U_e}\right)^3 + d\left(\frac{u}{U_e}\right)^4 + e\left(\frac{u}{U_e}\right)^5 \right] \quad (3-19)$$

where a,b,c,d,e are evaluated by using boundary conditions at the wall and at the outer edge of the boundary layer. These constants are also extremely difficult to verify experimentally. This model does, however, have the advantage of being able to predict the "S-shaped" crossflows which were discussed in Section 3.1 and observed experimentally by Klinksiek and Pierce (1970).

With these considerations in mind it was decided by the authors to employ the hodograph model as proposed by Mager (1951) in the form

$$\frac{w^+}{u^+} = \rho \left(1 - \frac{u^+}{\beta^+} \right)^2 \quad (3-20)$$

This choice seemed a good compromise between complexity and relative accuracy. In fact this correlation compares well with some experimental data as shown in Figure 3-5. Until such time as more reliable three-dimensional data become available, and in particular profile data, the use of a more sophisticated hodograph model does not seem warranted.

2.3 The Method of Solution

In order to solve equations (3-1), (3-2), and (3-3) they are first nondimensionalized using the shear velocity in the freestream direction. The result is

$$\begin{aligned} & \frac{u^*u^+}{h_1} \frac{\partial}{\partial s} (u^*u^+) + \frac{u^*w^+}{h_2} \frac{\partial}{\partial n} (u^*u^+) + v \frac{u^*}{v} \frac{\partial}{\partial y^+} (u^*u^+) \\ & + u^* \frac{\partial}{\partial s} \left(\frac{u^*w^+}{h_1 h_2} \frac{\partial h_1}{\partial n} \right) - \frac{u^* \frac{\partial}{\partial s} (u^*w^+)}{h_1 h_2} \frac{\partial h_2}{\partial s} = - \frac{1}{\rho h_1} \frac{\partial p}{\partial s} + \frac{u^*}{\rho v} \frac{\partial \tau_s}{\partial y^+} \end{aligned} \quad (3-21)$$

and

$$\begin{aligned} & \frac{u^*u^+}{h_1} \frac{\partial}{\partial s} (u^*u^+) + \frac{u^*w^+}{h_2} \frac{\partial}{\partial n} (u^*w^+) + v \frac{u^*}{v} \frac{\partial}{\partial y^+} (u^*w^+) \\ & + \frac{u^* \frac{\partial}{\partial s} (u^*w^+)}{h_1 h_2} \frac{\partial h_2}{\partial s} - \frac{u^* \frac{\partial}{\partial n} (u^*w^+)}{h_1 h_2} \frac{\partial h_1}{\partial n} = - \frac{1}{\rho h_2} \frac{\partial p}{\partial n} + \frac{u^*}{\rho v} \frac{\partial \tau_n}{\partial y^+} \end{aligned} \quad (3-22)$$

where the velocity v is determined from the continuity equation:

$$v = - \frac{v}{u^*} \int_0^{\delta^+} \left[\frac{1}{h_1 h_2} \frac{\partial}{\partial s} (h_2 u^* u^+) + \frac{1}{h_1 h_2} \frac{\partial}{\partial n} (h_1 u^* w^+) \right] dy^+ \quad (3-23)$$

Expressions for the partial derivatives with respect to both s and n are needed. Note that

$$u^+ = \text{fcn}(y^+, \alpha_s) \quad (3-24)$$

and

$$w^+ = \text{fcn}(y^+, \alpha_s, \theta, \delta^+) \quad (3-25)$$

Therefore,

$$\frac{\partial u^+}{\partial s} = \frac{\partial y^+}{\partial s} \frac{\partial u^+}{\partial y^+} + \frac{\partial \alpha_s}{\partial s} \frac{\partial u^+}{\partial \alpha_s} \quad (3-26)$$

$$\frac{\partial w^+}{\partial s} = \frac{\partial y^+}{\partial s} \frac{\partial w^+}{\partial y^+} + \frac{\partial \alpha_s}{\partial s} \frac{\partial w^+}{\partial \alpha_s} + \frac{\partial \theta}{\partial s} \frac{\partial w^+}{\partial \theta} + \frac{\partial \delta^+}{\partial s} \frac{\partial w^+}{\partial \delta^+} \quad (3-27)$$

plus similar expressions for the n derivatives. For the purpose of skin friction calculations, it is convenient to make the following non-dimensionalizations:

$$\lambda_1 = u_e^+ = (2/C_{fs})^{1/2}, \quad h_1^* = h_1/L, \quad h_2^* = h_2/L, \quad R_L = \frac{U_0 L}{\nu} \quad (2-28)$$

$$V = U_e(s, n)/U_0$$

where L is a reference length, and U_0 is a reference speed.

Then, from the definition of α_s

$$\frac{\partial \alpha_s}{\partial s} = \frac{\partial \alpha_s}{\partial \lambda_1} \frac{\partial \lambda_1}{\partial s} + \frac{\lambda_1^3}{R_L} \frac{\partial^2}{\partial s^2} \quad (1/\nu) \quad (3-29)$$

and

$$\frac{\partial \alpha_s}{\partial n} = \frac{\partial \alpha_s}{\partial \lambda_1} \frac{\partial \lambda_1}{\partial n} + \frac{\lambda_1^3}{R_L} \frac{\partial^2}{\partial n \partial s} \quad (1/\nu) \quad (3-30)$$

The partial derivatives of δ^+ with respect to s and n are more difficult to compute. Equation (3-7) integrates analytically to

$$\begin{aligned} u^+ &= \frac{1}{\kappa} \left[2(p-p_0) + \ln \left(\frac{p-1}{p+1} \frac{p_0+1}{p_0-1} \right) \right] \\ &\doteq \frac{1}{\kappa} \left[2(p-1) + \ln \left(\frac{p-1}{p+1} \left(\frac{4}{\alpha_s y^+} \right) \right) \right] \end{aligned} \quad (3-31)$$

where

$$p = (1 + \alpha_s y^+)^{1/2} .$$

At the edge of the boundary layer, equation (3-31) becomes

$$u_e^+ = \lambda_1 = \frac{1}{\kappa} \left[2(p_\delta - 1) + \ln \left(\frac{p_\delta - 1}{p_\delta + 1} \left(\frac{4}{\alpha_s y_0^+} \right) \right) \right] \quad (3-32)$$

where

$$p_\delta = (1 + \alpha_s \delta^+)^{1/2} .$$

Differentiating equation (3-32) with respect to s and n results in:

$$\frac{\partial \delta^+}{\partial s} = \left[\frac{\kappa(p_\delta - 1)}{\alpha_s p_\delta} \right] \frac{\partial \lambda_1}{\partial s} - \left[\frac{\alpha_s \delta^+ p_\delta^2 - p_\delta^3 + p_\delta}{\alpha_s^2 p_\delta^2} \right] \frac{\partial \alpha_s}{\partial s} \quad (3-33)$$

and a similar expression for the n derivative. Combining equations (3-26), (3-27), (3-29), (3-30), and (3-33) gives:

$$\frac{\partial u^+}{\partial s} = \frac{1}{\lambda_1} \frac{\partial \lambda_1}{\partial s} \left[-y^+ \frac{\partial u^+}{\partial y^+} + 3\alpha_s \frac{\partial u^+}{\partial \alpha} \right] \quad (3-34)$$

$$+ \frac{1}{V} \frac{\partial V}{\partial s} \left[y^+ \frac{\partial u^+}{\partial y^+} \right] + \frac{\lambda_1^3}{R_L} \left[\frac{\partial^2}{\partial s^2} \left(\frac{1}{V} \right) \right] \frac{\partial u^+}{\partial \alpha_s}$$

$$\frac{\partial u^+}{\partial n} = \frac{1}{\lambda_1} \frac{\partial \lambda_1}{\partial n} \left[-y^+ \frac{\partial u^+}{\partial y^+} + 3\alpha_s \frac{\partial u^+}{\partial \alpha} \right] \quad (3-35)$$

$$+ \frac{1}{V} \frac{\partial V}{\partial n} \left[y^+ \frac{\partial u^+}{\partial y^+} \right] + \frac{\lambda_1^3}{R_L} \left[\frac{\partial^2}{\partial n \partial s} \left(\frac{1}{V} \right) \right] \frac{\partial u^+}{\partial \alpha_s}$$

$$\begin{aligned}
\frac{\partial w^+}{\partial s} = & \frac{1}{\lambda_1} \frac{\partial \lambda_1}{\partial s} \left[-y^+ \frac{\partial w^+}{\partial y^+} + 3\alpha_s \frac{\partial w^+}{\partial \alpha_s} + \lambda_1 \frac{\kappa(p_\delta - 1)}{\alpha_s p_\delta} \frac{\partial w^+}{\partial \delta^+} \right. \\
& - 3\alpha_s \left. \frac{(\alpha_s \delta^+ p_\delta^2 - p_\delta^{3+p_\delta})}{\alpha_s^2 p_\delta^2} \frac{\partial w^+}{\partial \delta^+} \right] + \frac{1}{V} \frac{\partial V}{\partial s} \left[y^+ \frac{\partial w^+}{\partial y^+} \right] \quad (3-36) \\
& + \left[\frac{\partial w^+}{\partial \alpha_s} - \frac{(\alpha_s \delta^+ p_\delta^2 - p_\delta^{3+p_\delta})}{\alpha_s^2 p_\delta^2} \frac{\partial w^+}{\partial \delta^+} \right] \frac{\lambda_1^3}{R_L} \frac{\partial^2}{\partial s^2} \left(\frac{1}{V} \right) + \frac{\partial \theta}{\partial s} \frac{\partial w^+}{\partial \theta}
\end{aligned}$$

$$\begin{aligned}
\frac{\partial w^+}{\partial n} = & \frac{1}{\lambda_1} \frac{\partial \lambda_1}{\partial n} \left[-y^+ \frac{\partial w^+}{\partial y^+} + 3\alpha_s \frac{\partial w^+}{\partial \alpha_s} + \lambda_1 \frac{\kappa(p_\delta - 1)}{\alpha_s p_\delta} \frac{\partial w^+}{\partial \delta^+} \right. \\
& - 3\alpha_s \left. \frac{(\alpha_s \delta^+ p_\delta^2 - p_\delta^{3+p_\delta})}{\alpha_s^2 p_\delta^2} \frac{\partial w^+}{\partial \delta^+} \right] + \frac{1}{V} \frac{\partial V}{\partial n} \left[y^+ \frac{\partial w^+}{\partial y^+} \right] \quad (3-37) \\
& + \left[\frac{\partial w^+}{\partial \alpha_s} - \frac{(\alpha_s \delta^+ p_\delta^2 - p_\delta^{3+p_\delta})}{\alpha_s^2 p_\delta^2} \frac{\partial w^+}{\partial \delta^+} \right] \frac{\lambda_1^3}{R_L} \frac{\partial^2}{\partial n \partial s} \left(\frac{1}{V} \right) + \frac{\partial \theta}{\partial n} \frac{\partial w^+}{\partial \theta} .
\end{aligned}$$

After substituting the partial derivatives, equations (3-34) through (3-37), into equations (3-21) and (3-22) and integrating the resulting equations from $y^+ = 0$ ($\tau = \tau_w$) to $y^+ = \delta^+$ ($\tau = 0$), one obtains

$$\begin{aligned}
& \frac{1}{h_1^*} \frac{\partial \lambda_1}{\partial s} (G_1 - 3\alpha_s G_2) + \frac{\lambda_1}{\sqrt{h_1^*}} \frac{\partial V}{\partial s} (\lambda_1^2 \delta^+ - G_1) - \frac{\lambda_1}{\sqrt{h_2^*}} \frac{\partial V}{\partial n} G_3 \\
& + \frac{1}{h_2^*} \frac{\partial \lambda_1}{\partial n} (G_3 - 3\alpha_s G_4 + \lambda_1 G_5) - \frac{\lambda_1^4 G_2}{R_L h_1^*} \frac{\partial^2}{\partial s^2} \left(\frac{1}{V}\right) \\
& - \frac{\lambda_1^4 G_4}{R_L h_2^*} \frac{\partial^2}{\partial s \partial n} \left(\frac{1}{V}\right) + \frac{\lambda_1}{h_2^*} \frac{\partial e}{\partial n} G_6 - \frac{\lambda_1}{h_1^* h_2^*} \frac{\partial h_1^*}{\partial n} G_7 \\
& + \frac{\lambda_1}{h_2^* h_1^*} \frac{\partial h_2^*}{\partial s} G_8 = R_L V
\end{aligned} \tag{3-38}$$

$$\begin{aligned}
& \frac{1}{h_1^*} \frac{\partial \lambda_1}{\partial s} (G_3 - 3\alpha_s G_9 - G_{10}) + \frac{\lambda_1}{\sqrt{h_2^*}} \frac{\partial V}{\partial n} (\lambda_1^2 \delta^+ - G_{11}) - \frac{\lambda_1}{\sqrt{h_1^*}} \frac{\partial V}{\partial s} G_3 \\
& + \frac{1}{h_2^*} \frac{\partial \lambda_1}{\partial n} (G_{11} - 3\alpha_s G_{12} - \lambda_1 G_{13}) - \frac{\lambda_1^4 G_9}{R_L h_1^*} \frac{\partial^2}{\partial s^2} \left(\frac{1}{V}\right) \\
& - \frac{\lambda_1^4 G_{12}}{R_L h_2^*} \frac{\partial^2}{\partial n \partial s} \left(\frac{1}{V}\right) - \frac{\lambda_1}{h_1^*} \frac{\partial e}{\partial s} G_{14} - \frac{\lambda_1}{h_2^*} \frac{\partial e}{\partial n} G_{15} \\
& + \frac{\lambda_1}{h_1^* h_2^*} \frac{\partial h_1^*}{\partial n} G_{16} - \frac{\lambda_1}{h_2^* h_1^*} \frac{\partial h_2^*}{\partial s} G_{17} = e R_L V
\end{aligned} \tag{3-39}$$

The G coefficients in equations (3-38) and (3-39) are defined in terms of quadratures over the velocity correlations and various gradients of the velocity correlations. These are tabulated and evaluated in appendix A.

Equations (3-38) and (3-39) are two, coupled, non-linear, partial differential equations which have for dependent variables only the skin friction coefficient and

the tangent of the angle between the total surface shear stress vector and the shear stress in the freestream direction - no integral thicknesses need be calculated. The inviscid flow solution is assumed known, α_s may be computed from its definition, and δ^+ may be computed from equation (3-32). As should be the case, equation (3-38) reduces to the incompressible, two-dimensional analysis of White (1969) when $\frac{\partial}{h_2^* \partial n} = 0$, $w^+ = 0$, and $\frac{\partial}{h_1^* \partial s} = \frac{\partial}{\partial x^*}$.

3.4 Comparison with Experiment

3.4.1 The Rotating Disk Problem

A convenient starting point to test the validity of any three-dimensional theory is the problem of a smooth plane disk rotating in an otherwise stationary fluid. While axisymmetric, this problem exhibits the essential feature of a three-dimensional flow, namely crossflow and the resulting vector character of the surface shear stress. The present theory has been applied to the rotating disk problem in a paper by Lessmann and Christoph (1972) and is discussed below.

The boundary layer equations, equations (3-1), (3-2) and (3-3), may be reduced to those governing the boundary layer flow on a rotating disk by identifying s with the coordinate θ_1 and n with the coordinate r , both fixed in space. The metric coefficients become $h_1 = r$ and $h_2 = 1$ and the equations reduce to

$$\frac{1}{r} \frac{\partial}{\partial r} (rw) + \frac{\partial V}{\partial y} = 0 \quad (3-40)$$

$$w \frac{\partial u}{\partial r} + v \frac{\partial u}{\partial y} + \frac{uw}{r} = \frac{1}{\rho} \frac{\partial \tau}{\partial y} \theta_1 \quad (3-41)$$

and

$$w \frac{\partial w}{\partial r} + v \frac{\partial w}{\partial y} - \frac{u^2}{r} = -\frac{1}{\rho} \frac{\partial p}{\partial r} + \frac{1}{\rho} \frac{\partial \tau}{\partial y} r \quad (3-42)$$

All derivatives with respect to θ_1 have been eliminated because of symmetry.

The boundary conditions on the equations are that at the rotating plate $v=w=0$ and $u=-r\Omega$. Here Ω is the angular velocity of the rotating disk, assumed counterclockwise about the y axis. In the freestream u , v , and w as well as the shearing stresses are zero. As a consequence of this

$$\frac{\partial p}{\partial r} = 0 \quad (3-43)$$

For what follows, it will be convenient to transform equations (3-41) and (3-42) so as to obtain more conventional boundary conditions. Defining a new circumferential velocity as

$$u' = u + r\Omega \quad (3-44)$$

the boundary conditions at the plate become $u' = v=w=0$ and in the freestream $v=w=0$ while $u' = r\Omega$. Using equation (3-44) equations (3-41) and (3-42) become

$$w \frac{\partial u'}{\partial r} + v \frac{\partial u'}{\partial y} + \frac{u'w}{r} - 2\Omega w = \frac{1}{\rho} \frac{\partial \tau}{\partial y} \theta_1 \quad , \quad (3-45)$$

and

$$w \frac{\partial w}{\partial r} + v \frac{\partial w}{\partial y} + 2\Omega u' - r\Omega^2 = \frac{1}{\rho} \frac{\partial \tau_r}{\partial y} \quad . \quad (3-46)$$

Mager's crossflow velocity correlation, equation (3-20), will be used and since $\alpha_s = 0$,

$$u^+ = 2.5 \ln(y^+) + 5.5 \quad (3-47)$$

will be used for the streamwise velocity. Comparison of these two velocity correlations with the data of Cham and Head (1969) is shown in Figures 3-4 and 3-5. The velocity v is eliminated from equations (3-45) and (3-46) by the continuity equation, and the resulting equations are non-dimensionalized with respect to wall variables. For convenience u^* is related to the circumferential skin friction coefficient by

$$\lambda_1 = (2/c_{fs})^{1/2} = \frac{r\Omega}{u^*} \quad (3-48)$$

and r is non-dimensionalized by the relation

$$n = r(\Omega/v)^{1/2} \quad . \quad (3-49)$$

Note that n is the square root of the radial Reynolds number. In integrating the two momentum equations from $y^+ = 0$ to $y^+ = \delta^+$, the shear velocity in the radial direction, $v^* = (\tau_{rw}/\rho)^{1/2}$, will appear. The shear velocity

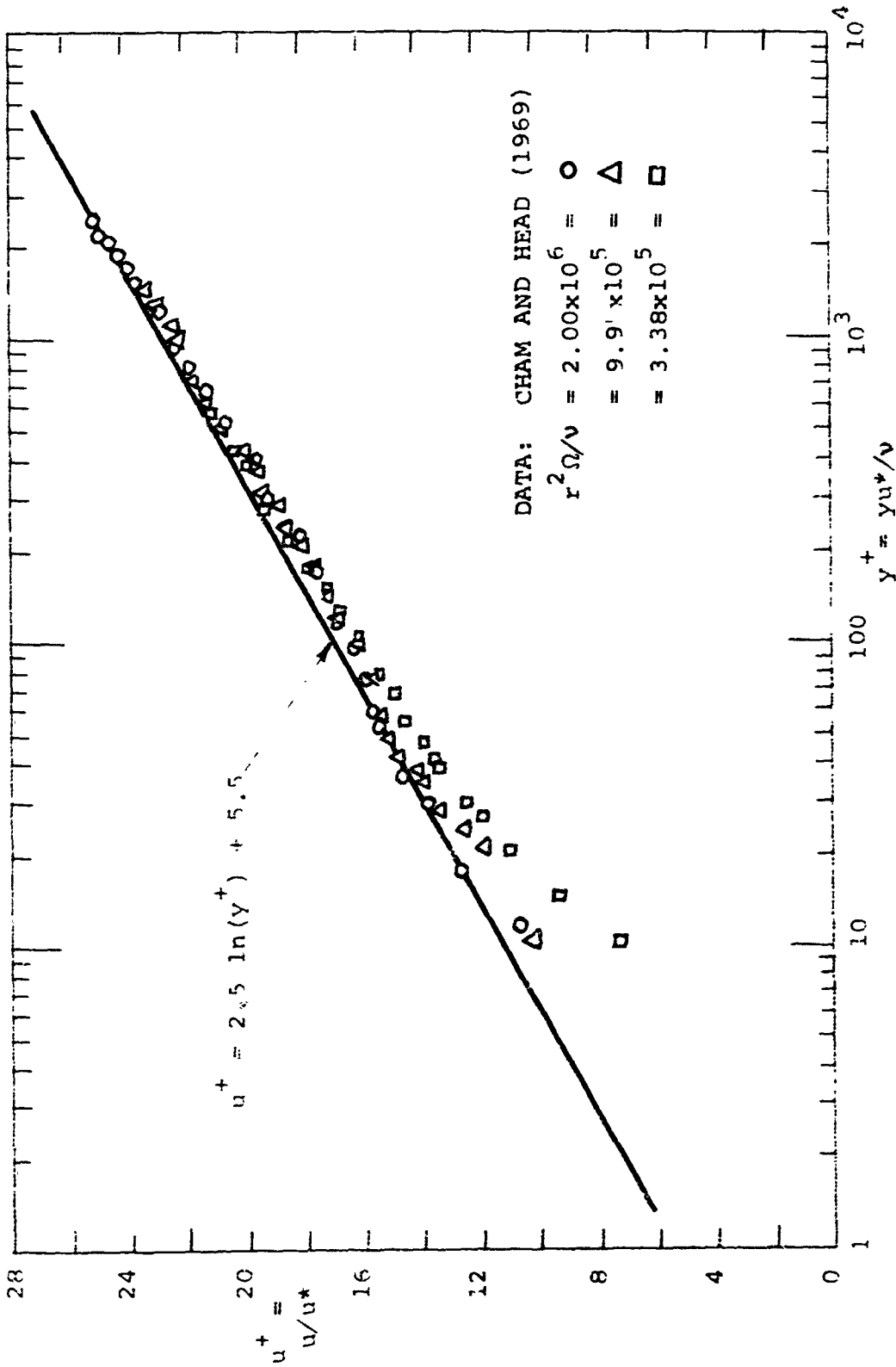


FIGURE 3.4. VERIFICATION OF THE STREAMWISE LAW-OF-THE-WALL FOR TURBULENT FLOW ON A ROTATING DISC.

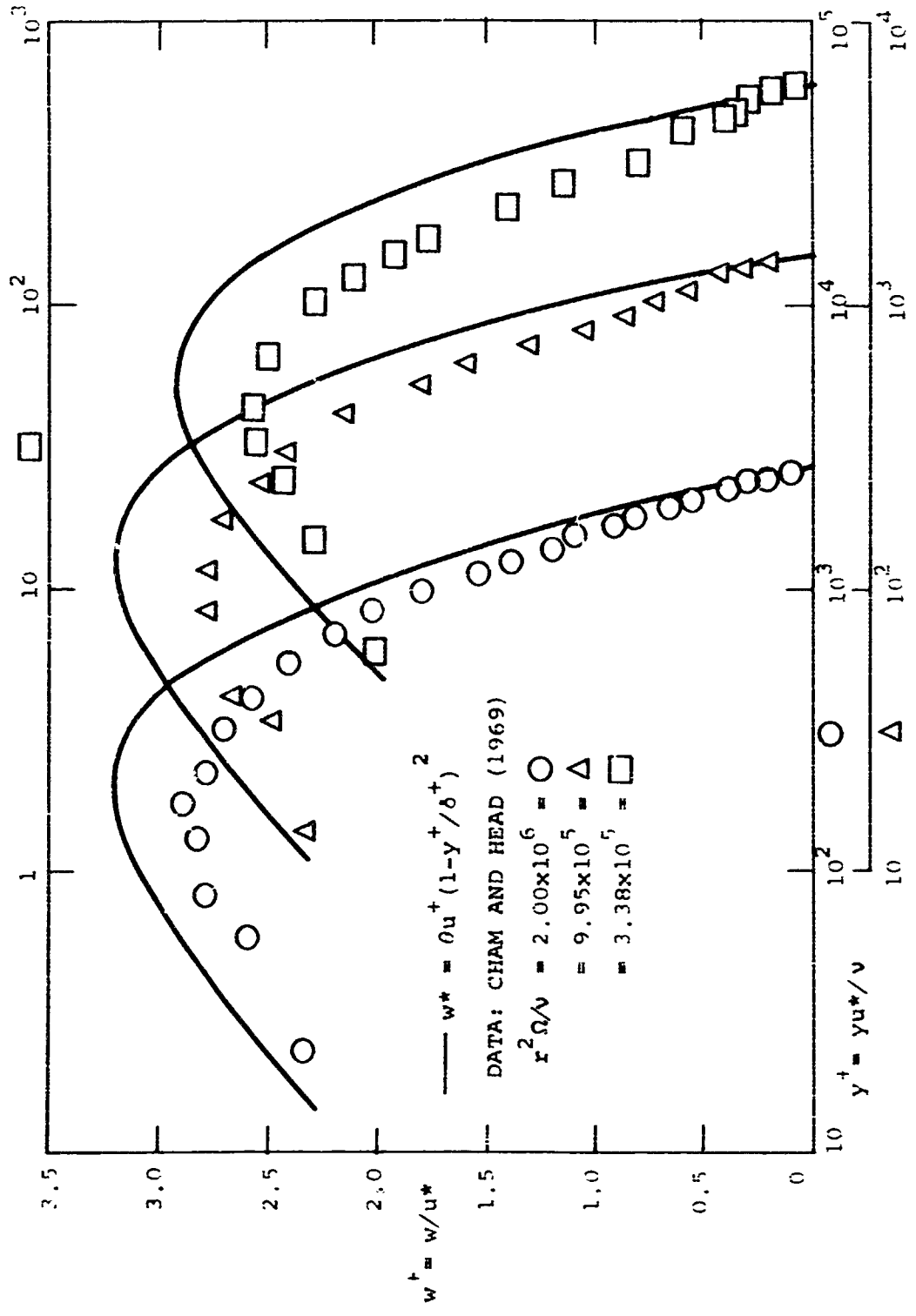


Figure 3.5. VERIFICATION OF MAGER'S HOLOGRAPH FOR ROTATING DISC FLOW.

v^* is eliminated in favor of u^* by the expression

$$\sigma = (v^*/u^*)^2 \quad (3-50)$$

The result is

$$E_1 \frac{d\lambda_1}{d\eta} + D_2 \frac{d\theta}{d\eta} + D_3 = \eta^2 \quad (3-51)$$

and

$$E_4 \frac{d\lambda_1}{d\eta} + E_5 \frac{d\theta}{d\eta} + D_6 = \theta \eta^2 \quad (3-52)$$

where

$$\begin{aligned} D_1 &= \int_0^{\delta^+} (\nu^+ w^+ + \kappa \lambda_1 \epsilon^+ \frac{\partial u^+}{\partial y^+} \int_0^{y^+} \frac{\partial w^+}{\partial \delta^+} dy^+) dy^+ \\ &= \epsilon \delta^+ (0.61 \lambda_1^2 - 3.95 \lambda_1 + 9.84) \end{aligned} \quad (3-53)$$

$$\begin{aligned} D_2 &= \lambda_1 \int_0^{\delta^+} \frac{\partial u^+}{\partial y^+} \left(\int_0^{y^+} \frac{\partial w^+}{\partial \delta^+} dy^+ \right) dy^+ \\ &= \delta^+ \lambda_1 (1.53 \lambda_1 - 9.84) \end{aligned} \quad (3-54)$$

$$\begin{aligned} D_3 &= \lambda_1 \int_0^{\delta^+} ((2u^+ - 2\lambda_1)w^+ - \frac{\partial u^+}{\partial y^+} \int_0^{y^+} w^+ dy^+) dy^+ \\ &= \epsilon \delta^+ \lambda_1 (4.58 \lambda_1 - 29.5) \end{aligned} \quad (3-55)$$

$$D_4 = \int_0^{\delta^+} \left(w^{+2} - \kappa \lambda_1 \delta^+ w^+ \frac{\partial w^+}{\partial \delta^+} + \kappa \lambda_1 \delta^+ \frac{\partial w^+}{\partial y^+} \right. \\ \left. - \int_0^{\delta^+} \frac{\partial w^+}{\partial \delta^+} dy^+ \right) dy^+ \quad (3-56)$$

$$\approx \delta^{+3} (8.33 - 3.41 \lambda_1 + 1.60 \lambda_1^2 - 0.08 \lambda_1^3),$$

$$D_5 = \lambda_1 \int_0^{\delta^+} \left(v^+ \frac{\partial w^+}{\partial \delta^+} - \frac{\partial w^+}{\partial y^+} \frac{\partial v^+}{\partial \delta^+} \right) dy^+; dy^- \quad (3-57)$$

$$\approx \delta^{+3} \lambda_1 (0.40 \lambda_1^2 - 5.00 \lambda_1 + 18.70)$$

$$D_6 = \lambda_1 \int_0^{\delta^+} \left(w^{+2} + 2\lambda_1 u^+ v^+ - u^{+2} - \frac{\partial w^+}{\partial y^+} \frac{\partial v^+}{\partial \delta^+} \right) dy^+ \quad (3-58)$$

$$\approx 12.50 \lambda_1 \delta^{+3} - \delta^{+2} \lambda_1 (18.75 - 5.00 \lambda_1 - 0.40 \lambda_1^2)$$

This problem reduces to the consideration of coupled ordinary differential equations as a result of the fact that the rotating disk is a two-coordinate problem.

The results of the present analysis consist of predictions, using equations (3-51) and (3-52), for the circumferential skin friction coefficient $c_{f\theta}$, and the ratio of the crossflow shearing stress to the circumferential shearing stress, δ . These are compared with experimental results in Figures 3-6 and 3-7. Figure 3-6 shows that the present calculation of $c_{f\theta}$ compares very favorably with the

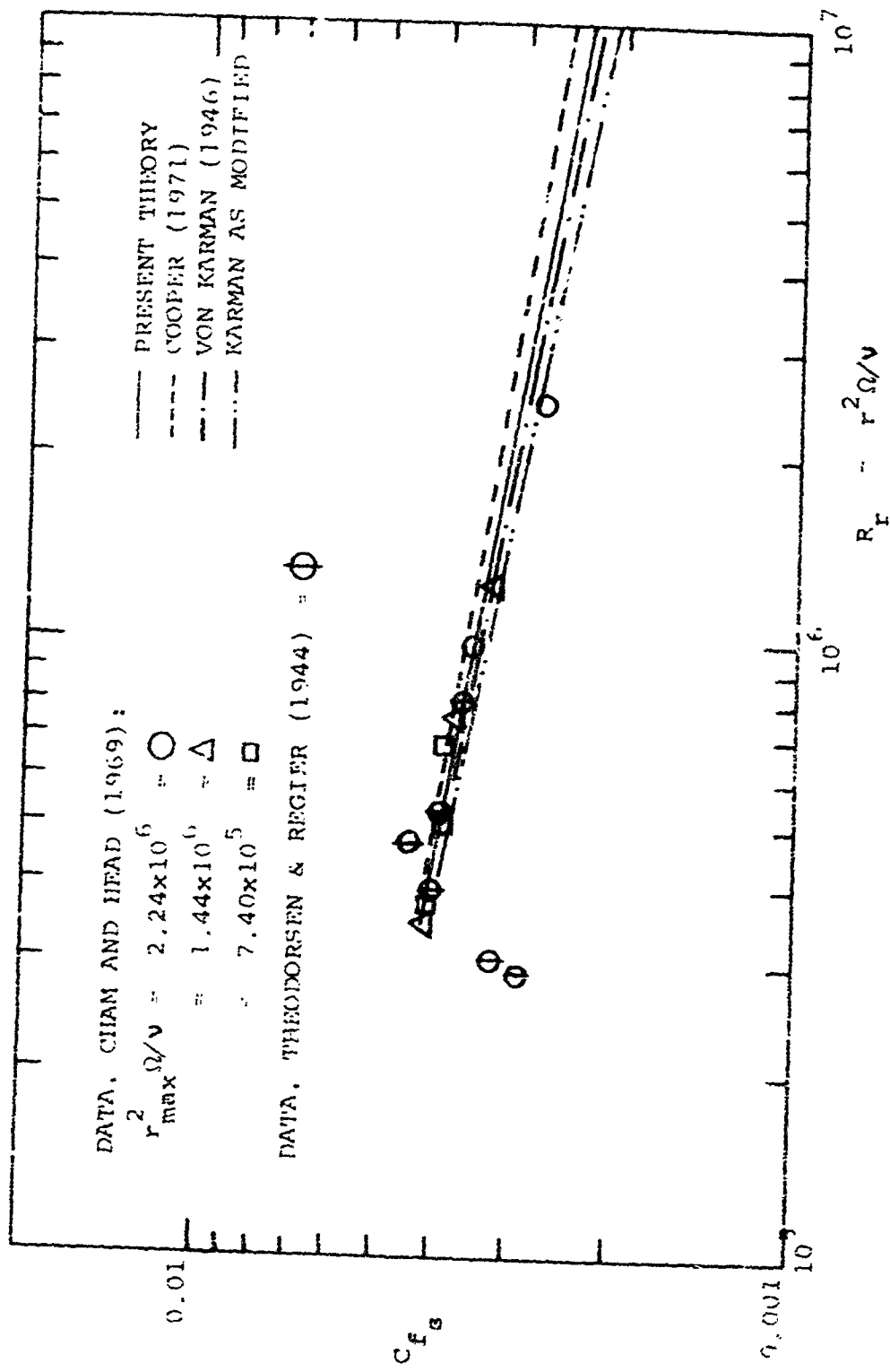


Figure 3.6. COMPARISON OF THEORY AND EXPERIMENT FOR STREAMWISE SKIN FRICTION ON A ROTATING DISC.

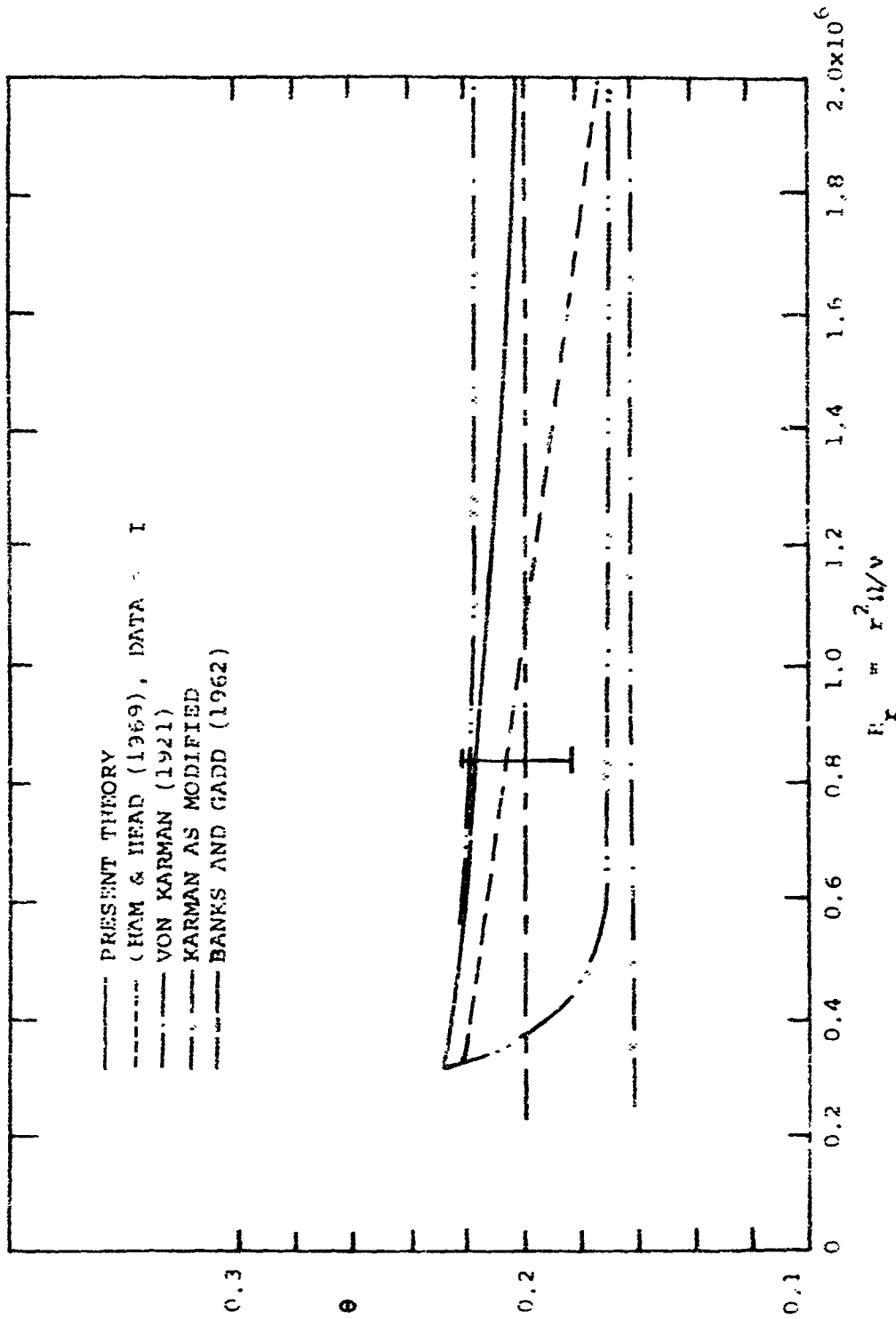


Figure 3.7. COMPARISON OF THEORY AND EXPERIMENT FOR THE WALL
STREAMLINE TANGENT ON A ROTATING DISC.

experimental data and falls approximately halfway between the results of Cooper (1971) and von Karman (1946). Cooper used a finite difference scheme based on the work of Smith and Gebeci (1966,1971). Figure 3-7 is reproduced from the work of Cham and Head (1969) and compares several predictions for α with one measured value. Unfortunately, the uncertainty associated with this single data point is relatively large. With this in mind, it can be seen that the present theory, as well as the entrainment method of Cham and Head (1969), and the prediction of Banks and Gadd (1962) give plausible results. Both the present calculation and that of Cham and Head show a tendency to fall with increasing radial Reynolds number, while the prediction of Banks and Gadd (1962) is for a constant value of α . Cooper (1971) did not concern himself with predicting total shear and hence no comparison with his work is possible on this point.

Since the present approach and the analysis of von Karman (1946) are integral methods it is informative to consider both the similarities and important differences between these two works. The velocity correlations used by von Karman are (in the present notation)

$$u = r\Omega(y/\delta)^{1/7} \quad (3-59)$$

and

$$w = \theta u(1-y/\delta) \quad (3-60)$$

These are to be compared with equations (3-47) and (3-20). It is well known that the 1/7 power law gives a good representation of fully turbulent velocity profiles; at least for a limited range of Reynolds number. This fact accounts for the relatively good agreement with the circumferential skin friction data. At the same time, the crossflow correlation used by von Kármán does not give a good representation of the radial velocity profile as is shown in Figure (3-8). Also, in order to get an exact solution of his equations, von Kármán assumed θ to be constant and the boundary layer thickness δ proportional to $r^{3/5}$. These facts account for the relatively poor prediction of $\theta = 0.162$. In order to carry through the calculation following von Kármán, one must express the wall shear stresses $\tau_{\theta w}$ and τ_{rw} as functions of θ and δ . This is in contrast to the present analysis in which the dependent variables are θ and the circumferential skin friction coefficient. No shear stress correlations are necessary. One can carry out von Kármán's analysis retaining the r dependence of θ and δ and also consider the effect of replacing (3-60) with Mager's correlation. As is shown in Figure 3-6, both of these lead to essentially the same skin friction curve, which is somewhat low. The effects of these changes on the prediction of θ is more drastic as shown in Figure 3-7. When one keeps the original velocity correlation but allows for r variation, the result is a

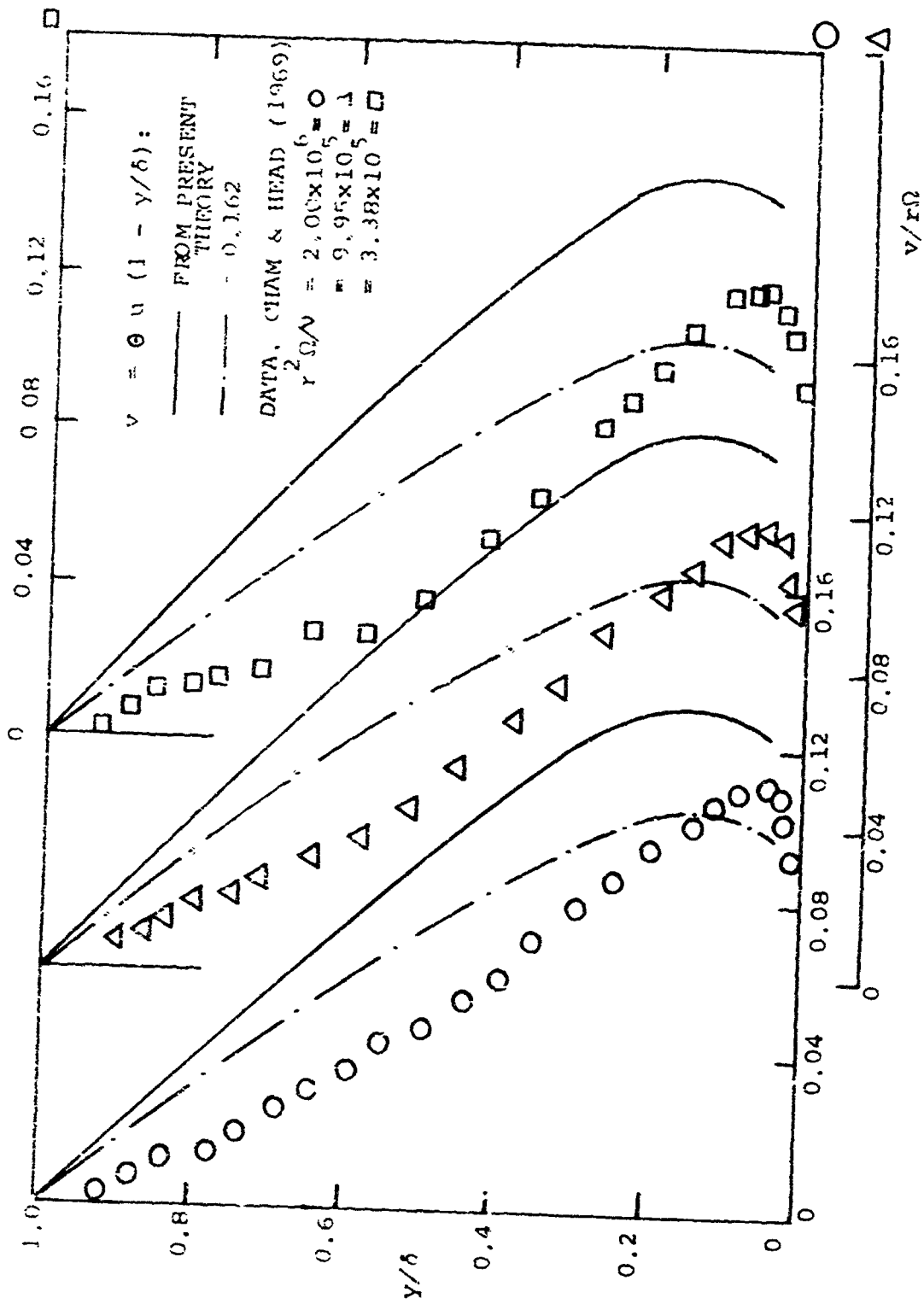


Figure 3.8. COMPARISON OF ROTATING DISC CROSSFLOW VELOCITY PROFILES WITH THE HODOGRAPH OF VON KARMAN (1946).

curve which falls rapidly to an asymptotic behavior approaching $\theta = 0.162$. Using Mager's correlation with von Kármán's approach gives a prediction for θ which agrees closely with the present method for small Reynolds number and becomes asymptotic to $\theta = 0.217$ for higher Reynolds number. Apparently this difference is due to the fact that the logarithmic law-of-the-wall properly accounts for Reynolds number variation, while the $1/7$ power law does not.

It should be pointed out that all calculations of θ in the present study assumed an initial value of $\theta = 0.228$. This initial value was chosen so as to generate a monotonic curve for θ as a function of r . It was found that perturbing this initial condition caused the calculation to rapidly converge to the curve shown in Figure 3-7.

3.4.2 Johnston's Swept, Forward-Facing Step

Johnston (1970) experimentally investigated the flow over a two inch high rectangular step, swept at forty five degrees to the main flow direction. While an example of a fully three-dimensional situation, this flow is not strictly a boundary layer due to the large variation of pressure in the normal direction. For the purpose of the present analysis the "freestream" velocity distribution was determined by fitting a polynomial to Johnston's pressure coefficient data. Three different such distributions were

considered, one corresponding to the wall pressure coefficient, one to the vertically averaged pressure coefficient, and one assuming a constant "freestream" velocity. As expected, use of the average pressure coefficient gave the best results but none of the calculations agreed well with the data.

Bradshaw (1971) also analyzed Johnston's data using a finite difference scheme. His calculations, using the wall pressure coefficient, showed similar behavior to the present results. In order to overcome this difficulty Bradshaw determined the local value of the "freestream" pressure gradient from the two-dimensional pressure coefficient data given by Johnston. With this additional complication Bradshaw's final results agreed fairly well with the data except in the region close to separation. In this context, separation refers to the condition where the surface flow in this "boundary layer" has become parallel to the step.

The present analysis follows directly from equations (3-38) and (3-39). Making the assumption that the sweep is infinite, and hence that all variations parallel to the step are zero, related derivatives in the s and n directions by

$$\frac{\lambda}{\lambda s} = \frac{\lambda}{\lambda n} \quad (3-61)$$

Also the metric coefficients h_1 and h_2 are equal to unity. These simplifications result in two ordinary differential

equations for λ_1 and θ as functions of $s^* = s/L$. The characteristic length L is taken to be the distance from the step to the initial point of the calculation, along the "freestream line".

The results of this analysis are shown on Figures 3-9 and 3-10. Also, Bradshaw's finite difference calculation is displayed for comparison. On Figure 3-9, it can be seen that use of the vertically averaged pressure coefficient gives good agreement with the skin friction up to about $s^* = 0.8$. The calculation using the wall pressure coefficient is low while use of a constant free stream velocity gives results which are much too high. Bradshaw's results are also in good agreement but extend as far as $s^* = 0.85$. None of these predictions agree with the measured separation, which occurs at about $s^* = 0.93$.

Figure 3-10 shows a comparison between the present theory and Johnston's data for θ . Again the average pressure gradient case gives the best agreement but predicts separation too early. Bradshaw's calculation is somewhat better but also shows early separation.

These results should not be construed as indicating some intrinsic deficiency in the present theory, since this flow is not truly a boundary layer flow. Actually, in order to accurately predict the swept step flow field one should use the full Navier-Stokes equations and not the boundary layer equations.

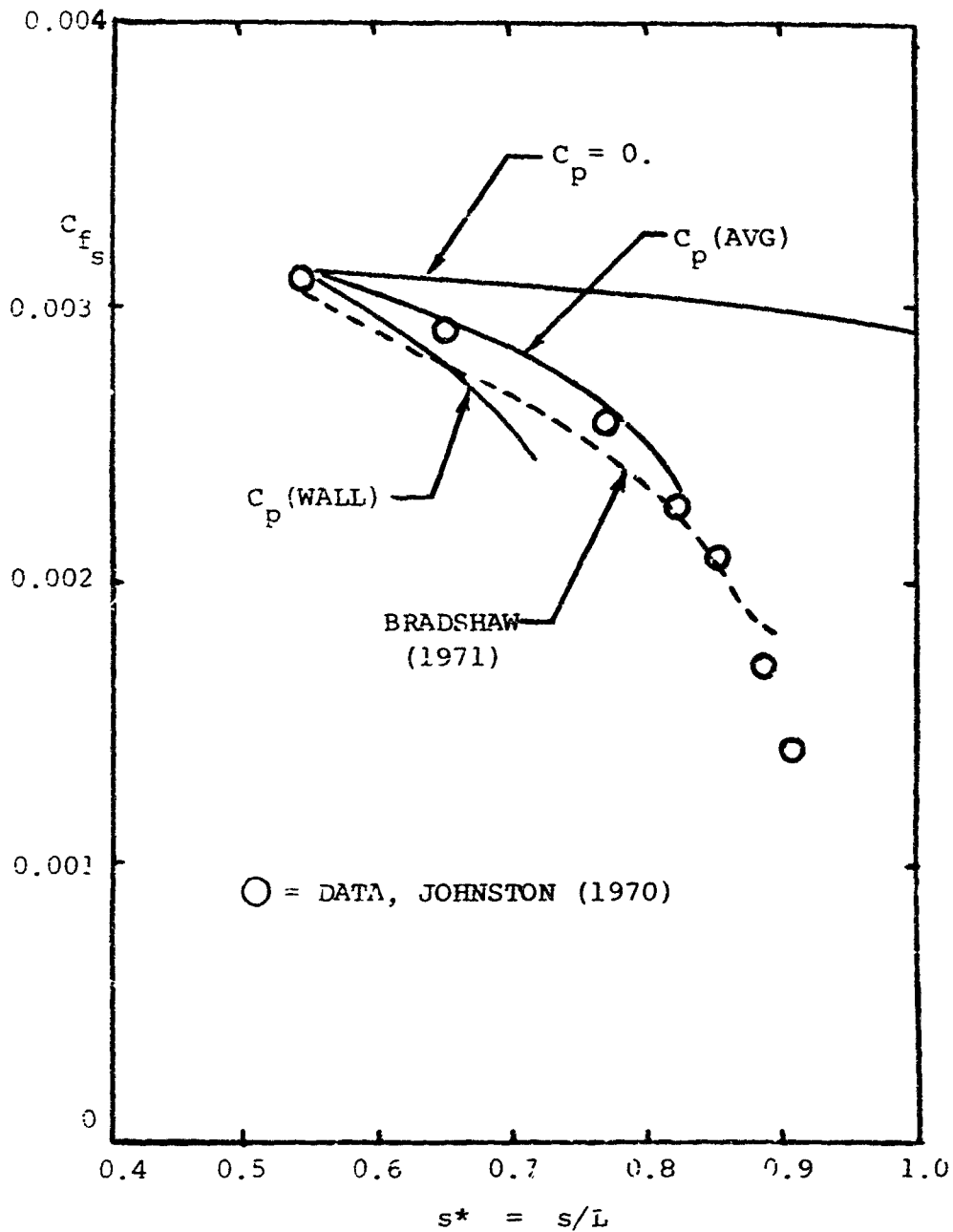


Figure 3.9. COMPARISON OF PRESENT THEORY FOR THREE PRESSURE DISTRIBUTION ASSUMPTIONS WITH THE STREAMWISE SKIN FRICTION DATA OF JOHNSTON (1970) FOR FLOW NEAR A 45° SWEEPED STEP.

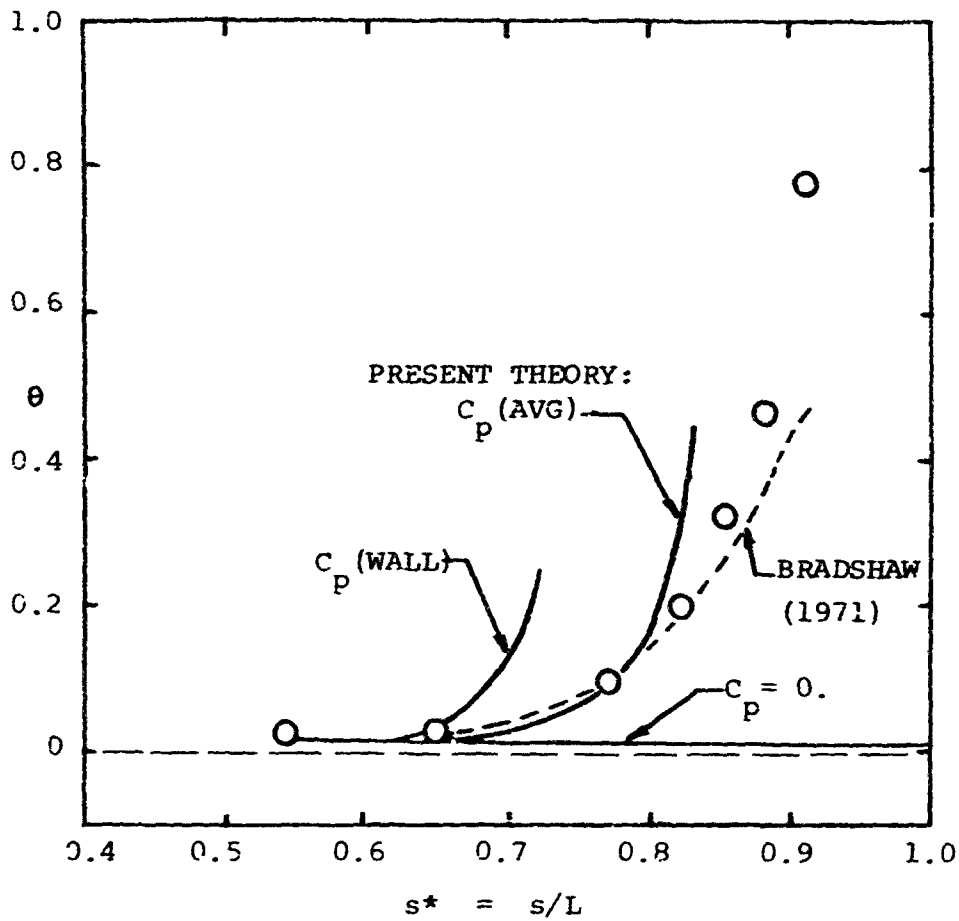


Figure 3.10. COMPARISON OF PRESENT THEORY FOR THREE PRESSURE DISTRIBUTION ASSUMPTIONS WITH THE WALL STREAMLINE TANGENT DATA OF JOHNSTON (1970) FOR FLOW NEAR A SWEEPED STEP.

3.4.3 Data of Francis and Pierce

Francis and Pierce (1967) measured α , the tangent of the angle between the total surface shear stress vector and the shear stress in the freestream direction, in a rectangular channel. The 10 inch wide channel consisted of a 48 inch straight inlet section followed by a curved section of either a 55 inch centerline radius of curvature (referred to as series 5) or a 25 inch centerline radius of curvature (referred to as series 2) and a 48 inch straight discharge section. Most of the measurements were taken on the centerline but a few of the measurements were taken 2 inches either side of the centerline. The Reynolds number was $1.07 \pm 0.03 \times 10^6$ per foot for both series 5 and series 2. The freestream velocity variation was about 0.3 percent per foot, while the crossflow velocity variation was from 30 to 54 percent per foot in the radial direction. This experiment provides the possibility of examining effects produced by a crossflow pressure gradient without the influence of a strong pressure gradient in the freestream flow direction.

Equations (3-38) and (3-39) are solved with the following simplifications:

$$\alpha_s = 0, \quad \frac{1}{h_1} \frac{\partial}{\partial s} = \frac{\partial}{\partial x^*}, \quad \frac{1}{h_2} \frac{\partial}{\partial n} = \frac{\partial}{\partial y^*}, \quad \frac{1}{h_1} \frac{\partial v}{\partial s} = 0, \quad (3-67)$$

$$\frac{1}{h_2 h_1} \frac{\partial h_2^*}{\partial s} = 0, \quad - \frac{1}{h_1 h_2} \frac{\partial h_1}{\partial n} = - \frac{1}{\rho U_e^2} \frac{\partial p}{\partial y^*} = \frac{1}{R^*}$$

Multiple copies of this report are available from the NTIS Document Supply Center, Springfield, Virginia 22161

where x^* , y^* , and R^* are respectively the streamwise flow direction, the direction normal to the streamwise flow direction, and the radius of curvature, all non-dimensionalized with respect to the length of the channel. This results in two coupled partial differential equations for λ_1 and ρ as functions of x^* and y^* . It is assumed that λ_1 and ρ are known along some initial line x_0^* - no side boundary conditions need be known. The partial derivatives occurring in these equations may be numerically approximated in a number of ways. For illustrative purposes, they were calculated by forward differences. Backward or central differences could have been used just as easily. Also, if more accuracy is desired it is possible to keep correcting $\frac{\partial \lambda_1}{\partial y^*}$ and $\frac{\partial \rho}{\partial y^*}$ with their average values iteratively.

The results of these calculations for the center streamline are compared to the measured values of ρ and to the skin friction as computed by Francis and Pierce using the Ludwig and Tillmann (1950) shear law, as shown in Figures 3-11, 3-12, 3-13, and 3-14. Agreement with the data over about the first half of both channels is quite good, but then the theory and the data diverge. The skin friction as computed by the present theory is lower than that computed by the Ludwig and Tillmann law, and the theoretical values of ρ are considerably higher than the measured values. One possible reason for these discrepancies is that Mager's profile may not adequately represent Francis and Pierce's data. Shanebrook and Hatch (1970) suggested a more

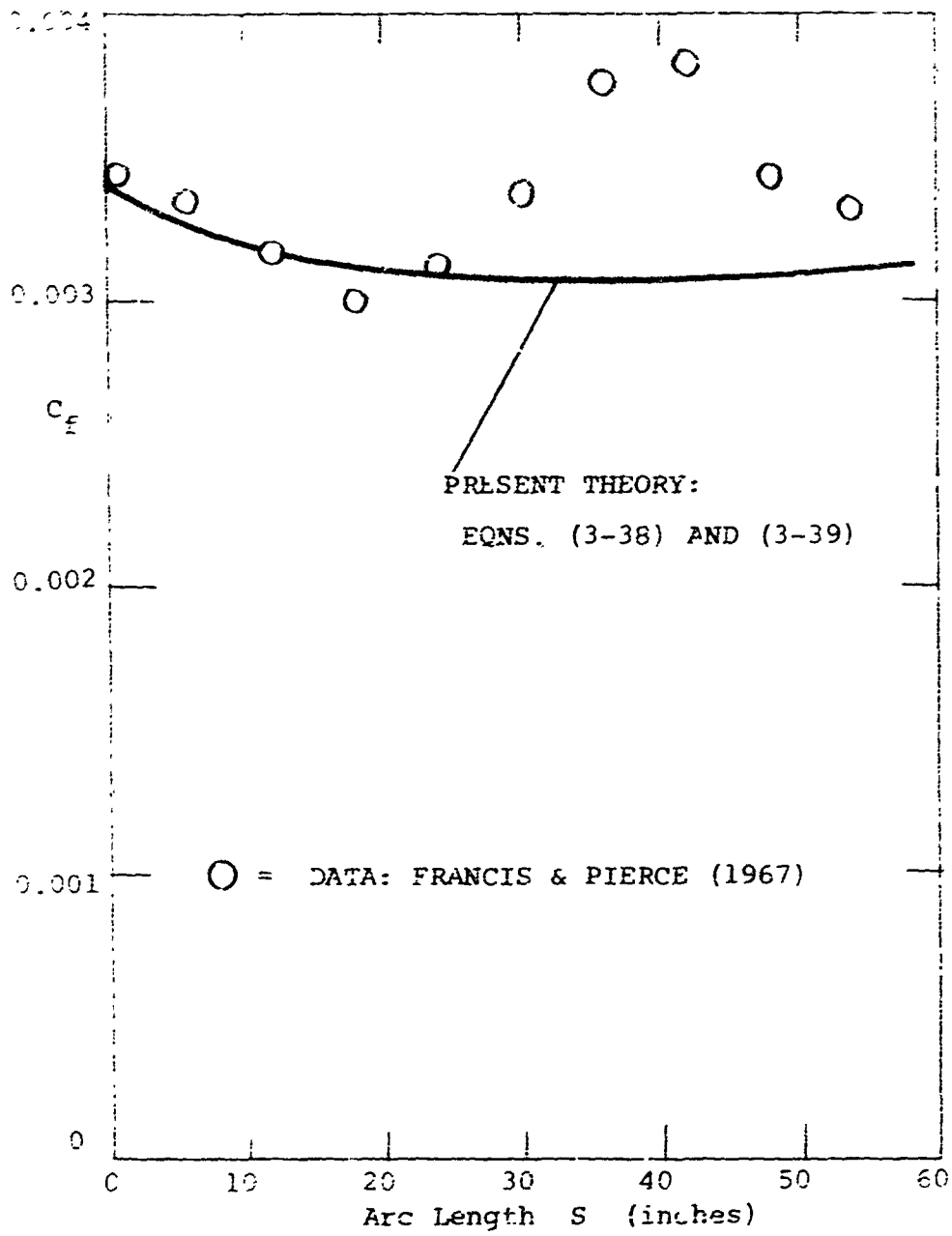


Figure 3-11. COMPARISON OF PRESENT THEORY WITH THE CURVED DUCT EXPERIMENT OF FRANCIS AND PIERCE (1967), SERIES 5.

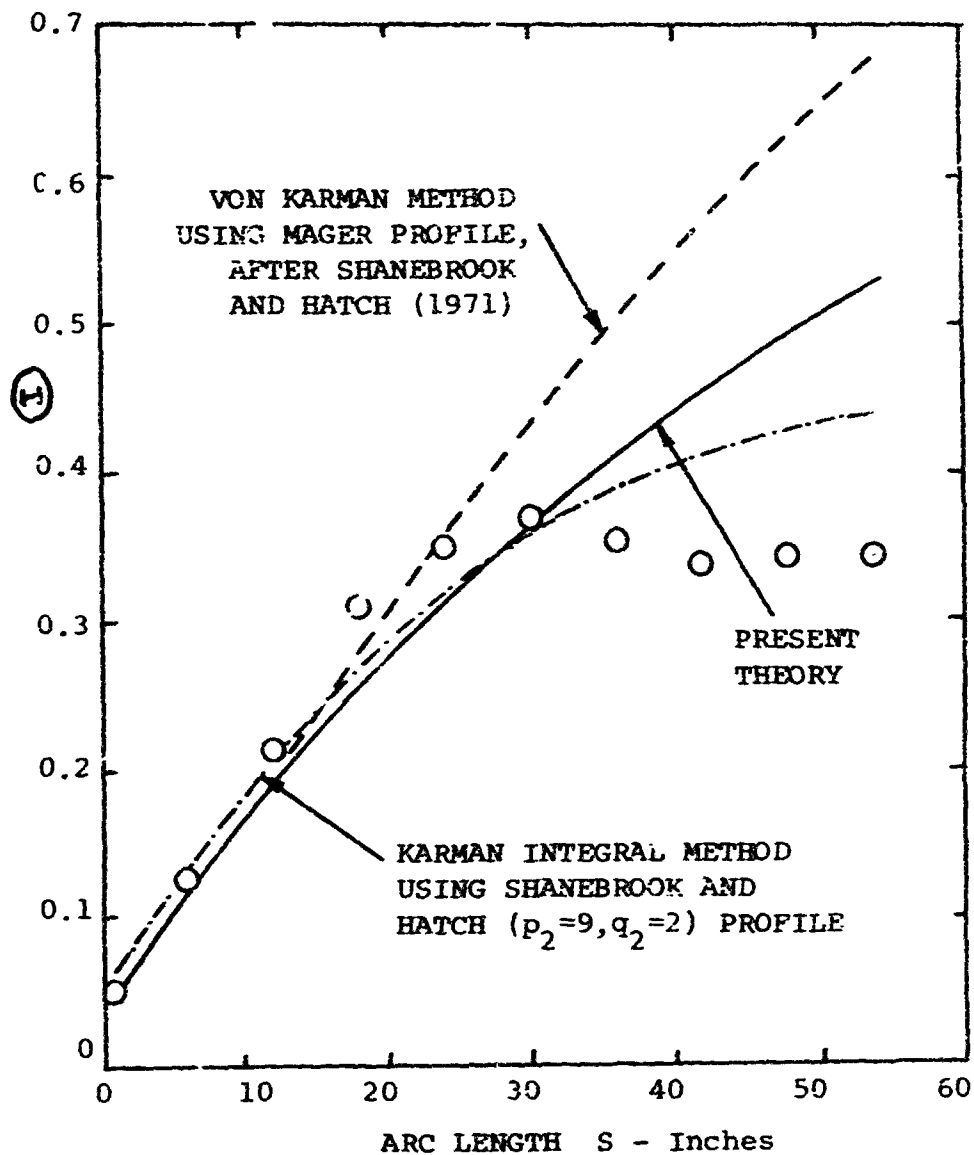


Figure 3-12. COMPARISON OF THEORY WITH WALL STREAMLINE TANGENT DATA OF FRANCIS AND PIERCE (1967), SERIES 5.

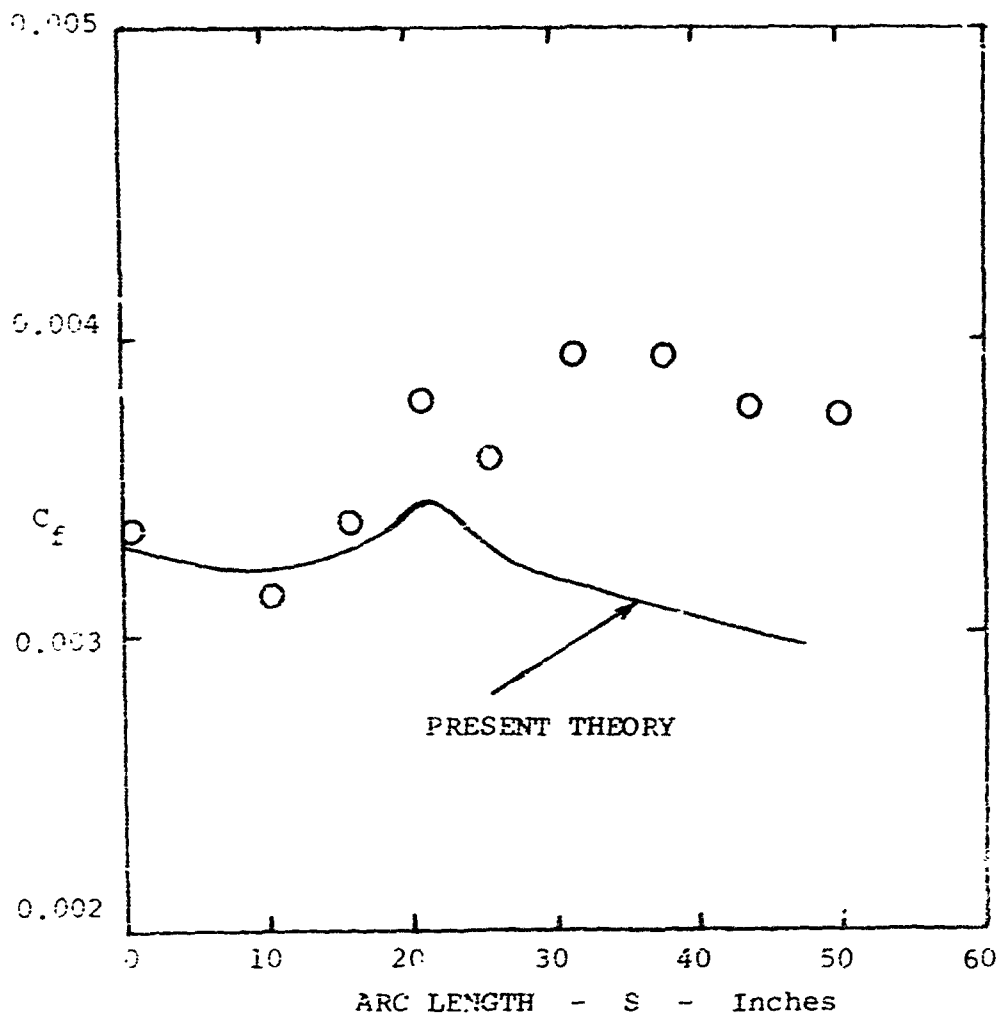


Figure 3.13. COMPARISON OF PRESENT THEORY WITH EXPERIMENTAL SKIN FRICTION AS ESTIMATED IN A CURVED DUCT BY FRANCIS & PIERCE (1967), SERIES 2.

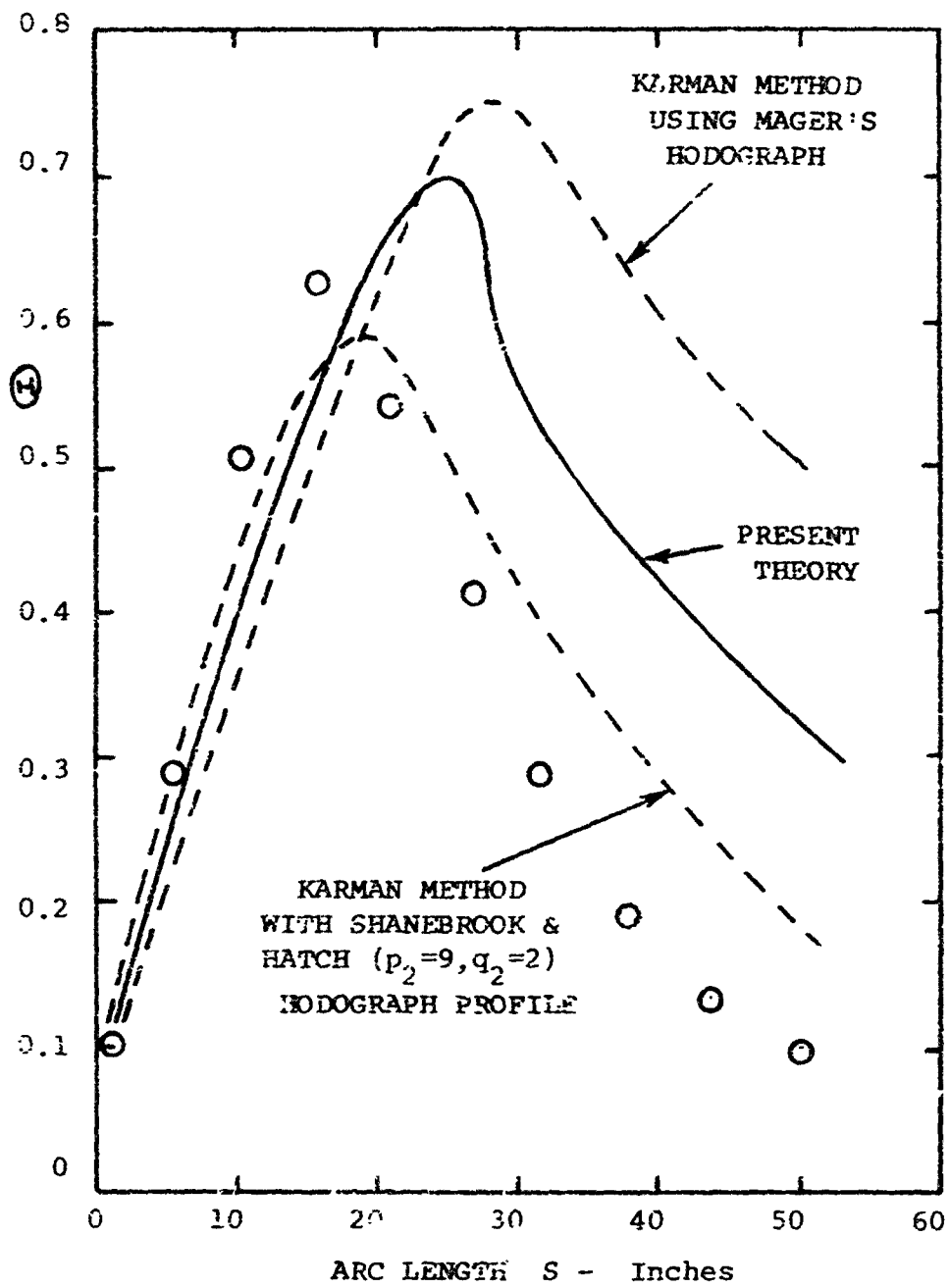


Figure 3.14. COMPARISON OF THEORY WITH WALL STREAMLINE TANGENT DATA OF FRANCIS AND PIERCE (1967), SERIES 2.

sophisticated family of hodograph models for crossflow profiles. Their method extended Eichelbrenner's (1966) polynomial representation by forcing consecutive higher order derivatives to be zero at the wall and at the boundary layer edge. This family is called the (p_i, q_j) family of hodograph models where p_i is the number of consecutive zero derivatives at the wall beginning with the i th derivative and q_j is the number of consecutive zero derivatives at the boundary layer edge beginning with the j th derivative. Besides containing many terms, Shanebrook and Hatch's hodograph models also contain the angle β that is used in Johnston's (1957) triangular model, Figure 3-3. By the use of the momentum integral equations and an entrainment equation, Shanebrook and Hatch compared their hodograph model with Mager's velocity correlation for Francis and Pierce's data. Shanebrook and Hatch's model shows better agreement with the data, but the same trends as the present theory, as seen in Figures 3-12 and 2-14. However, Nash and Patel (1972) showed that Mager's correlation was in excellent agreement with the crossflow velocity data for Francis and Pierce's experiment.

Therefore, it is felt that the disagreement between the present theory and Francis and Pierce's data is not the fault of the assumed crossflow velocity correlation. Rather, it is believed, as Nash and Patel pointed out, that the

boundary layer in Francis and Pierce's curved channel was dominated by the effects of corner flow at the junction of the side walls and the floor of the channel. These effects were not accounted for in the present analysis.

3.4.4 Data of Klinksiek and Pierce

As is pointed out in the introduction to this chapter, Mager's velocity correlation is not capable of representing the so-called S-shaped crossflow velocity profiles, Figure 3-2. However, it is believed that the present theory will give accurate results even if the crossflow velocity profile is only grossly approximated; as long as θ is well predicted, and apparently Mager's correlation predicts θ accurately. Klinksiek and Pierce (1970) conducted an experiment in which they obtained S-shaped crossflow velocity profiles. Their experiments were conducted in a doubly curved channel of rectangular cross section. An initial straight section of 78.7 inches was followed by a 60 degree bend with a 25 inch centerline radius of curvature. This in turn was followed by a 12 inch straight section and a 60 degree bend in the opposite direction with a 55 inch centerline radius of curvature. The same equations (3-38) and (3-39) that were used to compare with the data of Francis and Pierce apply to this situation. The results are shown in Figures 3-15 and 3-16. The theoretical values of θ are considerably above the data, presumably again because of side wall influence. The S-shaped profiles were observed

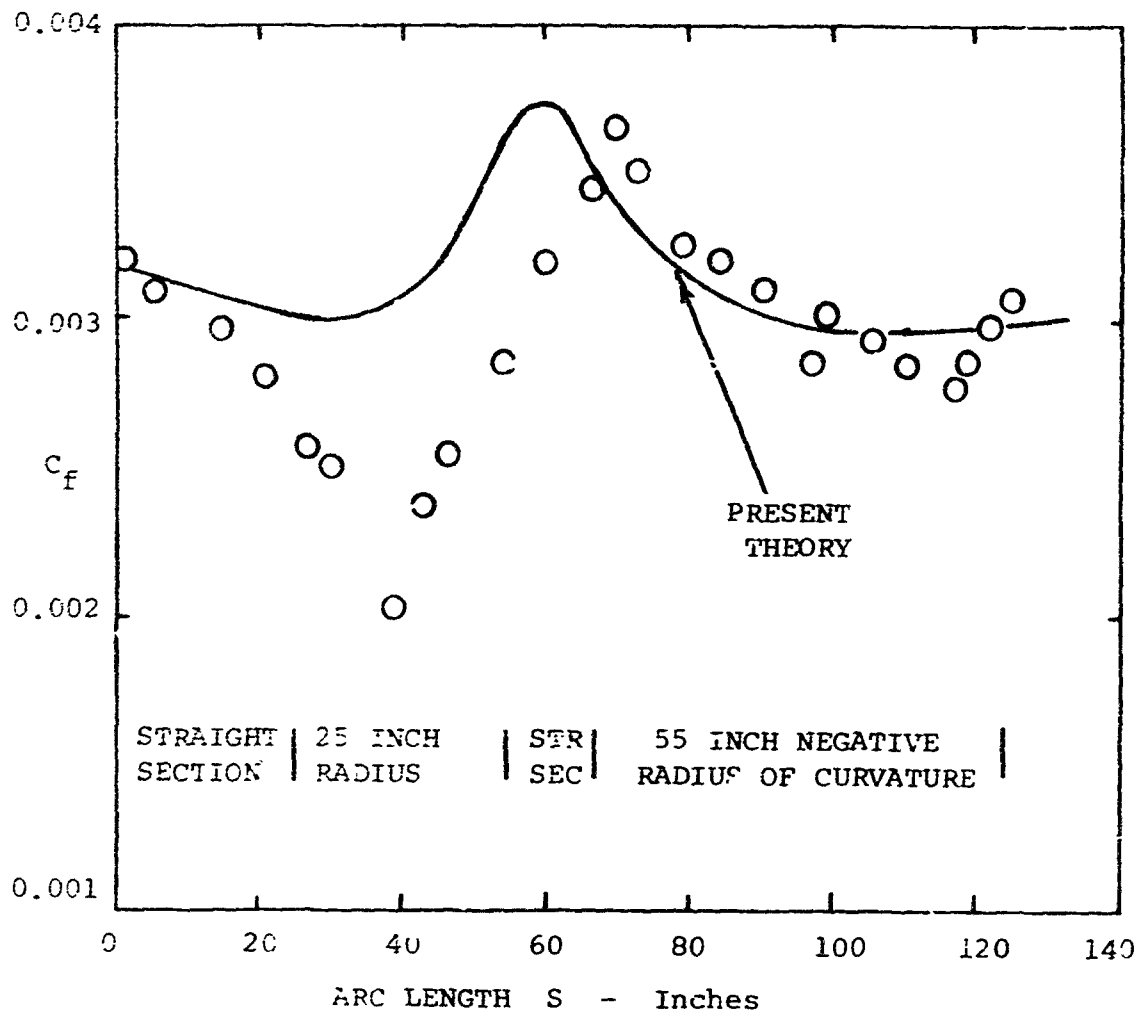


Figure 3.15. COMPARISON OF PRESENT THEORY WITH ESTIMATED SKIN FRICTION IN THE CURVED DUCT EXPERIMENT OF KLINSIEK & PIERCE (1970).

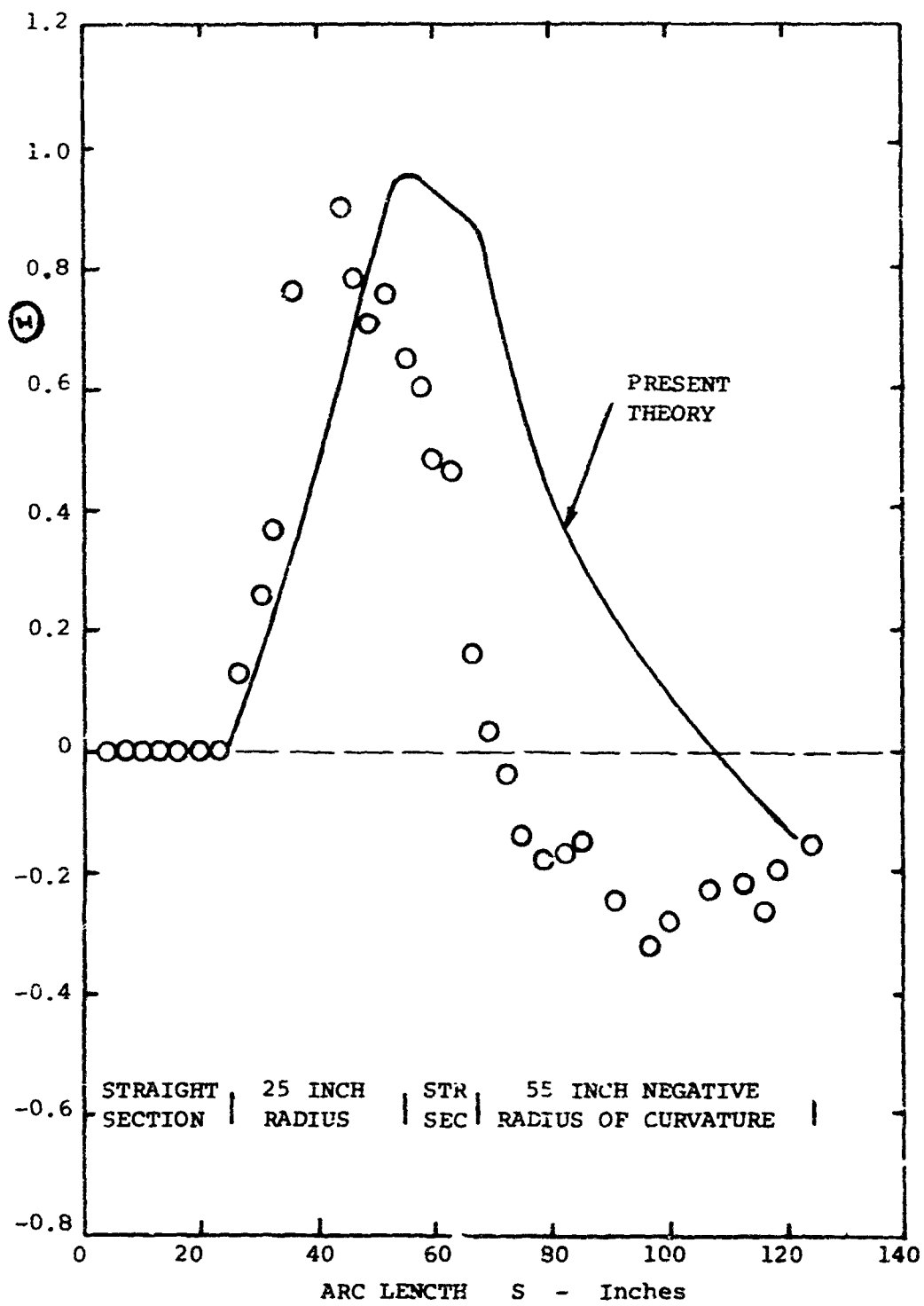


Figure 3.16. COMPARISON OF PRESENT THEORY WITH WALL STREAMLINE TANGENT DATA OF KLINKSIEK & PIERCE (1971).

in the latter curved portion of the channel with the 55 inch centerline radius of curvature (starting at 66.5 inches in Figures 3-15 and 3-16). By this point in the calculation the theory considerably diverges from the data. Thus no conclusion can be drawn about the general use of Mager's correlation in situations where bilateral skewing of the crossflow profile is present.

3.5 Summary

The approach to calculating three-dimensional skin friction presented in this chapter seems to offer great promise. It is an integral method which utilizes "law-of-the-wall" velocity correlations and results in two, coupled, partial differential equations having the streamwise skin friction and the angle between the total surface shear stress vector and the shear stress in the freestream direction as the dependent variables. This analysis contains significantly less empiricism than "classical" integral methods and is computationally much simpler than currently available differential approaches.

An area requiring more study is the problem of specifying a suitable crossflow velocity correlation. Mager's hodograph model was used here as it would seem to offer the best current compromise between accuracy and complication. However, it is not capable of predicting crossflow profiles with reversed skewing; and this must

be regarded as a deficiency for any generally applicable theory. It is felt that the development of a more accurate crossflow model must wait upon the availability of more accurate profile data.

The approach developed here compares extremely well with the rotating disk data of Cham and Head and with other predictions of this flow. The relatively poor performance of the present method when compared to the data of Johnston, Francis and Pierce, and Klinksiek and Pierce should not be taken as an indication of any serious deficiency in the theory. Johnston's swept step flow was not truly a boundary layer due to the presence of a large vertical pressure gradient and the Francis/Pierce and Klinksiek/Pierce data sets were strongly influenced by channel corner flows. Thus, serious evaluation of the present method must await the availability of a clean set of experimental data for a three-dimensional boundary layer flow. Such a set of data should include direct measurements of skin friction in both the freestream and crossflow directions as well as accurate measurements of the pressure gradient along the freestream line and velocity profile data.

APPENDIX A

A.1. The coefficients H_1 for use in the heat transfer differential equations, Eqns.(1-29,30), are defined as:

$$H_1 = \int_0^{\delta^+} \left(\frac{u^+}{T^+} - \beta u^+ \frac{\partial u^+}{\partial \beta} + 2\gamma \frac{u^+ \partial u^+}{T^+ \partial \gamma} + \frac{\beta}{\mu_w} \frac{\partial u^+}{\partial \gamma} \frac{\partial \psi}{\partial \beta} - \frac{2\gamma}{\mu_w} \frac{\partial u^+}{\partial \gamma} \frac{\partial \psi}{\partial \gamma} \right) dv^+$$

$$H_2 = \int_0^{\delta^+} \left(\frac{u^+}{T^+} \frac{\partial u^+}{\partial \alpha} - \frac{1}{\mu_w} \frac{\partial u^+}{\partial \gamma} \frac{\partial \psi}{\partial \alpha} \right) dv^+$$

$$H_3 = \int_0^{\delta^+} \left(\frac{u^+}{T^+} \beta \frac{\partial u^+}{\partial \beta} - \frac{\beta}{\mu_w} \frac{\partial u^+}{\partial \gamma} \frac{\partial \psi}{\partial \beta} \right) dv^+$$

$$H_4 = \int_0^{\delta^+} \left(\frac{1}{2} \frac{u^{+2}}{T^+} - \beta \frac{u^+}{T^+} \frac{\partial u^+}{\partial \beta} + \frac{\beta}{\mu_w} \frac{\partial u^+}{\partial \gamma} \frac{\partial \psi}{\partial \beta} \right) dv^+$$

$$H_5 = \int_0^{\delta^+} \left(\frac{\gamma u^{+3}}{T^+} - P_T \frac{\beta u^+}{2T^+} \frac{\partial T^+}{\partial \beta} + P_T \gamma \frac{u^+}{T^+} \frac{\partial T^+}{\partial \gamma} + \frac{P_T \beta}{2\mu_w} \frac{\partial T^+}{\partial \gamma} \frac{\partial \psi}{\partial \beta} \right. \\ \left. - P_T \frac{\gamma}{\mu_w} \frac{\partial T^+}{\partial \gamma} \frac{\partial \psi}{\partial \gamma} - \gamma \beta \frac{u^{+2}}{T^+} \frac{\partial u^+}{\partial \beta} + 2\gamma^2 \frac{u^{+2}}{T^+} \frac{\partial u^+}{\partial \gamma} \right. \\ \left. + \gamma \beta \frac{u^+}{\mu_w} \frac{\partial u^+}{\partial \gamma} \frac{\partial \psi}{\partial \beta} - 2\gamma^2 \frac{u^+}{\mu_w} \frac{\partial u^+}{\partial \gamma} \frac{\partial \psi}{\partial \gamma} \right) dv^+$$

$$H_6 = \int_0^{\delta^+} \left(\frac{P_T u^+}{2T^+} \frac{\partial T^+}{\partial \alpha} - \frac{P_T}{2\mu_w} \frac{\partial T^+}{\partial \gamma} \frac{\partial \psi}{\partial \alpha} + \frac{\gamma u^{+2}}{T^+} \frac{\partial u^+}{\partial \alpha} - \frac{\gamma u^+}{\mu_w} \frac{\partial u^+}{\partial \gamma} \frac{\partial \psi}{\partial \alpha} \right) dv^+$$

$$H_{\gamma} = \int_0^{\delta^+} \left(\frac{\beta P_T}{2} \frac{u^+}{T^+} \frac{\partial T^+}{\partial \beta} - \frac{\beta P_T}{2u_w} \frac{\partial T^+}{\partial y^+} \frac{\partial \psi}{\partial \beta} + \gamma \beta \frac{u^{+2}}{T^+} \frac{\partial u^+}{\partial \beta} - \gamma \beta \frac{u^+}{u_w} \frac{\partial u^+}{\partial y^+} \frac{\partial \psi}{\partial \beta} \right) dy^+$$

$$H_{\beta} = \int_0^{\delta^+} \frac{1}{2} (P_T u^+ - P_T \frac{\beta u^+ \partial T^+}{2T^+ \partial \beta} + \frac{\beta P_T}{2u_w} \frac{\partial T^+}{\partial y^+} \frac{\partial \psi}{\partial \beta} - \gamma \beta \frac{u^{+2}}{T^+} \frac{\partial u^+}{\partial \beta} + \frac{\gamma u^{+3}}{T^+} + \gamma \beta \frac{u^+}{u_w} \frac{\partial u^+}{\partial y^+} \frac{\partial \psi}{\partial \beta}) dv^+$$

The various partial derivatives which are needed in the above expressions may be evaluated as follows:

$$\frac{\partial u^+}{\partial \alpha} = \int_0^{u_e^+} \left[T^+ y^+ + \alpha y^+ \int_0^{u^+} \frac{-\beta y^+ du^+}{(1 + \alpha y^+)^2} \right] \frac{du^+}{2T^+(1 + \alpha y^+)}$$

$$\frac{\partial u^+}{\partial \beta} = \int_0^{u_e^+} \frac{du^+}{2T^+} \left[\int_0^{u^+} \frac{du^+}{1 + \alpha y^+} \right]$$

$$\frac{\partial u^+}{\partial \gamma} = \int_0^{u_e^+} \frac{-du^+}{T^+} \left[\int_0^{u^+} 2u^+ du^+ \right]$$

$$\frac{\partial T^+}{\partial \alpha} = \int_0^{u_e^+} \frac{-\beta y^+ du^+}{(1 + \alpha y^+)^2}$$

$$\frac{\partial T^+}{\partial \beta} = \int_0^{u_e^+} \frac{du^+}{1 + \alpha y^+}$$

$$\frac{\partial T^+}{\partial \gamma} = \int_0^{u_e^+} -2 u^+ du^+ = -u_e^2$$

$$\frac{1}{u_w} \frac{\partial \psi}{\partial \alpha} = \int_0^{u_e^+} \frac{\kappa y^+ du^+}{(1 + \alpha y^+)^{1/2} T^{5/2}} \left[T^+ \frac{\partial u^+}{\partial \alpha} - u^+ \int_0^{u^+} \frac{-\{\beta y^+ + 2\alpha \gamma y^+ \frac{\partial u^+}{\partial \alpha} (1 + \alpha y^+)\}}{(1 + \alpha y^+)^2} du^+ \right]$$

$$\frac{1}{u_w} \frac{\partial \psi}{\partial \beta} = \int_0^{u_e^+} \frac{\kappa y^+ du^+}{(1 + \alpha y^+)^{1/2} T^{5/2}} \left[T^+ \frac{\partial u^+}{\partial \beta} - u^+ \int_0^{u^+} \frac{\{1 - 2\gamma(1 + \alpha y^+) \frac{\partial u^+}{\partial \beta}\}}{(1 + \alpha y^+)} du^+ \right]$$

$$\frac{1}{u_w} \frac{\partial \psi}{\partial \gamma} = \int_0^{u_e^+} \frac{\kappa y^+ du^+}{(1 + \alpha y^+)^{1/2} T^{5/2}} \left[T^+ \frac{\partial u^+}{\partial \gamma} - u^+ \int_0^{u^+} \frac{-2\{u^+ + \gamma(1 + \alpha y^+) \frac{\partial u^+}{\partial \gamma}\}}{(1 + \alpha y^+)} du^+ \right]$$

The following are curve-fit expressions for the coefficients H_1 :

$$H_1 = 8.5 \exp \left\{ \frac{0.475 u_e^+ (1 + 0.22 \gamma u_e^{+2})}{[1 + 0.1(\alpha \delta^+)^{1/2}](1 + 0.3\beta u_e^+)} \right\}$$

$$H_2 \doteq 0.062 \exp\left\{ \frac{0.94 u_e^+ (1 + 0.22 \gamma u_e^{+2})}{[1 + 0.12(\alpha\delta^+)^{1/2}] (1 + 0.3 \beta u_e^+)} \right\}$$

$$H_3 \doteq 10.0 \beta \exp\left\{ \frac{0.52 u_e^+ (1 + 0.22 \gamma u_e^{+2})}{[1 + 0.08(\alpha\delta^+)^{1/2}] (1 + 0.22 \beta u_e^+)} \right\}$$

$$H_4 \doteq 2.75 \exp\left\{ \frac{0.5 u_e^+ (1 + 0.32 \gamma u_e^{+2})}{[1 + 0.09(\alpha\delta^+)^{1/2}] (1 + 0.3 \beta u_e^+)} \right\}$$

$$H_5 \doteq -0.2 \gamma^2 \exp\left\{ \frac{(0.7 + 400 \gamma) u_e^+}{[1 + 0.02(\alpha\delta^+)^{1/2}]} \right\} - \frac{3.58}{1-15\beta} \exp\left\{ \frac{(0.482-3.7\beta) u_e^+}{[1 + 0.1(\alpha\delta^+)^{1/2}]} \right\}$$

$$+ \frac{\beta \gamma}{1 + (2000 \gamma)^{7.6}} \exp\left\{ \frac{(0.68 + 400\gamma) u_e^+}{[1 + 0.03(\alpha\delta^+)^{1/2}]} \right\}$$

$$H_6 \doteq 0.051 \exp\left\{ \frac{0.435 u_e^+ (1 + 35 \gamma u_e^+)}{[1 + 0.25(\alpha\delta^+)^{1/2}]} \right\}$$

$$- 0.14 \beta \exp\left\{ \frac{(0.8 - 5 \beta) u_e^+}{[1 + 0.25(\alpha\delta^+)^{1/2}]} \right\}$$

$$H_7 \doteq \frac{3.5 \beta}{1 - 15\beta} \exp\left\{ \frac{(0.482 - 3.7\beta) u_e^+}{[1 + 0.1(\alpha\delta^+)^{1/2}]} \right\} \\ + \frac{10000. \beta \gamma}{1 + \beta(3200 \gamma)^{7.4}} \exp\left\{ \frac{(0.46 + 260\gamma - 3\beta) u_e^+}{[1 + 0.05(\alpha\delta^+)^{1/2}]} \right\}$$

$$H_8 \doteq 0.33 \exp\left\{ \frac{0.46 u_e^+ (1 + 0.33 \gamma u_e^{+2})}{[1 + 0.1(\alpha\delta^+)^{1/2}] (1 + 0.25 \beta u_e^+)} \right\}$$

In order to use these curve-fit expressions, one first evaluates α , β , and γ from their definitions, Eqns. (1-32), and then evaluates δ^+ from the two-dimensional law-of-the-wall, Eqn. (1-33). The only other parameter in the formulas for H_i is u_e^+ , which is directly related to skin friction by the relation $u_e^+ = \lambda (T_e/T_w)^{1/2}$.

A.2. The coefficients G_1 for use in the three-dimensional theory, Eqns.(3-38,39), are defined as follows:

$$G_1 = \int_0^{\delta^+} u^{+2} dy^+$$

$$G_2 = \int_0^{\delta^+} \left[u^+ \frac{\partial u^+}{\partial \alpha_s} - \frac{\partial u^+}{\partial y^+} \int_0^{y^+} \frac{\partial u^+}{\partial \alpha_s} dy^+ \right] dy^+$$

$$G_3 = \int_0^{\delta^+} u^+ w^+ dy^+$$

$$G_4 = \int_0^{\delta^+} \left\{ w^+ \frac{\partial u^+}{\partial \alpha_s} - \frac{\partial u^+}{\partial y^+} \left[\int_0^{y^+} \frac{\partial w^+}{\partial \alpha_s} dy^+ \right] + \left[\frac{\alpha_s \delta^+ p_\delta^2 - p_\delta^3 + p_\delta}{\alpha_s^2 p_\delta^2} \right] \frac{\partial u^+}{\partial y^+} \int_0^{y^+} \frac{\partial w^+}{\partial \delta^+} dy^+ \right\} dy^+,$$

$$\text{where } p_\delta = (1 + \alpha_s \delta^+)^{1/2}.$$

$$G_5 = \int_0^{\delta^+} \left[\frac{\kappa(p_\delta^2 - 1)}{\alpha_s p_\delta} \frac{\partial u^+}{\partial y^+} \int_0^{y^+} \frac{\partial w^+}{\partial \delta^+} dy^+ \right] dy^+$$

$$G_6 = \int_0^{\delta^+} \left[\frac{\partial u^+}{\partial y^+} \int_0^{y^+} \frac{\partial w^+}{\partial \delta} dy^+ \right] dy^+$$

$$G_7 = \int_0^{\delta^+} \left[u^+ w^+ - \frac{\partial u^+}{\partial y^+} \int_0^{y^+} w^+ dy^+ \right] dy^+$$

$$G_8 = \int_0^{\delta^+} \left[w^{+2} + \frac{\partial u^+}{\partial y^+} \int_0^{y^+} u^+ dv^+ \right] dy^+$$

$$G_9 = \int_0^{\delta^+} \left\{ u^+ \frac{\partial w^+}{\partial \alpha_s} - \frac{\partial w^+}{\partial y^+} \left[\int_0^{y^+} \frac{\partial u^+}{\partial \alpha_s} dy^+ \right] - \left(\frac{\alpha_s \delta^+ p_\delta^2 - p_\delta^3 + p_\delta}{\alpha_s^2 p_\delta} \right) u^+ \frac{\partial w^+}{\partial \delta^+} \right\} dy^+$$

$$G_{10} = \int_0^{\delta^+} \frac{\kappa(p_\delta^2 - 1)}{\alpha_s p_\delta} u^+ \frac{\partial w^+}{\partial \delta^+} dy^+$$

$$G_{11} = \int_0^{\delta^+} w^{+2} dy^+$$

$$G_{12} = \int_0^{\delta^+} \left\{ w^+ \frac{\partial w^+}{\partial \alpha_s} - \frac{\partial w^+}{\partial y^+} \left[\int_0^{y^+} \frac{\partial w^+}{\partial \alpha_s} dv^+ \right] - \left(\frac{\alpha_s \delta^+ p_\delta^2 - p_\delta^3 + p_\delta}{\alpha_s^2 p_\delta} \right) \left[w^+ \frac{\partial w^+}{\partial \delta^+} - \frac{\partial w^+}{\partial v^+} \int_0^{y^+} \frac{\partial w^+}{\partial \delta^+} dv^+ \right] \right\} dy^+$$

$$G_{13} = \int_0^{\delta^+} \frac{\kappa(p_\delta^2 - 1)}{\alpha_s p_\delta} \left[w^+ \frac{\partial w^+}{\partial \delta^+} - \frac{\partial w^+}{\partial v^+} \int_0^{y^+} \frac{\partial w^+}{\partial \delta^+} dy^+ \right] dy^+$$

$$G_{14} = \int_0^{\delta^+} u^+ \frac{\partial w^+}{\partial \theta} dy^+$$

$$G_{15} = \int_0^{\delta^+} \left[w^+ \frac{\partial w^+}{\partial \theta} - \frac{\partial w^+}{\partial y^+} \int_0^{y^+} \frac{\partial w^+}{\partial \theta} dy^+ \right] dy^+$$

$$G_{16} = \int_0^{\delta^+} \left[u^{+2} + \frac{\partial w^+}{\partial y^+} \int_0^{y^+} w^+ dy^+ \right] dy^+$$

$$G_{17} = \int_0^{\delta^+} \left[u^+ w^+ - \frac{\partial w^+}{\partial y^+} \int_0^{y^+} u^+ dy^+ \right] dy^+$$

Using the law-of-the-wall and the Mager hodograph, these integrals may be evaluated numerically as functions of the parameters λ_1 , α_s , θ , and δ^+ . The following curve-fits are suggested for the numerical results:

$$G_1 \approx 8.5 \exp[0.475 \lambda_1 / (1 + 0.1(\alpha_s \delta^+)^{1/2})]$$

$$G_2 \approx 0.062 \exp[0.84 \lambda_1 / (1 + 0.12(\alpha_s \delta^+)^{1/2})]$$

$$G_3 \approx \theta \delta^+ [0.33 \lambda_1^2 - 3.06 \lambda_1 + 9.84 - \alpha_s \delta^+ (0.78 \lambda_1 - 1.50 \alpha_s \delta^+)]$$

$$G_4 \approx 32500. \theta \exp[0.285 \lambda_1 / (1 + 0.3(\alpha_s \delta^+)^{1/2})]$$

$$G_5 \approx \theta \delta^+ [0.33 \lambda_1 - \alpha_s \delta^+ (0.13 \lambda_1 - 0.3 \alpha_s \delta^+)]$$

$$G_6 \approx \delta^+ [1.53 \lambda_1 - 9.84 - \alpha_s \delta^+ (0.1 \lambda_1 - 0.2 \alpha_s \delta^+)]$$

$$G_7 \approx \theta \delta^+ [0.33 \lambda_1^2 - 4.59 \lambda_1 + 19.65 - \alpha_s \delta^+ (0.6 \lambda_1 - 1.1 \alpha_s \delta^+)]$$

$$G_8 \doteq \delta^+ [2.50 \lambda_1 - 12.5 - \alpha_s (0.08 \lambda_1 - 0.15 \alpha_s \delta^+)] + \\ + \theta^2 \delta^+ (0.2 \lambda_1^2 - 2.28 \lambda_1 + 8.33)$$

$$G_9 \doteq - 0.71 \theta \exp[0.83 \lambda_1 / (1 + 0.12(\alpha_s \delta^+)^{1/2})]$$

$$G_{10} \doteq \theta \delta^+ [0.07 \lambda_1^2 - 0.28 \lambda_1 + 0.42 - \alpha_s \delta^+ (0.92 \lambda_1 - 2.0 \alpha_s \delta^+)]$$

$$G_{11} \doteq \theta^2 \delta^+ [0.2 \lambda_1^2 - 2.28 \lambda_1 + 8.33 - \alpha_s \delta^+ (0.48 \lambda_1 - 0.82 \alpha_s \delta^+)]$$

$$G_{12} \doteq - 5.50 \theta \exp[0.63 \lambda_1 / (1 + 0.1(\alpha_s \delta^+)^{1/2})]$$

$$G_{13} \doteq \theta^2 \delta^+ [0.08 \lambda_1^2 - 0.58 \lambda_1 + 0.83 - \alpha_s \delta^+ (0.45 \lambda_1 - 0.94 \alpha_s \delta^+)]$$

$$G_{14} \doteq G_3 / \theta$$

$$G_{15} \doteq \theta \delta^+ (0.40 \lambda_1^2 - 5.0 \lambda_1 + 18.7 - 0.30 \alpha_s \delta^+ \lambda_1)$$

$$G_{16} \doteq \delta^+ [\lambda_1^2 - 5.0 \lambda_1 + 12.5 - \alpha_s \delta^+ (4.0 \lambda_1 - 4.0 \alpha_s \delta^+)] \\ - \theta^2 \delta^+ (0.2 \lambda_1^2 - 1.5 \lambda_1 + 6.95)$$

$$G_{17} \doteq \theta \delta^+ [0.87 \lambda_1^2 - 6.11 \lambda_1 + 19.65 - \alpha_s \delta^+ (0.87 \lambda_1 - \alpha_s \delta^+)]$$

It is these curve-fits which were used to compare the present theory, Eqns. (3-38,39), with the three-dimensional flow experiments of Figures 3.9 through 3.16.

REFERENCES

- Allen, J.M. (1970) "Experimental Preston Tube and Law-of-the-Wall Study of Turbulent Skin Friction on Axisymmetric Bodies at Supersonic Speeds", NASA TN D-5660, February.
- Banks, W.H. and Gadd, G.E. (1962) "A Preliminary Report on Screw Propellers and Simple Rotating Bodies", National Physical Laboratory, Ship Division, Report No. 27.
- Beckwith, I.E. (1969) "Recent Advances in Research on Compressible Turbulent Boundary Layers", Symposium on Analytical Methods in Aircraft Aerodynamics, NASA SP-228, October, pp 355-416.
- Bradshaw, P., Ferriss, D.H. and Atwell, N.P. (1967) "Calculation of Boundary Layer Development Using the Turbulent Energy Equation", Journal of Fluid Mechanics, Vol 28, No 3, pp 593-616 (See also N.P.L. Aero. Report No 1182, 1966).
- Bradshaw, P. (1971) "Calculation of Three-Dimensional Turbulent Boundary Layers", Journal of Fluid Mechanics, Vol 46, pp 417-445.
- Brand, R.S. and Persen, L.N. (1964) "Implications of the Law of the Wall for Turbulent Boundary Layers." ACTA Polytechnica Scandinavica, PH 30, UDC 532.526.4, Trondheim, Norway, pp 1-61.
- Brott, D.L., Yanta, W.J., Voisinet, R.L., and Lee, R.E. (1969) "An Experimental Investigation of the Compressible Turbulent Boundary Layers with a Favorable Pressure

- Gradient", AIAA Paper No 69-685, June. (See also Naval Ordnance Laboratory Report 69-143, 25 August 1969).
- Bushnell, D.M. and Beckwith, I.E. (1969) "Calculation of Nonequilibrium Hypersonic Turbulent Boundary Layers and Comparisons with Experimental Data", AIAA Paper 69-684. June.
- Cebeci, T. (1970) "Laminar and Turbulent Incompressible Boundary Layers on Slender Bodies of Revolution in Axial Flow", ASME Transactions, Journal of Basic Engineering, Vol 92, No 3. September, pp 545-554.
- Cebeci, T. (1971) "Calculation of Compressible Turbulent Boundary Layers with Heat and Mass Transfer", AIAA Journal Vol 9, No 6. June. pp 1091-1097.
- Chaz, T-S. and Head, M.R. (1969) "Turbulent Boundary Layer Flow on a Rotating Disk", Journal of Fluid Mechanics, Vol 37, Part 1. pp 129-147.
- Chi, S.W. and Spaulding, D.B. (1966) "Influence of Temperature Ratio on Heat Transfer to a Flat Plate Through a Turbulent Boundary Layer in Air", Proceedings of the Third International Heat Transfer Conference, Vol II, Chicago, Ill., August. pp 41-49.
- Colburn, A.P. (1933) "A Method of Correlating Forced Convection Heat Transfer Data and A Comparison with Fluid Friction", Transactions of the American Institute of Chemical Engineers, Vol 29, pp 174-210.

- Coles, D.E. (1964) "The Turbulent Boundary Layer in a Compressible Fluid", The Physics of Fluids, Vol 2, No 6. September. pp 1403-1423.
- Cooke, J.C. (1958) "A Calculation Method for Three-Dimensional Turbulent Boundary Layers", Aeronautical Research Council, Reports and Memoranda No 3199.
- Cooke, J.C. and Hall, M.G. (1962) "Boundary Layers in Three Dimensions", Progress in Aeronautical Sciences, Vol 2, Pergamon Press.
- Cooper, P. (1971) "Turbulent Boundary Layer on a Rotating Disk Calculated With an Effective Viscosity", AIAA Journal, Vol 9, February. pp 255-261.
- Coosteix, J., Quemard, C. and Michel, R. (1971) "Application d'un Schema Ameliore de Longueur de Malange a L'etude des Couches Turbulentes Tridimensionnelles", AGARD Conference Proceedings No 93 on Turbulent Shear Flows, September. pp 7.1-7.11.
- Cumpsty, N.A. and Head, M.R. (1967) "The Calculation of Three-Dimensional Turbulent Boundary Layers. Part I: Flow over the Rear of an Infinite Swept Wing", Aeronautical Quarterly, Vol 18, Part I. pp 55-84.
- Cumpsty, N.A. and Head, M.R. (1967) "The Calculation of Three-Dimensional Turbulent Boundary Layers. Part II: Attachment-Line Flow on an Infinite Swept Wing", Aeronautical Quarterly, Vol 18, Part II. pp 150-164.

- Deissler, R.G. and Loeffler, A.L. (1959) "Analysis of Turbulent Flow and Heat Transfer on a Flat Plate at High Mach Numbers with Variable Fluid Properties", NASA TR R-17, pp 1-33.
- Eckert, E.R.G. (1955) "Engineering Relations for Heat Transfer and Friction in High Velocity Laminar and Turbulent Boundary Layer Flow Over Surfaces with Constant Pressure Temperature", Journal of the Aeronautical Sciences, Vol 22, pp 585-587.
- Eichelbrenner, E.A. and Peube, J-L. (1966) "The Role of S-Shaped Profiles in Three-Dimensional Boundary Layer Theory", Laboratoire de Mechanique des Fluides, Poitiers, Final Report.
- Francis, G.P. and Pierce, F.J. (1967) "An Experimental Study of Skewed Turbulent Boundary Layers in Low Speed Flows", ASME Transactions, Journal of Basic Engineering, September. pp 597-607.
- Head, M.R. (1956) "Entrainment in the Turbulent Boundary Layer", Aeronautical Research Council, Reports and Memoranda No 3152.
- Herring, J.H. and Mellor, G.L. (1968) "A Method of Calculating Compressible Turbulent Boundary Layers", NASA CR-1144, September.
- Johnston, J.P. (1970) "Measurements in a Three-Dimensional Turbulent Boundary Layer Induced by a Swept, Forward-Facing Step", Journal of Fluid Mechanics, Vol 42, Part 4, pp 627-644.

- Johnston, J.P. (1957) "Three-Dimensional Turbulent Boundary Layers", M.I.T. Gas Turbine Lab. Report 39; see also ASME Transactions, Journal of Basic Engineering, Series D, Vol 82, No 4, December 1960, pp 622-628.
- Joubert, P.N., Perry, A.E. and Brown, K.C. (1967) "Critical Review and Current Developments in Three-Dimensional Turbulent Boundary Layers", Fluid Mechanics of Internal Flows, Elsevier.
- Kepler, C.E. and O'Brien, R.L. (1959) "Turbulent Boundary Layer Characteristics in Supersonic Streams Having Adverse Pressure Gradients", United Aircraft Research Department R-1285-11, September. (See also ISA Journal, Vol 29, pp 1-10).
- Klinksiek, W.F. and Pierce, F.J. (1970) "Simultaneous Lateral Skewing in a Three-Dimensional Turbulent Boundary-Layer Flow", ASME Transactions, Journal of Basic Engineering, March. pp 83-90.
- Lee, R.E., Yanta, W.J. and Leonas, A.C. (1969) "Velocity Profile, Skin Friction Balance and Heat Transfer Measurements of the Turbulent Boundary Layer at Mach 5 and Zero Pressure Gradient", NOLTR 69-106. June.
- Lessmann, R.C. and Christoph, G.H. (1972) "A Modified Integral Approach to the Calculation of Three Dimensional Turbulent Skin Friction", Submitted to the AIAA Journal for Publication. April.

- Ludwig, H. and Tillman, W. (1950) "Investigation of the Wall Shearing Stress in Turbulent Boundary Layers", NACA Tech. Memo. No 1285.
- Mager, A. (1951) "Generalization of Boundary Layer Momentum Integral Equations to Three-Dimensional Flows Including Those of a Rotating System", NACA Tech. Note 2310.
- Mangler, W. (1946) "Boundary Layers on Bodies of Revolution in Symmetrical Flow", M.A.P. Vlkenrode Ref. MAP-VG 45-55t.
- Mellor, G.L. (1966) "The Effects of Pressure Gradients on Turbulent Flow Near a Smooth Wall", Journal of Fluid Mechanics, Vol 24, Part 2. pp 255-274.
- Moore, D.R. (1962) "Velocity Similarity in the Compressible Turbulent Boundary Layer with Heat Transfer", Report DRL-480, CM 1014, Defense Res. Lab. Univ. of Texas.
- Moretti, P.M. and Kays, W.M. (1965) "Heat Transfer for a Turbulent Boundary Layer with Varying Free-Stream Velocity and Varying Surface Temperature - an Experimental Study", International Journal of Heat and Mass Transfer, Vol 8, pp 1187-1202.
- Nash, J.F. (1969) "The Calculation of Three-Dimensional Turbulent Boundary Layers in Incompressible Flow", Journal of Fluid Mechanics, Vol 37, pp 625-642.
- Nash, J.F. and Patel, V.C. (1972) Three Dimensional Turbulent Boundary Layers, Atlanta, Georgia: Scientific and Business Consultants, Inc.

- Nielsen, J.N., Kuhn, G.D. and Lynes, L.L. (1969) "Calculation of Compressible Turbulent Boundary Layers with Pressure Gradients and Heat Transfer", NASA CR-1303.
- Prandtl, L. (1946) "Über Reibungsschichten bei dreidimensionalen Strömungen", British M.A.P. Volkenrode Report and Translation No 64.
- Rao, G.N.V. (1967) "The Law of the Wall in a Thick Axisymmetric Turbulent Boundary Layer", Journal of Applied Mechanics, Vol 34, No 1, March. pp 237-238.
- Reshotko, E. and Tucker, M. (1957) "Approximate Calculation of the Compressible Turbulent Boundary Layer with Heat Transfer and Arbitrary Pressure Gradient", NACA TN-4154.
- Reynolds, O. (1874) "On the Extent and Action of the Heating Surface for Steam Boilers", Proceedings of Manchester Literary Philosophical Society, Vol 14. pp 7-12.
- Richmond, R.L. (1957) "Experimental Investigation of Thick Axially Symmetric Boundary Layers on Cylinders at Subsonic and Hypersonic Speeds", Ph.D. Thesis, Calif. Inst. of Technology, (also GALCIT Hypersonic Research Project Memo. No 39, 1957).
- Rubesin, M.W. (1953) "A Modified Reynolds Analogy for the Compressible Turbulent Boundary Layer on a Flat Plate", NACA TN 2917.
- Sasman, P.K. and Cresci, R.J. (1966) "Compressible Turbulent Boundary Layer with Pressure Gradient and Heat Transfer", AIAA Journal, Vol 4, No 1, January. pp 19-25.

- Schlichting, H. (1968) Boundary Layer Theory, Sixth edition. New York: McGraw Hill Book Company, Inc.
- Shanebrook, J.R. and Hatch D.E. (1971) "A Family of Hodograph Models for the Cross Flow Velocity Component of Three-Dimensional Turbulent Boundary Layers", ASME Paper No 71-FE-1.
- Shanebrook, J.R. and Sumner, W.J. (1970) "Entrainment Theory for Axisymmetric, Turbulent Incompressible Boundary Layers", Journal of Hydronautics, Vol 4, No 4, October. pp 159-160.
- Simpson, R.L., Whitten, D.G. and Koffatt, R.J. (1970) "An Experimental Study of the Turbulent Prandtl Number of Air with Injection and Suction", International Journal of Heat and Mass Transfer, Vol 13, pp 125-1-3.
- Smith, P.D. (1966) "Calculation Methods for Three-Dimensional Turbulent Boundary Layers", Aeronautical Research Council, Reports and Memoranda No 3523.
- Smith, T. and Harrop, R. (1946) "The Turbulent Boundary Layer with Heat Transfer and Compressible Flow", Tech. Note Aero. 1759, R.A.E. (British).
- Sommer, S.C. and Short, B.J. (1955) "Free-Flight Measurements of Turbulent Boundary Layer Skin Friction in the Presence of Severe Aerodynamic Heating at Mach Numbers from 2.9 to 7.0", NACA TN 3391, March.

- Spalding, D.B. and Chi, S.W. (1964) "The Drag of a Compressible Turbulent Boundary Layer on a Smooth Flat Plate with and without Heat Transfer", Journal of Fluid Mechanics, Vol 16, Part 1. pp 117-143.
- Tetervin, N. (1969) "Approximate Calculation of Reynolds Analogy for Turbulent Boundary Layer with Pressure Gradient", AIAA Journal, Vol 7, No 6, June. pp 1079-1085.
- Tetervin, N. (1969) "A Generalization to Turbulent Boundary Layers of Mangler's Transformation Between Axisymmetric and Two-Dimensional Laminar Boundary Layers", U.S. Naval Ordnance Laboratory, Report NOLTR 69-47, June 12.
- Theodorsen, T. and Regier, A. (1944) "Experiments on Drag of Revolving Disks, Cylinders and Streamline Rods at High Speeds", NACA Report No 793.
- Van Driest, E.R. (1956a) "On Turbulent Flow Near a Wall", Journal of the Aerospace Sciences, Vol 23, No 11, November. pp 1007-1011.
- Van Driest, E.R. (1956b) "The Problem of Aerodynamic Heating", Aeronautical Engineering Review, Vol 15, No 10, October. pp 26--1.
- Van Driest, E.R. (1952) "Turbulent Boundary Layer on a Cone in a Supersonic Flow at Zero Angle of Attack", Journal of Aeronautical Sciences, Vol 19, No 1, pp 55-60.
- von Kármán, Th. (1946) "On Laminar and Turbulent Friction", NACA TM 1092.

- von Kármán, Th. (1939) "The Analogy Between Fluid Friction and Heat Transfer", Transactions of the ASME, Vol 61, No 8, pp 705-710.
- White, F.M. (1969) "A New Integral Method for Analyzing the Turbulent Boundary Layer with Arbitrary Pressure Gradient", ASME Transactions, Journal of Basic Engineering, September. pp 371-378.
- White, F.M. (1972) "An Analysis of Axisymmetric Turbulent Flow Past a Long Cylinder", Journal of Basic Engineering, March. pp 200-206.
- White, F.M. and Christoph, G.H. (1970) "A Simple New Analysis of Compressible Turbulent Two-Dimensional Skin Friction Under Arbitrary Conditions", Technical Report AFFDL-TR-70-133, Air Force Flight Dynamics Laboratory, Wright-Patterson Air Force Base, Ohio. November.
- White, F.M. and Christoph, G.H. (1971) "A Simple Analysis of Two-Dimensional Turbulent Skin Friction with Arbitrary Wall and Freestream Conditions", Paper No. 20, Proceedings AGARD Conference on Turbulent Shear Flows, London, England, September.
- Winter, K.G., Smith, K.G. and Rotta, J.C. (1965) "Turbulent Boundary on a Waisted Body of Revolution in Subsonic and Supersonic Flow", AGARDograph 97, pp 933-962.
- Young, A.D. (1953) "The Equations of Motion and Energy and the Velocity Profile of a Turbulent Boundary Layer in a

Compressible Fluid", College of Aeronautics, Cranfield,
England, Report No 42.